NASA CR-143675

EARTH OBSERVATORY SATELLITE SYSTEM DEFINITION STUDY

REPORT NO. 7: EOS SYSTEM DEFINITION REPORT

• Appendixes A through D

GRUMMAN

EARTH OBSERVATORY SATELLITE SYSTEM DEFINITION STUDY

REPORT NO. 7: EOS SYSTEM DEFINITION REPORT

• Appendixes A through D

Prepared For

NATIONAL AERONAUTICS AND SPACE ADMINISTRATION

GODDARD SPACE FLIGHT CENTER

GREENBELT, MARYLAND 20771

Prepared By

GRUMMAN AEROSPACE CORPORATION

BETHPAGE, NEW YORK 11714

NAS 5-20520

September 1974

APPENDIX A CONTENTS

APPENDIX A1 CONTENTS

TABLE

APPENDIX A2 CONTENTS

ILLUSTRATION

TABLES

APPENDIX A3 CONTENTS

ILLUSTRATIONS

TABLE

APPENDIX A4 CONTENTS

ILLUSTRATIONS

TABLES

APPENDIX A5 CONTENTS

ILLUSTRATIONS

APPENDIX A6 CONTENTS

APPENDIX A6 CONTENTS (Cont)

APPENDIX A6 ILLUSTRATIONS

APPENDIX A6 TABLES

APPENDIX B CONTENTS

APPENDIX B ILLUSTRATIONS

TABLES

C7

APPENDIX C CONTENTS

ILLUSTRATION

TABLES

APPENDIX D CONTENTS

APPENDIX D ILLUSTRATIONS

TABLE

APPENDIX A DATA MANAGEMENT SYSTEM

A1 OBSERVATORY TO PRIMARY GROUND STATION COMMUNICATION LINKS

A1.1 INTRODUCTION

Three NASA Spaceflight Tracking and Data Network (STDN) ground stations will be used in the EOS System as Primary Ground Stations (PGS). In this mode, the system will provide space-to-ground data-transfer capability at rates up to 240 Mbps. For example, simultaneous transfer of 100 Mbps Thematic Mapper (TM) and 16 Mbps Multi-Spectral Scanner (MSS) data can be provided. The PGSs will receive the modulated signals from the spacecraft, track these signals with their 9 or 12 meter steerable antennas, and demodulate, tape record, and process the data. The three STDN locations of interest are; Engineering Training Center (ETC), Greenbelt, Maryland, Goldstone (GDS), California, and Fairbanks, Alaska (ULA). It has also been specified that QPSK (quaternary phase-shift keyed) modulation will be used, and that the spacecraft EIRP is ≥ 30 DBW when operating at the baseline X-band frequency. As an alternate, Ku band operation may be implemented where the EIRP is assumed to be 36 dBW.

Each STDN terminal location has a different complement of equipment as shown in Table A1-1. Also indicated in this table are the planned Ku-band modifications. The indicated 9-meter antennas will be equipped with dual S/Ku-band feeds, allowing full transmit and receive capability on both bands. Reviewing this data, it is seen that if the primary link is operated at Ku-band, no terminal modifications beyond those already planned by STDN are required, with the possible exception of the demodulators. Therefore, the remaining paragraphs will be concerned with only the X-band (baseline) approach.

Table A1-1 STDN Antenna Systems – S-Band Capability

LOCATION	27 m TELEMETRY (RECEIVE ONLY)	12 m COMMAND & TELEMETRY (RECEIVE AND TRANSMIT)	12 m TELEMETRY (RECEIVE ONLY)	9 m COMMAND & TELEMETRY (RECEIVE AND TRANSMIT)	Ku-BAND MODIFICATIONS PLANNED?
ENGRG TEST CENTER				1	YES
				2	NO
			X		NO
GOLDSTONE		X		X	YES
FAIRBANKS	X				NO
			X		NO
				X	YES

A7T-7

A1.2 SUMMARY OF TERMINAL MODIFICATIONS

At E.T.C., two fully USB-capable (receive and transmit) antennas exist. One of these will be modified for Ku-band. For the EOS application, the other 9-meter antenna must be equipped with a dual-frequency S/X-band feed. In addition, all the other X-band reception components (preamplifier, receiver, demodulator) are also required. Tracking will be done at S-band (the EOS spacecraft also has an S-band transmitter for telemetry purposes). Thus, E.T.C. is relatively uncomplicated, since only one antenna is needed to fully serve EOS. An alternative is to modify the 12-meter antenna for dual band (receive only) capability. This is less desirable, despite the higher antenna gain, because the 12-meter antenna cannot transmit commands at S-band.

At Goldstone (GDS), the sole existing 9-meter antenna is slated to be modified for S/Ku band. It is unlikely that a 3-band (S/Ku/X) feed could be developed for this antenna. It is also unlikely that the large 27-meter antenna would or should be equipped for X-band. Therefore, this location will require installation of a second 9-meter antenna system with and S/X-band feed and full S-band receive-transmit capability. It is understood that NASA has spare units of this type, and therefore no development or procurement costs are necessary. The feed assembly (S/X-band) as well as all X-band electronics will be the same here as at ETC. The new 9-meter system will fully support EOS.

Alaska (ULA) has a 9-meter antenna system, but this antenna is scheduled for the S/Ku-band feed, and is, therefore, not a candidate for X-band receive capability. The 12-meter antenna at this location is used for telemetry reception at S-band and some lower frequencies. This antenna could be modified using the same basic S/X-band feed approach as used for the 9-meter antennas at other locations. The additional gain of several dB achieved with this approach would probably be beneficial for this terminal. A disadvantage is that the 9-meter antenna would have to be used for S-band commands, thus requiring that the EOS spacecraft be tracked by two antennas. The other modifications (X-band receive equipment) will be the same at ULA as at the other locations.

A1.3 TRADEOFF AREAS

The motivation for designating STDN sites as Primary Ground Stations was to take advantage of installed equipment, particularly antennas and related subsystems, to as great an extent as possible. In particular, the development of a dual frequency S/X-band feed to replace the S-band feed is clearly cost-effective as compared to the procurement of a new, separate antenna. Retention of the existing S-band capability, rather than complete conversion to X-band, is mandatory in light of other STDN missions. Furthermore, if the dual feed is properly designed with both gain peaks coincident, and with retention of the S-band tracking system, the latter can be utilized to track EOS, thereby greatly simplifying and making less expensive the X-band electronics required. One approach retains the S-band Cassegrain feed system, but adds an X-band prime-focus receive feed. The subreflector will have to be dichroic, passing X but reflecting S-band signals. Such and approach should minimize performance degradation introduced by the multiple-frequency performance requirements. An alternative is a dual-band pure Cassegrain feed which is feasible since no autotrack is needed at X-band.

It is also recommended that at Goldstone, where an additional antenna is required, this be one of the USB system 9-meter units; either a spare or one retired

from service elsewhere. This will save on development and procurement costs. The feed assembly would be the same modified S/X-band unit. At ULA, a 12-meter receive-only antenna is to be modified. The feed modification can be essentially the same as for the 9-meter antenna although the transmit capability at S-band is not required.

System performance calculations show that with a 30 dBW spacecraft EIRP, a 9-meter ground antenna, a 240 Mbps data rate, and QPSK modulation, the system noise temperature at the PGSs must be under 350^{o}K. Such values are achievable only with parametric amplifiers. The only tradeoff is between cooled and uncooled paramps. The uncooled units are less expensive and, because of the lack of cryogenic equipment, more reliable. The state-of-the-art can provide a paramp with approximately 125^{o}K noise temperature, which in turn enables the system to achieve Te = 200^{o}K. This gives a margin of 5.3 dB in the worst-case power budget. Therefore, it is concluded that a cooled paramp is not warranted for the low noise preamplifier in the Primary Ground Station.

The preamp is typically mounted as close to the antenna feed as possible. Therefore, it must have sufficient gain (30 dB) so that the waveguide losses and/or down-converter noise figure do not noticeably degrade the system noise figure. Since the preamplifier is mounted on the antenna structure, it must be fixed-tuned and broad-banded over the entire applicable operating frequency range.

The use of QPSK (or variants) has been specified for the Primary links based on performance (low E_b/N_o requirement) and spectral efficiency (BW = R/2). There are three variants possible: conventional QPSK, offset QPSK, or two BPSK channels in phase quadrature. The differences at the demodulator are minor, having to do with manipulating the demodulated bit stream. For reasons of flexibility, the demodulator should be capable of outputting two separate data streams as would be derived from and I-Q (inphase/quadrature) modulation system. The data rates required for EOS (up to 240 Mpbs total) represent fairly sophisticated technology. Therefore, the specification has allowed for performance 2 dB off the theoretical

curve over the range $P_e = 5x10^{-7}$ to $1x10^{-2}$ (the nominal error rate is $P_e = 10^{-6}$). The intermediate frequency for such rates must be in the UHF region; 700 MHz has been specified. One important area in which the EOS PGS demodulator differs from other high rate PSK units is that it does not need to operate at low data rates. Therefore, the loop bandwidths are large, and rapid acquisition is assured. Also, the internal frequency stability requirement can be quite modest. Availability of the demodulator need not exceed good commercial practice. Since this is the most complex subsystem in the PGS receiving configuration, it may be desirable to employ two units in parallel for redundancy.

A2 LOCAL USER SYSTEM

A2.1 GENERAL

The LUS terminal is composed of three subsystems: an RF/IF, a Data Handling/Recording, and a Processor and Display subsystem. These subsystems were studied in detail during the EOS System Definition Study. They are described in the following paragraphs.

A2.2 LUS RF/IF SUBSYSTEM

Differential phase shift keyed (DPSK) modulation is used onboard the EOS to transmit payload data at 16 to 20 Mbps rates to the LUS. The baseline also assumes X-band signals, a satellite antenna characteristic which provides good performance only at LUS look angles above 50^{o}, and a spacecraft EIRP of 22 dBW. (An alternative is to operate the Ku band with 20 dBW EIRP).

The emphasis at the LUS's is on low cost. Given DPSK modulation operating at and E_b/N_o of 12 dB and the cited EIRP, a ground terminal with a G/T of 11 $dB/^{o}K$ will operate with about 3 dB margin above the worst-case power budget. This is considered adequate margin for this application. At Ku band, the limitations of space transmitter tube availability and the resulting low EIRP result in a required G/T of about 22 dB. Consequently, even with the largest antenna (12 ft) which is reasonable for a local user, a lower noise temperature front end is required. The emphasis is on the X-band (baseline) approach.

A2.2.1 ANTENNA AND DRIVE

The three major tradeoff areas with regard to the antenna system are:

- Size (gain)
- Mount type
- Tracking System

Antenna size is determined by the tradeoff between receiving noise temperature and aperture size. Because field effect transistors (FET) preamplifiers with relatively excellent performance are inexpensive the smallest practical antenna dish should be used at X-band, about 1.8 m (6 ft). Such an antenna is structurally and aesthetically more attractive than larger alternatives. This is an important consideration for the local users, who may mount an antenna on a rooftop, for example.

The antenna mount type is influenced by coverage considerations and cost factors. Specifically, one does not want a "keyhole" or tracking mode changeover at zenith, and would prefer a mount that minimizes the number of required simultaneous two axis tracking corrections per EOS pass. At this time the polar type of mount appears to be the best alternative.

The most important tradeoff is tracking technique. The simplest extreme is a manually turned mount (human muscle power). The next step, "manually" steered, refers to a system with remote electrical position readouts and remotely-controllable steering motors. The operator steers the antenna and updates the position every 30 seconds or so based partly on previously prepared steering charts and partly on "peaking-up" the signal strength. This approach is relatively inexpensive, but operationally inconvenient. Nevertheless, its low cost would make it the recommended approach except that the cost increment for the next step up is small.

Once the readouts and motors (servos) for remote manual control have been assumed, it is straightforward to replace the operator by a machine - specifically, an interface unit and a computer. This is the programmed track approach. The computer does not add to the cost because it is available in the processor/display subsystem. Thus only a computer/antenna servo interface unit and software need be added to implement programmed track.

The next, more sophisticated approach is step track where the control loop is closed and the computer adjusts antenna pointing for strongest signal strength, doing so in discrete position steps. It is not clear whether such a system could be made

to perform properly with low orbit satellites. However, it is not likely to perform better than programmed track, assuming that the programmed track steering data are accurate. The additional interface with the receiver (for signal strength) and the comparison logic or software would add to the cost.

The most sophisticated approach is autotrack, which employs more complex antenna feeds and receivers to continuously track the received signal. This is clearly undesirable for the LUS because of its high cost.

It appears that programmed track is the best choice of the three (manual, program, step) techniques for the LUS's. This conclusion is based on the necessary system performance being provided at the least cost with reasonable local operator convenience.

A2.2.2 LOW NOISE PREAMPLIFIER

The field effect transistor (FET) preamplifier has supplanted the tunnel diode preamp as the accepted low cost, moderately low-noise approach for RF preamplification at microwave frequencies. However, there is no reason why a TDA could not be employed, or even a low-noise (image enhanced Schottky barrier) mixer, if it can match the FET. The state-of-the-art system noise temperature when using such units is expected to be 900^{o}K, at costs in the several thousand dollar category.

A2.2.3 DOWNCONVERTER-RECEIVER

The downconverter-receiver for the LCGS is quite straightforward and presents no significant technical tradeoffs. The output (IF) has been specified at the standard 70-MHz frequency for which off-the-shelf equipment is available.

A2.3 DATA HANDLING/RECORDING SUBSYSTEM (DRS)

The DRS consists of a demodulator, data acquisition tape recorder/reproduce and a pixel decommutator. The demodulator receives a modulated IF signal at 70 MHz and provides an NRZ-M baseband signal output. The NRZ-M format is converted to NRZ-L prior to recording by the acquisitive recorder.

Tape recorder/pixel decommatator performance/cost tradeoffs have indicated that serial data recording rather that decommutated data recording is less expensive. Therefore, pixel decommutation is performed upon playback of the raw data into the processor/display subsystem.

A2.3.1 DEMODULATOR

System tradeoffs have previously shown that only three modulation techniques might be cost and performance competitive: BPSK, DPSK, and m-ary FSK. However, further study showed that the FSK alternative could offer only negligible advantages in cost or performance, whereas PSK represented a lower technical risk, being closer to developments under way for many NASA, military, and INTELSAT programs. It has been concluded that DPSK (differentially coherent PSK) is a better choice for the LUS than BPSK, because it solves the ambiguity problem with an 0.8 dB performance loss.

The PSK demodulator is a well developed, almost off-the-shelf item, and no significant system level tradeoffs exist with regard to its implementation. Performance has been specified as within 1.5 dB of theoretical performance, and, like the PGS demodulators, loop bandwidths can be made wide so that acquisition, tracking, and frequency stability are not a problem.

A2.3.2 LUS ACQUISITION TAPE RECORDER

Basic characteristics of the recorder/reproducer are: store 16 to 20 Mbps data received over a period of 5 to 15 minutes with playback rates between 1 and 3 Mbps through the pixel decommutator into the PDS computer. Other characteristics as well as candidate equipment, are shown in Table A2-1. The currently recommended unit is the RCA LC 20G recorder which is estimated to cost $25K in quantities of 10 or more.

Table A2-1. Suitable High Density Digital Tape Recorders for 20 Mbps Data Acquisition

MANUFACTURER AND MODEL	RCA CVR 102D	RCA LC 20G	BELL & HOWELL VR3700B (PCM)	AMPEX	LEC HD7000/20
• RECORDING TECHNIQUE	ROTARY HEAD TRANSVERSE RECORDING	ROTARY HEAD TRANSVERSE RECORDING	LONGITUDINAL MULTITRACK	LONGITUDINAL MULTITRACK	LONGITUDINAL MULTITRACK
• NUMBER OF TRACKS	1 DATA (TRANSVERSE) 2 AUDIO (LONGITUDINAL) 1 CONTROL (LONGITUDINAL)	1 DATA (TRANSVERSE) 2 AUDIO (LONGITUDINAL) 1 CONTROL (LONGITUDINAL)	14 TOTAL (IRIG) 8 DATA –	14 TOTAL (IRIG) 12 DATA –	7 TOTAL (IRIG) 7 DATA –
• IN-TRACK PACKING DENSITY	10 KBPI	10 KBPI	30 KBPI	15 KBPI	25 KBPI
• RECORD TAPE SPEED	10 IPS LONGITUDINAL 2000 IPS HEAD TO TAPE	10 IPS LONGITUDINAL 2000 IPS HEAD TO TAPE	120 IPS –	120 IPS –	120 IPS –
• PLAYBACK SPEED OF RECORDED DATA				1-7/8 IPS (MINIMUM)	15 IPS (MINIMUM)
• MAX. RECORD/PLAYBACK RATIO	32:1	32:1	8:1	–	–
• MAGNETIC TAPE				GOOD QUALITY	VENDOR RECOMMENDED
–TYPE	COMM. GRADE VIDEO	COMM. GRADE VIDEO	CERTIFIED INSTR. TAPE	INSTR. TAPE	3M 971
–WIDTH	2 IN.	2 IN.	1 IN.	1 IN.	1/2 IN.
–REEL DIAMETER	6-1/2 IN.	6-1/2 IN.	14 IN.	10-1/2 IN.	14 IN.
• RECORDING CODE	RCA PROPRIETARY	RCA PROPRIETARY	ENHANCED NRZ	MILLER	HDDR II
• RECORD TIME	15 MINUTES	15 MINUTES	15 MINUTES	22 MINUTES	10 MINUTES

A7T-10

A2.4 PROCESSOR AND DISPLAY SUBSYSTEM (PDS)

Three levels of PDS capability have been considered for the LUS terminals. The terminals are labeled Basic, Enhanced I, and Enhanced II depending on their capability and cost. Table A2-2 lists the terminal equipment.

Figure A2-1 diagrams the Enhanced II LUS. Of significance with the minicomputer system is the use of a multiport core. This feature increases the processing throughout because data input and output operations can occur simultaneously without affecting the computing operations.

Table A2-2 PDS Terminals Vs Capabilities

LUS MODEL	HARDWARE	CAPABILITIES
BASIC	1 - MINICOMPUTER (32K MEMORY) 1 - DISK AND DRIVE (29M BY) 2 - MAGNETIC TAPES[a] AND DRIVES 1 - OPERATOR I/O CRT/KEYBOARD 1 - B & W IMAGE STORAGE DISPLAY 1 - DATA REPRODUCER INTERFACE	DISPLAY - B & W IMAGES (1024 PIXELS) DATA PROCESSING - YES (SLOW) IMAGE ANALYSIS - YES (VERY SLOW) HARDCOPY - YES (CAMERA)
ENHANCED I	BASIC HARDWARE PLUS 1 - MINICOMPUTER (MULTIPROCESSOR) 1 - LINE PRINTER 1 - INTERACTIVE COLOR DISPLAY 1 - FLOATING POINT AND HARDWARE MULTIPLY/DIVIDE FOR MINI-COMPUTERS	DISPLAY - B&W OR COLOR IMAGES DATA PROCESSING - MODERATE SPEED IMAGE ANALYSIS - INTERACTIVE HARDCOPY - CAMERA AND LINE PRINTER FOR THEMATIC MAPS, ETC.
ENHANCED II	BASIC, ENHANCED I HARDWARE PLUS 1 - DISK AND DRIVE (29 MBY) 2 - MAGNETIC TAPES AND DRIVES 1 - B&W AND COLOR IMAGE RECORDER 1 - COLOR IMAGE DISPLAY	DISPLAY - 2 SIMULTANEOUS B&W OR COLOR IMAGES DATA PROCESSING - REASONABLY FAST IMAGE ANALYSIS-INTERACTIVE, CHANGE ANALYSIS, MODERATE SPEED HARDCOPY - LINE PRINTER AND FIRST GENERATION PHOTO PRODUCTS (70 MM TO 4" x 5" SIZES)

(a) 75 IPS AND 1600 BPI

A7T-11

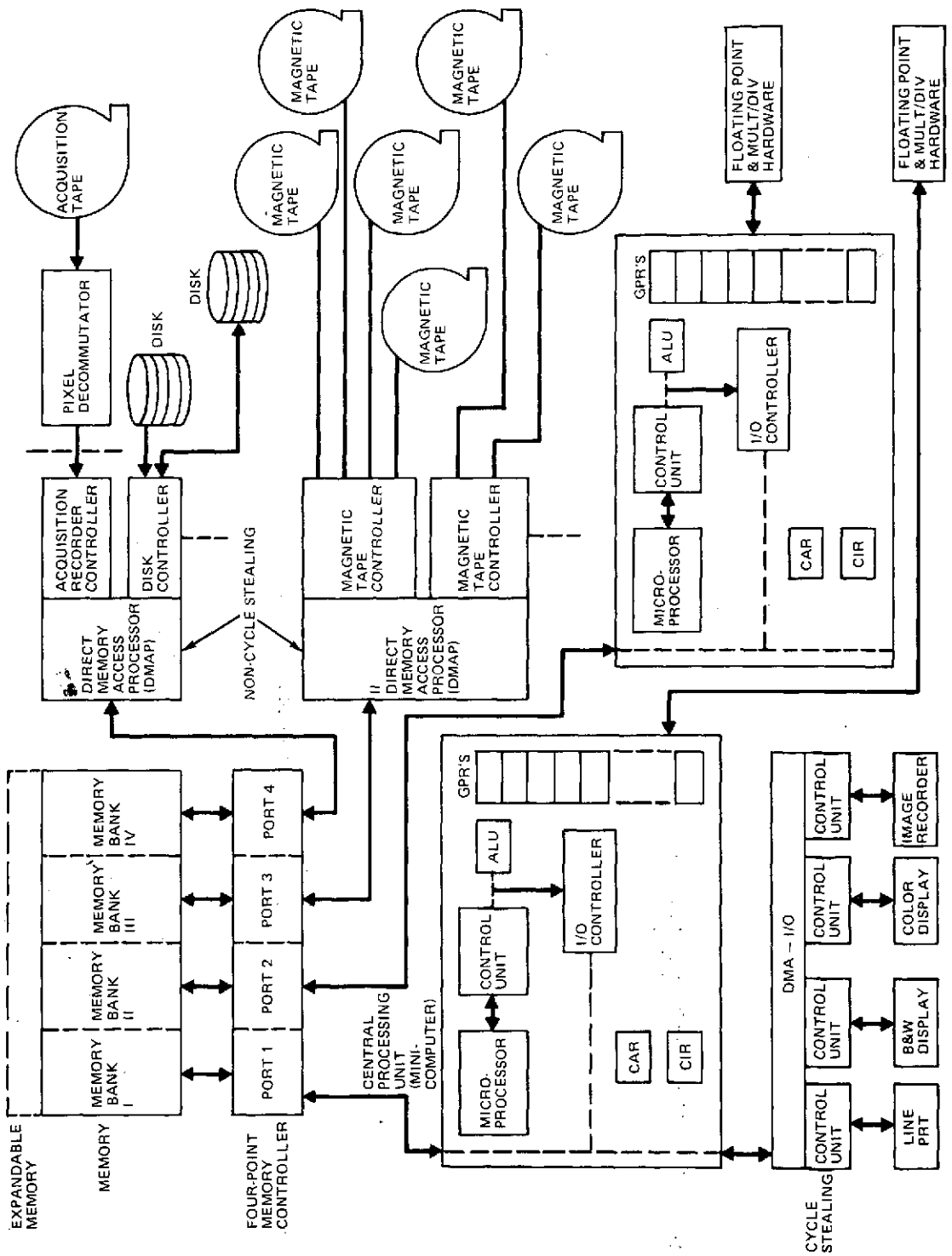

Fig. A2-1 LUS Enhanced II Processing System

A3 CONICAL SCANNER VS LINEAR SCANNER PROCESSING COSTS

A3.1 INTRODUCTION

One of the candidate approaches to the Thematic Mapper (TM) design is the image-plane scanner developed by Minneapolis Honeywell. Advantages to this alternative design include a rotating rather than an oscillating mirror, better scan linearity, and possibly lighter weight of the overall instrument. A disadvantage is that, in order to keep the optics as simple as possible, the image is scanned at an angle with the result that the earth is scanned with conical rather than linear scan lines. More precisely, the path of the scanner for any particular sweep of the earth can be envisioned as following a path along the rim of a cone. The cone has some thickness since each sweep produces 18 scan lines at a time. Each is 27 meters wide in the north-south direction. Although the rim of such a cone would intersect a flat surface with no overlap of the scan lines, the intersection with a sphere will result in an overlapping of the 18 scan stripes near the edge of the scan. This effect, and the shape of the scan lines on the curved earth, will be dependent on the angle with which the cone intersects the earth. Also, picture samples can be taken during the forward or backward looking portion of the scan. Generally, then, we are dealing with scan patterns that are sectors of circles which are concave forward with respect to the ground track for a scan at the rear of the nadir point, or convex forward when scanning ahead of the spacecraft. These two options have no clear advantages over one another. The cone orientation can also be selected to scan through the nadir point. Although this option may produce slightly less image distortion, it will not be considered in the following discussion (scan lines become parabolas rather than circles and the mathematical complications could obscure the first-order effects which are the only effects to be included in the analysis).

Our goal here is to compare the conical-scan and linear-scan Thematic Mappers in terms of the processing that must be performed to achieve precise geometric correction of the resulting digital images. By geometric correction, we shall refer to all of the digital processing steps that are necessary to produce a precise map in a UTM coordinate system. We will attempt to quantify the extra storage and the extra machine instructions (if any) required to correct the conical scan data compared to the linear scan data.

In Subsection 3.2, the conical-scan geometry is described for a simple flat-earth case. This case should be adequate to reveal the major (first-order) geometric distortions. Complexity and costs are then estimated in Subsection 3.3 for the processing of these images and these are compared to the costs for the linear case. Since a definitive set of numbers for the conical scan parameters are not available at present, the necessary numbers have been assumed. The results should be adequate for the type of cost estimates which are attempted here. Subsection 3.4 includes a summary comparison of the linear and conical scan cases.

A3.2 ASSUMED GEOMETRY OF THE CONICAL SCANNER

The relationship of the conical scan pattern with respect to the 185 km swath is shown in Figure A3-1. We assume that six segments are used on the scan wheel and that the scan is to be 80 percent efficient. Active scanning therefore covers $0.8 \times 360 = 288^{\circ}$ and each segment covers 48°. In Figure A3-2, we show the detailed geometry of the scan lines within the 185 km swath. For the case shown, the bow in the scan lines is given by the distance b which is

$$b = R - x = 227.418 \text{ km } [1 - \cos \Theta/2] = 19.66 \text{ km}$$

With a resolution of 27 meters, 728 resolution elements or 43 sweeps of the scanner are contained in the bowed region.

In Figure A3-3, we show in more detail the relationship of the conical scan lines to the resampling grid structure. This drawing is approximately to scale and we have assumed a 10 x 10 resampling grid. The large 185 x 185 km rectangular

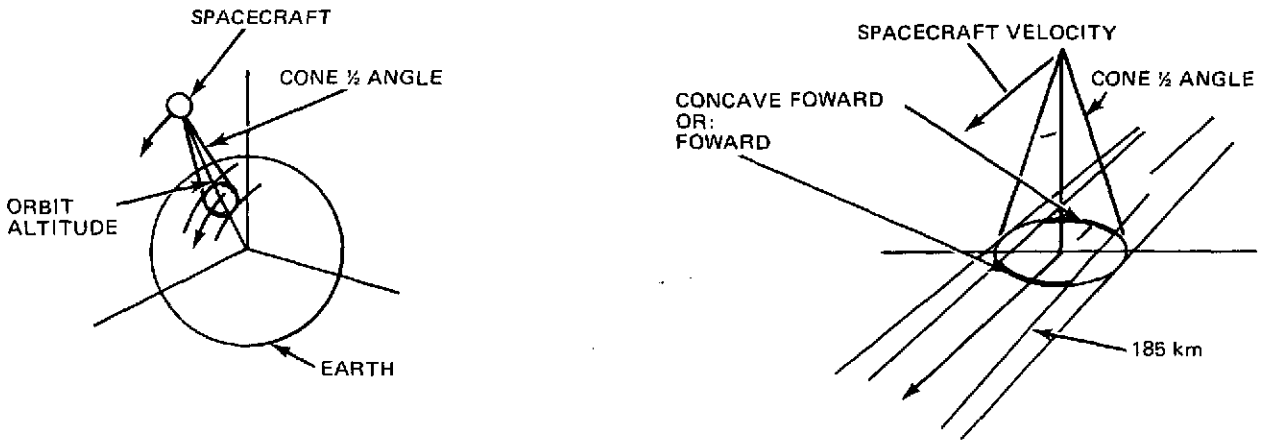

A7-2 **Fig. A3-1 Basic Conical Scan Pattern and Flat-Earth Assumption**

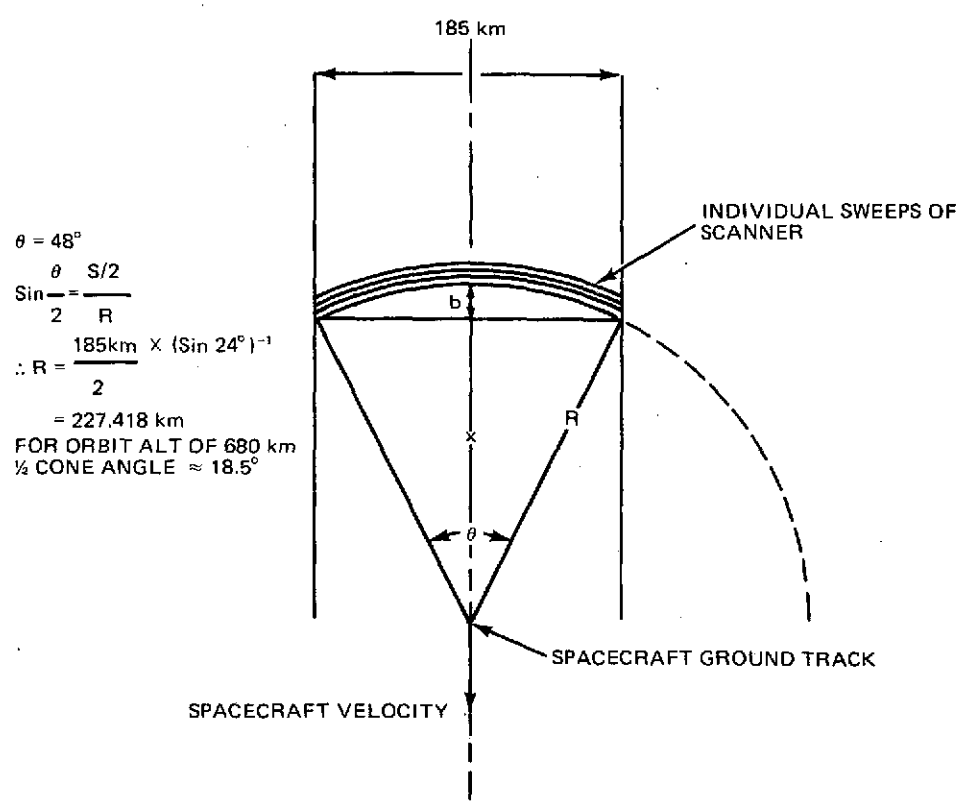

A7-3 **Fig. A3-2 Geometry of Backward Conical Scan**

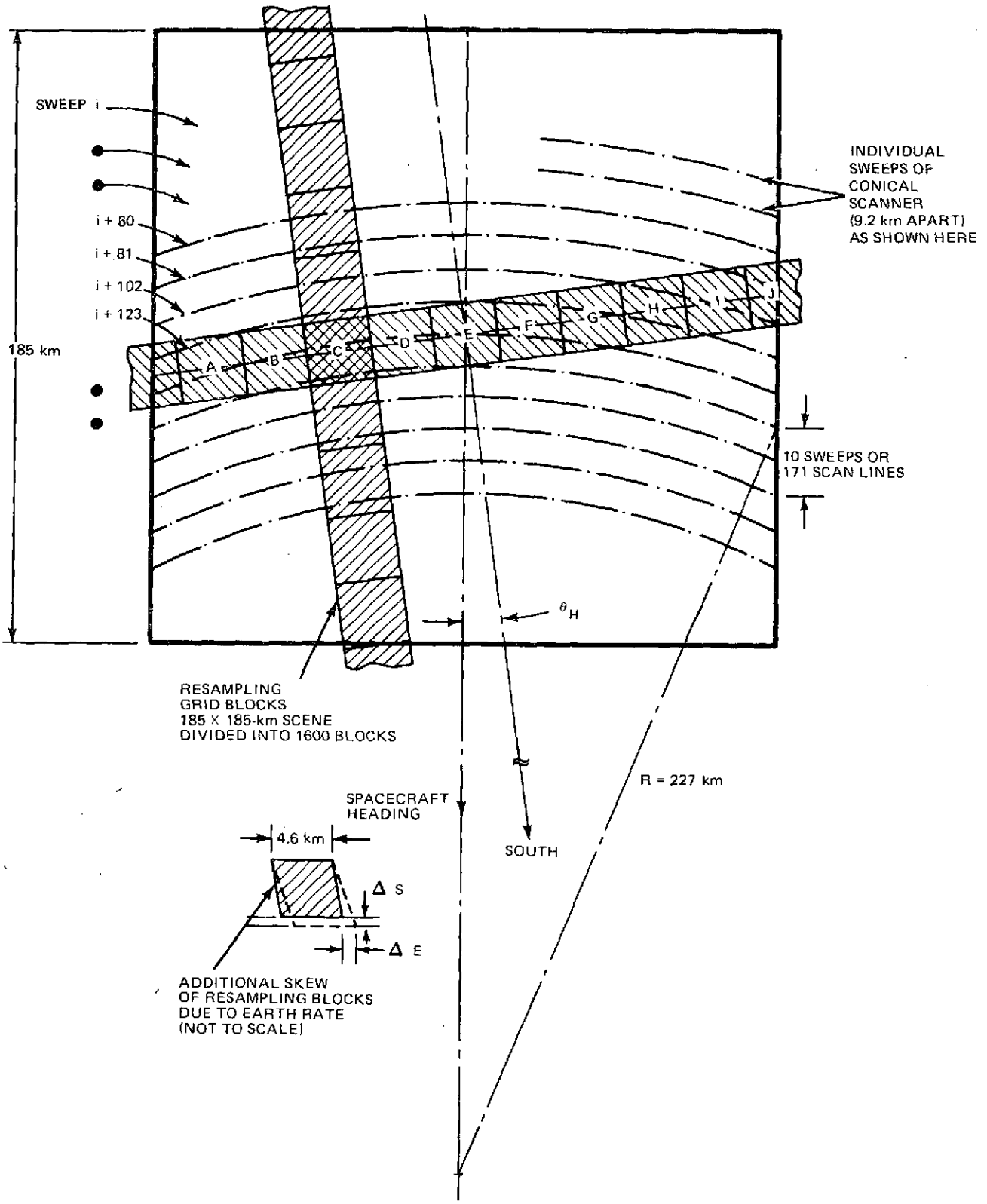

Fig. A3-3 Location of Resampling Grid Blocks Within the 185 x 185 Km Scene

area corresponds to the "scene" taken by the sensor. Within this scene, there are 6852 individual scan lines representing approximately 380 sweeps of the sets of 18 detectors in each band. Each sweep of the scanner traces out an arc of a circle with radius 227 km. The scanner produces pixels at equal-angle increments within the $\pm 24^{o}$ sector with the individual elements representing angles of approximately 97 μ radians (this should not be confused with the 38 μ rad resolution of the TM from orbit altitude).

The scan pattern is normal to the S/C heading which is itself oriented by Θ_H^o with respect to south (Θ_H^o measured clockwise with respect to due south). This heading angle is given by

$$\Theta_H = \sin^{-1}\left[\frac{\sin \Theta_E}{\cos \lambda}\right] \tag{1}$$

where

Θ_E is the polar inclination (6^{o} assumed)

λ is the latitude.

For a latitude of approximately 37^{o}, the heading angle is 7.5^{o}. Therefore, we show the orientation of the resampling grid blocks within the scene as oriented at an angle of nominally 7.5^{o} with respect to the S/C ground track. There are approximately 100 of these blocks representing a 10 x 10 subdivision of the desired output grid. Each of these blocks is subjected to an additional skew due to the earth's rate of rotation. This skew can be estimated as

$$\Delta S = V_E \, \delta t \cos \Theta_H \cos \lambda \tag{2}$$

$$\Delta E = V_E \, \delta t \sin \Theta_H \cos \lambda \tag{3}$$

Where V_E is the velocity of the earth at the equator (463.38 m/s) and δt is the time for one sampling block to be scanned (approximately 1/10 of the scene time or

2.7 seconds). For a 6^{o} inclination at 37^{o} latitude, we obtain $\Delta S = 130$ meters and $\Delta E = 990$ meters. Compared to the skew due to ground - track heading (approximately 18.5 km x tan (7.5^{o}) = 2423 meters) these additions are fairly small but they do add to the overall skew of the resampling blocks with respect to the image data.

Even for a linear scanner, the skew of the resampling grid relative to the scan pattern causes some complication in collecting together the data needed for the blocks. This complication is increased for the conical scan lines. For example, sweep (i + 123) in Figure A3-3 contributes to block A but is not needed again until blocks G, H, and I. To reconstruct a single output scan line, say the top line in all blocks A through J, the number of scan lines that must be accessed (hence stored) is determined by the bow in the scan lines (d = 19.66 km corresponding to 728 scan lines) plus the tilt due to the heading angle (185 km x tan 7.5^{o} corresponding to 24.2 km or 899 scan lines). The conical scanner, therefore, requires 1627 scan lines to produce one output line which is an increase of 80 percent over the linear scanner. An additional complexity concerns the algorithm that must be used to compute the coordinates of the desired output data points with respect to the conical scan data.

A3.3 PROCESSING COMPLEXITY

A3.3.1 INTRODUCTION

Some of the processing which must be performed on the TM data is peculiar to the conical scan pattern and will, therefore, require more processing than for the linear case. A second factor that must be considered is the increase in storage required to process the conical scan data. Finally, the third factor that must be considered is the accessability of the resampling blocks from the intermediate storage device which we will assume to be a disk.

A3.3.2 CALCULATION OF COORDINATES OF THE CONICAL SCAN DATA IN THE OUTPUT COORDINATE SYSTEM

The main computational complication in resampling the conical scan data is the determination of the coordinates of the original data points (line number and pixel number within the line) for each desired point in the output grid blocks. In Figure A.3-4 we show a worst case situation where we are resampling the data in grid block "I" of Figure A3-3. The cross-track distance to a general point (x, y) in this block is

$$d = \frac{S}{2} - [(G - y) \sin \beta + x \cos \beta] \tag{4}$$

where G is the dimension of the grid block (assumed square) and β is the total tilt angle. Given d and R* one can find Θ as

$$\Theta = \sin^{-1} \left\{ d/R \right\} \tag{5}$$

and the distance D is then found as

$$D = R \cos \Theta + y \cos \beta \tag{6}$$

If the angle Θ is known, then the element (or nearest element) in a particular scan line is known. If D is known, we can find the nearest scan line to the desired output point. This situation is shown at the left of Figure A3-4. Here we show the original array of sampling points as squares and these points define an array of data indexed by Θ and D (P (Θ, D)). The coordinates x and y define the coordinates of the points in the desired output array R(x,y). Given x and y, one can solve for d by using (3). Pixel number is then found by using (5) to obtain Θ. Finally, knowing Θ, one finds line number from D in (6).

---

* The assumption is made here that R is a constant. Actually, the radius differs slightly for the scan lines within each set of 18 which comprise one sweep. Equations (5) and (6) are, therefore, a simplification of the actual algorithms that would be used.

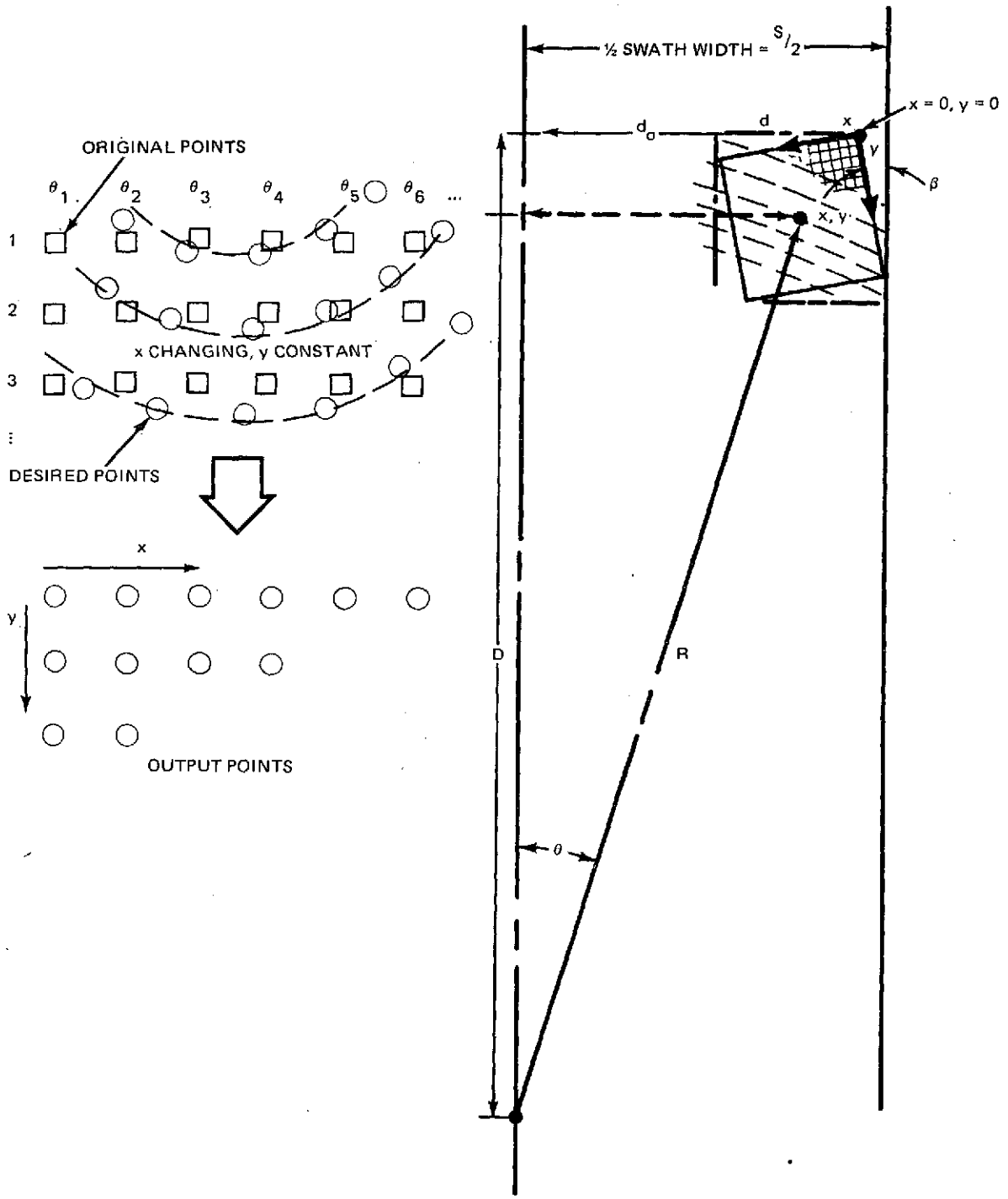

A7-5 **Fig. A3-4 Resampling Geometry for One Grid Block**

It is clear that (4), (5) and (6) give a nonlinear set of equations for Θ and D as a function of x and y. Assume first, that we want a set of coordinates for a particular line in the output array where y remains constant at a value Y_o. To find Θ and D by straightforward techniques, one would solve (4), (5), and (6) as follows

Constants: $S/2$, $(G - Y_o) \sin \beta$, $\cos \beta$, R

	Floating Pt Mply.	Ft. Pt. Divide	Ft. Pt. Add	Trig. Function
Equation (4) $x \cos \beta$	1			
$\left[x \cos \beta + (G - Y_o) \sin \beta \right]$			1	
$S/2 - \left[\quad \right] = d$			1	

	Floating Pt Mply.	Ft. Pt. Divide	Ft. Pt. Add	Trig. Function
Equation (5) d/R		1		
$\sin^{-1} \left[\quad \right] = \Theta$				1
Equation (6) $\cos \Theta$				1
$R \cos \Theta$	1			
$R \cos \Theta + Y_o \cos \beta = D$			1	
TOTAL	2	1	3	2

Using the equivalences:

Floating Point Multiply = 5 interger add times
Floating Point Divide = 11 interger add times
Trigonometric Function = 22 interger add times
Floating Point Add = 3 interger add times

we obtain a total of 74 machine instructions for the coordinate computation of each output point. This is an intolerable processing load (equivalent roughly to the operations required for "cubic convolution" interpolation) and a simple recursive implementation of (4) through (6) must be found.

We can assume resampling according to Fig. A3-5 and that output samples are required on a grid with $\Delta x = \Delta y = 27$ meters.

Considering one output line in the block, we first assume that y is constant ($Y_o = O$) and then let x assume the values $X_o = O$, $X_1 = 27$ meters, $X_2 = 54$ meters, and so on. The initial values of θ_{oo} and D_{oo} are:

$$d_{oo} = s/2 - G \sin \beta$$

$$\Theta_{oo} = \sin^{-1}\left[d_{oo}/R\right]$$

$$D_{oo} = R \cos \theta_{oo}$$

The partial derivative of Θ with respect to x is

$$\frac{\partial \Theta}{\partial x} = \left[1 - (d/R)^2\right]^{-1/2} \frac{\partial (d/R)}{\partial x}$$

$$= -\frac{\cos \beta}{R}\left\{1 - \left(\frac{S/2 - (G-y) \sin \beta + x \cos \beta}{R}\right)^2\right\}^{-1/2} \qquad (7)$$

Using the approximation

$$(s + t)^n \cong s^n + n\, s^{n-1}\, t + \ldots . \quad ; \; |s| > |t|$$

we can approximate $\left[A - 1\right]$ as

$$\frac{\partial \Theta}{\partial x} \cong -\frac{\cos \beta}{R}\left\{1 + 1/2\left(\frac{s/2 - \left[(G-y) \sin \beta + x \cos \beta\right]}{R}\right)^2\right\} \qquad (8)$$

similarly,

$$\frac{\partial \Theta}{\partial y} \cong +\frac{\sin \beta}{R}\left\{1 + 1/2\left(\frac{s/2 - \left[(G-y) \sin \beta + x \cos \beta\right]}{R}\right)^2\right\} \qquad (9)$$

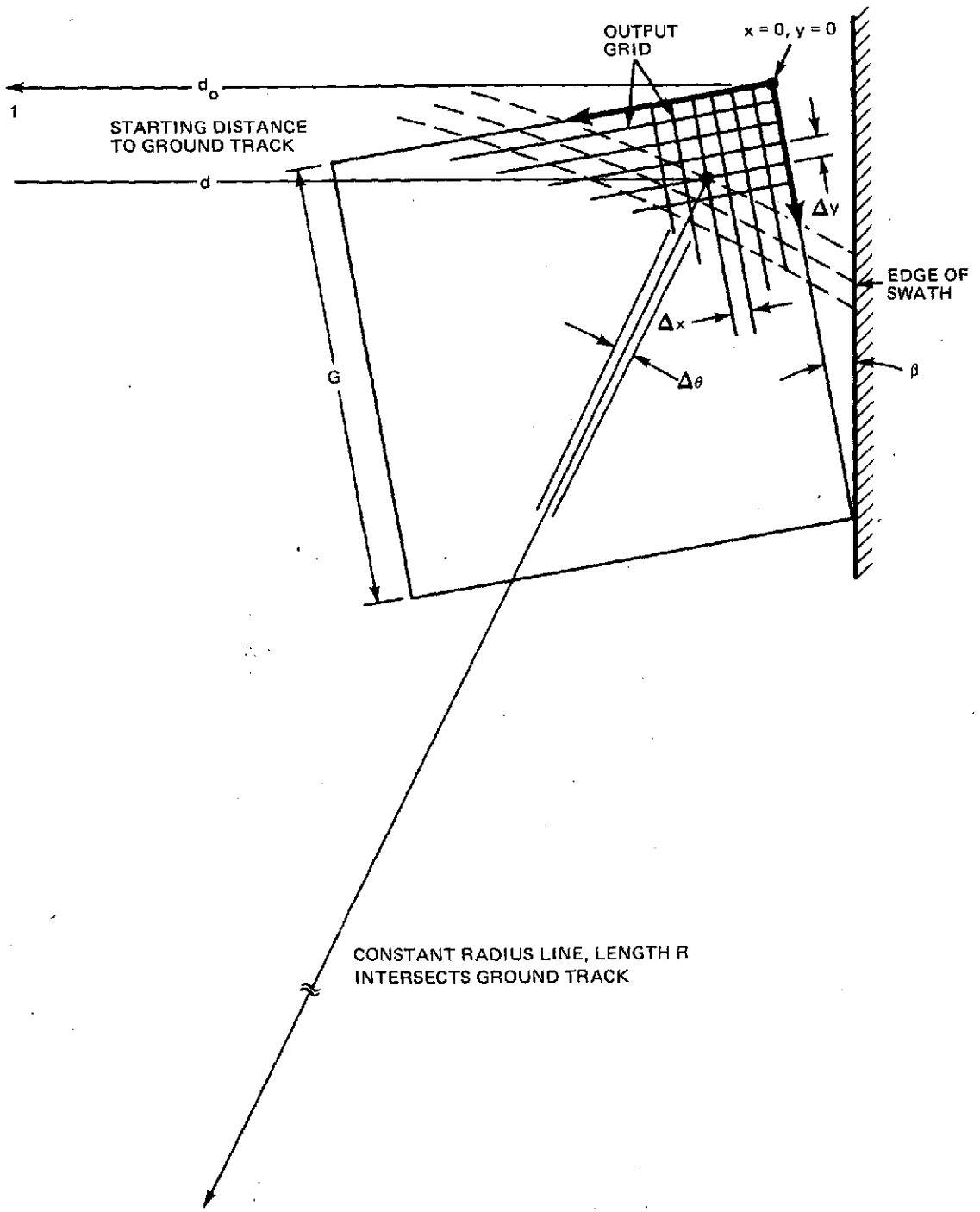

Fig. A3-5 Detail of the Resampling Within One Grid Block

the second partials become

$$\frac{\partial^2 \Theta}{\partial x^2} \cong + \left(\frac{\cos \beta}{R}\right)^2 \left(\frac{s/2 - [(G-y) \sin \beta + x \cos \beta]}{R}\right) \tag{10}$$

$$\frac{\partial^2 \Theta}{\partial y^2} \cong + \left(\frac{\sin \beta}{R}\right)^2 \left(\frac{s/2 - [(G-y) \sin \beta + x \cos \beta]}{R}\right) \tag{11}$$

and, finally, the third partials are

$$\frac{\partial^3 \Theta}{\partial x^3} \cong - \left(\frac{\cos \beta}{R}\right)^3 \tag{12}$$

$$\frac{\partial^3 \Theta}{\partial y^3} \cong + \left(\frac{\sin \beta}{R}\right)^3 \tag{13}$$

Still considering only the resampling in the x direction, we find

$$\frac{\partial D}{\partial x} = - R \sin \Theta \frac{\partial \Theta}{\partial x} \tag{14}$$

$$\frac{\partial^2 D}{\partial x^2} = - R \cos \Theta \frac{\partial^2 \Theta}{\partial x^2} \tag{15}$$

$$\frac{\partial^3 D}{\partial x^3} = + R \sin \Theta \frac{\partial^3 \Theta}{\partial x^3} \tag{16}$$

where higher order partials are zero. Although trigonometric functions appear in (14) and (16), these can be computed recursively as

$$\sin(\Theta + \Delta\Theta) = \sin \Theta \cos \Delta\Theta + \cos \Theta \sin \Delta\Theta$$

$$\cos(\Theta + \Delta\Theta) = \cos \Theta \cos \Delta\Theta - \sin \Theta \text{ son } \Delta\Theta$$

where $\Delta\Theta$ is small enough that these can be approximated as

$$\sin(\Theta + \Delta\Theta) = \sin\Theta\,(1 - \epsilon^2/2) + \epsilon\cos\Theta$$

$$\cos(\Theta + \Delta\Theta) = \cos\Theta\,(1 - \epsilon^2/2) - \epsilon\sin\Theta$$

by assuming that ϵ is a constant.

We can now postulate a recursive algorithm as shown in Fig. A3-6 which should allow the computation of Θ and D as x moves in equal increments along the resampling block. The accuracy of this approximation must be tested by simulation. However, it does appear that the computation of Θ and D can be accomplished in much less than 74 additions. In the figure, 26 additions (8 adds, 6 multiplies) is estimated for the recursive approach.

For the purposes here, we will use the estimate of 26 instructions/pixel for the recursive conical scan coordinate computation. The major contributors to processing load are summarized as:

	Instructions/Pixel				
	Linear		Conical		
Radiometric Correction	2		2		
Line Stretching	0.64*		0.64*		
Resampling Grid	0.17*		0.17*		
Coordinate Computation for Resampling	0.48*		4.16*		
Interpolation		Totals		Totals	Excess for Conical Scan
Nearest Neighbor (NN)	8.0	11.3	8.0	15.0	+ 32%
Bilinear (BI)	25.0	28.3	25.0	32.0	+ 13%
Cubic Convolution (CC)	60.0	63.3	60.0	67.0	+ 6%
GCP Location	Negligible for 4 per scene/baseline ACS.				

* Divided by 6.25 since one computation serves for all bands.

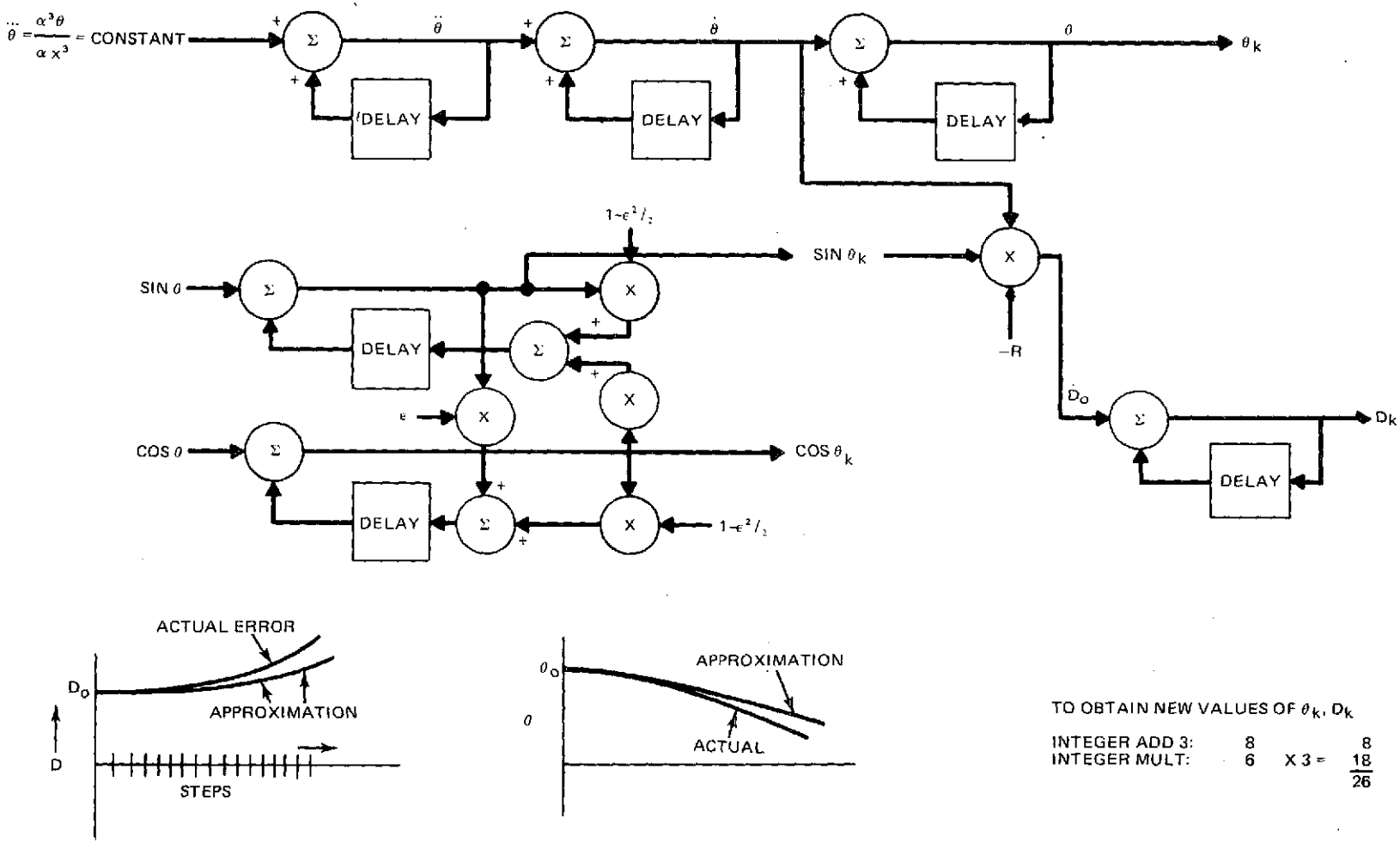

Fig. A3-6 Recursive Computation of θ and D.

A3.3.3 ADDITIONAL STORAGE REQUIRED TO HOLD THE DATA REQUIRED TO PRODUCE A SINGLE OUTPUT GRID BLOCK

A second factor in processing the conical scan data is the storage required to hold the individual blocks. If we consider a block as 1/1600 of a scene, then the number of pixels in a block are approximately

$$N_{PB} = 6852 \frac{\text{LINES}}{\text{SCENE}} \times 6852 \frac{\text{PIXELS}}{\text{LINES}} \times \frac{1}{1600} \times 6.0625 \text{ bands} = 1.77 \times 10^5 \text{ PIXELS/BLOCK}$$

In Table A.3-1 we show the percentage extra pixels that must be stored to process a single block of data as a function of satellite latitude, for an orbit inclination of 98^{o} (differences with orbit altitude in the range 640 - 775 km are negligible). If we express N_{PB} in terms of bits, and assign a cost of \$0.05 per bit for high-speed storage, we can extimate the costs of this extra storage as shown in the table.

In the comparison above, we are assuming that the individual blocks, each containing 1.77×10^5 eight-bit bytes of data (all bands), are processed individually in the computer.

Table A3-1 Extra Pixel Storage Requirements

LATITUDE, DEG,	HEADING ANGLE, DEG,	EXTRA STORAGE REQUIRED, %		COST (@ 5¢ bit), $	
	θ_H	Linear	Conical	Linear	Conical
56	14.2	47.6	97.2	$3.39 x 10^4	$6.90 x 10^4
49	12.0	40.7	95.1	$2.89 x 10^4	$6.75 x 10^4
36.5	9.8	33.4	92.4	$2.38 x 10^4	$6.55 x 10^4
19.5	8.4	28.8	90.5	$2.00 x 10^4	$6.44 x 10^4
0	8.0	27.6	89.9	$1.96 x 10^4	$6.40 x 10^4

A7T-8

A3.3.4 DISK INPUT/OUTPUT TIME

The final factor that enters into the evaluation of the conical scanner is the input/output time required to access the data on an intermediate storage device and to load these data points into core storage. To make these estimates, we will assume two hypothetical disk to core data transfer rates of 8 megabits per second and 192 megabits per second. The time required to read one scan is then:

Case I, 8 Mbps - 772 milliseconds

Case II, 192 Mbps - 32 milliseconds

For the linear scanner, we must access extra lines of data to account for the fact that the resampling grid is tilted with respect to the original data. For the linear scanner, the extra lines are approximately.

$$N_{\ell} = 2\ G \tan \beta$$

where G is the number of lines in the grid square (approximately 171). We will obtain our estimates of extra lines from Figure A3-6 by assuming that a square-root relationship exists between extra lines stored and extra pixels. From this figure, for a 40 x 40 subdivision, and a nominal 41 scans/block we obtain at approximately 35^{o} latitude:

Nominal, No Tilt	Linear Scanner	Conical Scanner
10 scans	11 scans	14 scans
171 lines	187 lines	234 lines

These numbers give the following times required to read 100 augmented blocks of data from disk to core storage.

	Linear Scan	Conical Scanner
Case I - 772 milliseconds to read an entire scan	13,600 seconds (226 minutes)	17300 seconds (288 minutes)
Case II - 32 milliseconds to read an entire scan	564 seconds (94 minutes)	717 seconds (119 minutes)

There are a total of 2.94×10^{8} pixels/scene so that a processor that is capable of 1 Mips (10^{6} operations/second) requires 330 seconds to perform one operation on each pixel. Figure A3-7 plots the number of seconds required to process one scene as a function of the number of operations performed on each pixel. We have added to these times the input transfer times above. When the processing time per block is less than the transfer time, the latter will determine the throughput rate. When the transfer times becomes negligible, throughput rate is determined by the number of operations per pixel.

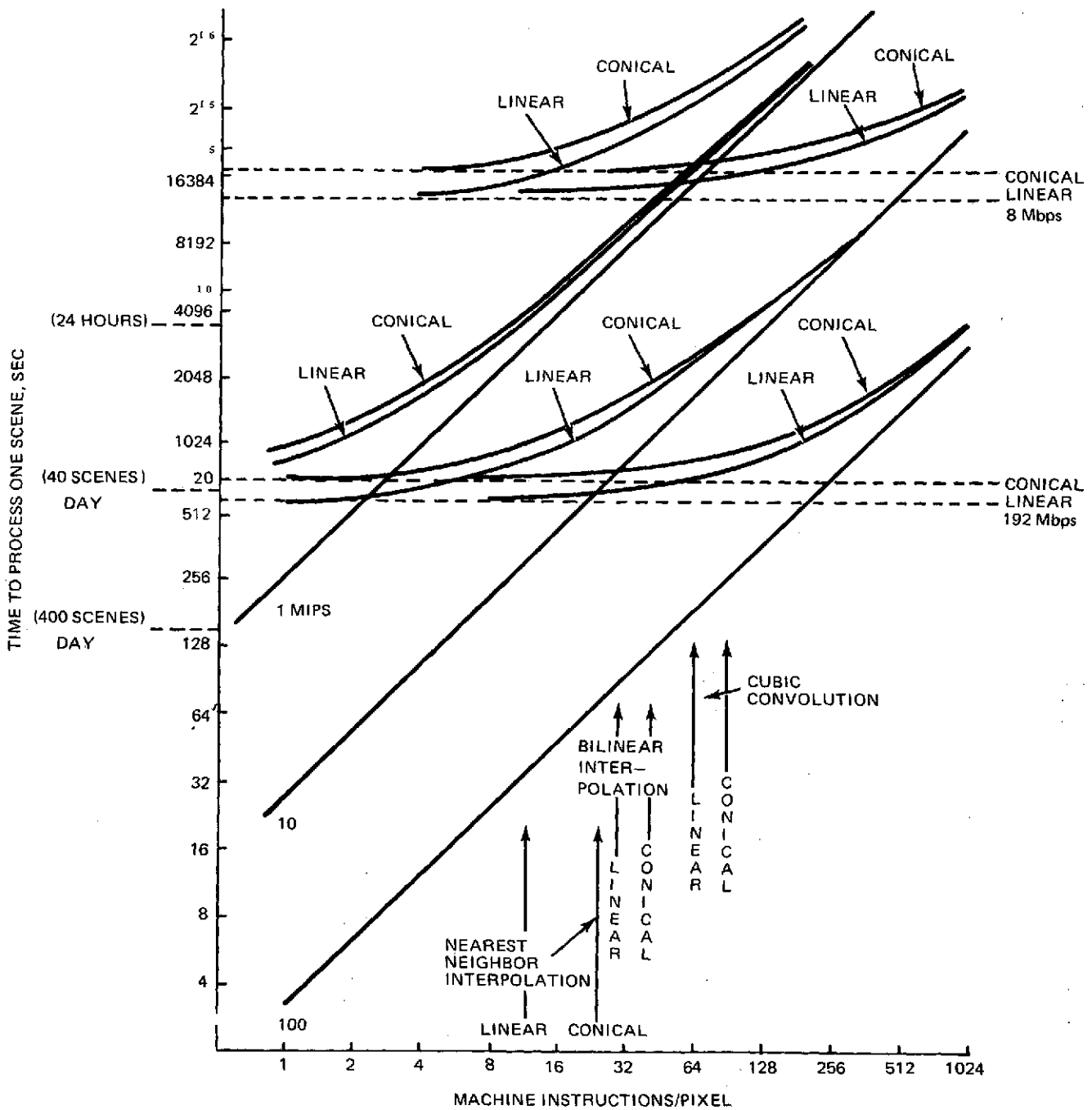

A7-8

Fig. A3-7 The Required to Process One Scene vs Number of Instructions Performed for Each Pixel

For Case I (8 Mbps), almost 4 hours is consumed in data transfer for each scene. The slow processor (1 Mips) becomes processing limited at approximately 64 instructions/pixel and the 10 Mips processor at about 500 instructions/pixel. Clearly, this type of data transfer results in a marginal throughput rate even at the lowest input load (20 scenes/day) and would be considered only for the lower cost processing configurations.

For the case where complete scans can be read simultaneously from the disk, the 1 Mips processor is always limited by the processing time, and the 10 Mips, processor becomes limited at only 20 instructions/pixel. Only for this case can the 100-Mips (hypothetical) processor be effectively utilized. Note that none of the configurations will handle 400 scenes/day.

A general conclusion from Figure A3-7 is that the conical scan has only modest impact on throughput (10 to 20% reduction) in the region where the processing is limited by the data transfer. When processor speed is the limitation, the conical scan has an impact only in the extra instructions/pixel required for coordinate computation. From Paragraph A3.2 these increases amount to 32, 13, and 6%, for nearest neighbor, bilinear, and cubic interpolation, respectively.

A3.4 COMPARISON OF SCAN TECHNIQUES

We can now summarize the impact of the conical scanner, as compared to the linear scanner, in the three major areas:

- Extra instructions required for coordinate computation : at 3.3×10^8 pixels/scene and $\$10^{-8}$/operation, we have the following dollar cost per scene:

	Linear	Conical	Increase	Increase
Nearest Neighbor	$ 33.00	$ 44.00	32%	$11.00
Bilinear	$ 83.00	$ 94.00	13%	$11.00
Cubic Convolution	$186.00	$197.00	6%	$11.00

- Additional storage required -

  From Table A3-1, we estimate the additional storage costs to process the conical scan data as $70,000 ($35,000 per bank and two are required). For a 5-year system that processes 20 scenes/day, this extra cost amounts to $1.92 per scene. For the baseline system (90 scenes/day) this reduces to $0.42 per scene, and for expanded capability system (400 scenes/day) to $0.10 per scene. These prorated costs are negligible compared to the above, even for the low cost system.

- Reduction in throughput due to input transfer time -

  By referring to Figure A 3-7 we can estimate the reduction in throughput (if any) due to data transfer.

Several cases can be identified in Figure A 3-7 and these are summarized in the table below. A 192 Mbps data transfer is assumed. The table contains two entries: (1) approximate number of scenes/day and, (2) the throughput reduction due to data transfer caused by the conical scan. Note that the extra instructions are not included in these estimates since these are accounted for above.

Interpolation Algorithm	PROCESSOR SPEED 1 Mips	10 Mips	100 Mips
• Nearest Neighbor			
— Scenes/day	20	100	145
— Reduction in throughput	4% ($1.25)	17% ($15.30)	25% ($149.00)
• Bilinear Interpolation			
— Scenes/day	10	60	130
— Reduction in throughput	2% ($2.20)	11% ($15.30)	23% ($148.00)
• Cubic Convolution			
— Scenes/day	5	35	95
— Reduction in throughput	1 ($1.90)	7% ($15.80)	20% ($148.00)

The third entry in the table assigns a dollar cost to throughput reduction by simply converting the seconds of extra processing cost for each scene to dollars using $\$10^{-8}$ per operation. An obvious conclusion from these costs is that the penalty in requiring the extremely fast processor to wait for input data is sever. Using the 10 Mip processor as more representative, cost penalties are comparable to those listed above.

In conclusion, the coordinate computation is the main contributor to cost increases in processing the conical scan data. The percent increase in cost of processing a single scene ranges from 32% (N. N.) to 6% (cubic convolution). The prorated cost of extra storage is significant (equivalent to the cost of extra operations) for the minimum 20 scene/day system but is reduced to a negligible amount when the system processes 400 scenes/day. Throughput reduction due to data transfer is only a moderate factor as long as data - transfer and processing loads are reasonably balanced. Very high data-transfer rates are required, however, to achieve this balance with processors with 10 Mips capability and above.

A4 TECHNIQUES FOR RECOGNIZING GROUND CONTROL POINTS

A4.1 INTRODUCTION

This Appendix presents the results of a comparison of candidate techniques for recognition of ground control points (GCP) in support of geometric correct activities for EOS imagery. The classes of techniques investigated were:

- Manual techniques
- Optical correlation
- Digital template matching
- Digital cluster based techniques.

Another item studied was the use of artificial landmarks to enhance any of the above techniques.

An optical correlation system has been developed for ERTS, with manual backup. In practice, the use of the optical system was relegated a coarse location of landmarks with the job of fine alignment left to the operator. Eventually the optical system was displaced by the human. For this study, no further development of optical correlation techniques was considered to be a feasible alternative for the EOS.

Although digital template matching techniques correspond closely with the optical technique, there is the possibility that the improved S/N ratio achievable with the digital data could result in improved performance. Therefore, three standard techniques - direct correlation, Fast Fourier Transforms (FFT) and Sequential Similarity Detection Algorithms (SSDA) were evaluated in the context of EOS. The potential for using clustering techniques which are widely used in multispectral classification problems but which have received little attention for GCP recognition was studied.

NOTE

Cited references are listed in paragraph A4.8.

The conclusions of the study can be summarized as follows:

- A manual system should be considered primary - at least initially - with a systematic plan for phasing into an automatic mode if highly reliable recognition of GCP's is found to be possible, i.e., the system design should recognize the possibility that automatic schemes may not work.
- Although supported by considerable attention in the literature, template matching techniques are high technology risk items for an operational system due to uncertainties in relative locations, seasonal variations and control point/background contrast.
- The highest cost factor is associated with the Fast Fourier Transform due to its inherent storage requirements.
- The Sequential Similarity Detection Algorithms and cluster based techniques merit further experimentation with real data. Some such approach should be employed in the operational system as a parallel to the manual system for a source of refinement data.
- The use of low cost passive artificial landmarks is worthy of attention in the overall system design .

A4.2 PERSPECTIVE OF PROBLEM

A schematic diagram of interrelated data processing functions for GCP's is shown in Figure A4-1. The ability to "locate" the input imagery based entirely upon ephemeris and pointing data is the basic determining factor in sizing the ground control point recognition system. If a typical ground control point is described by an mxm mask, and the location of a given point is known from ephemeris and pointing data within $\pm$ n pixels (assumed for the present equal in-track and cross-track), the portion of the input imagery which must be searched is a region of

$(m + 2n + 1)^2$ pixels. Some GCP recognition schemes require relative little storage in addition to that required to store the data for this size region, however, as is the case for the FFT the recognition scheme can require storage for multiples of this number, in addition to the data itself.

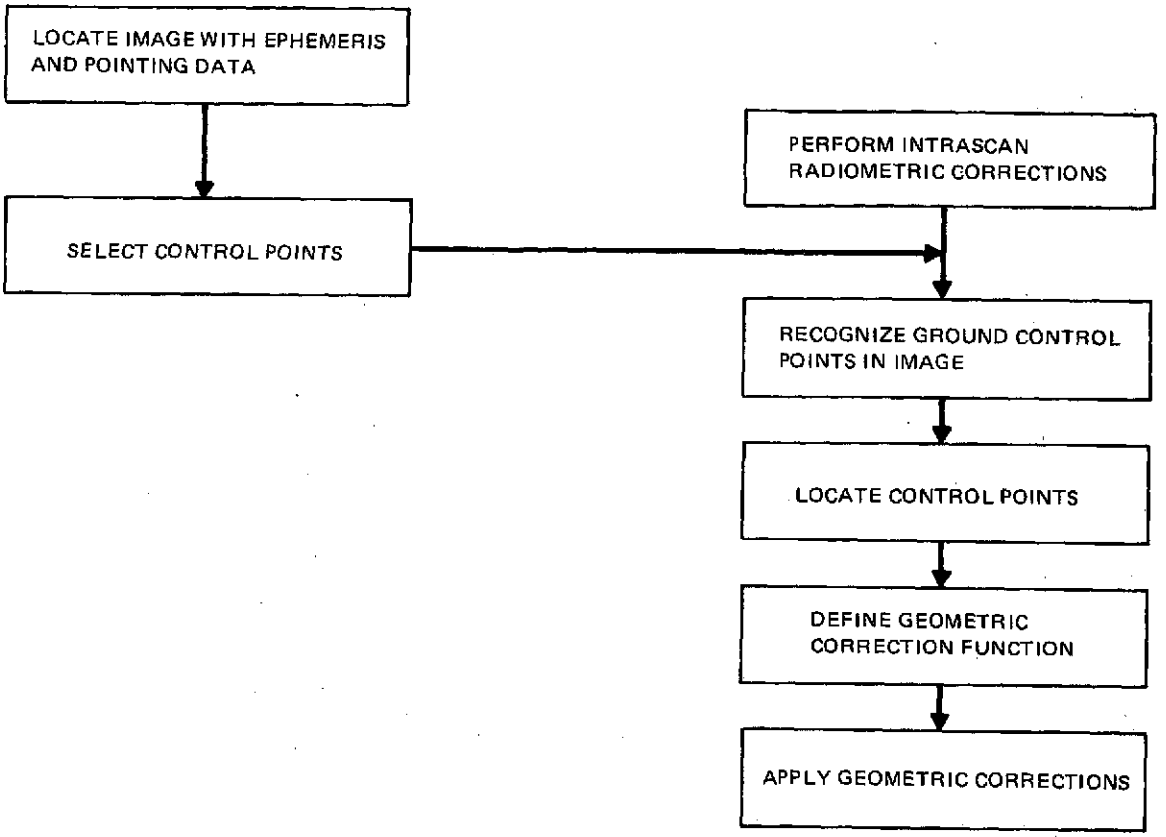

A 7-9

Fig. A4-1 Interrelated Data Processing Functions

Ephemeris error affects scale, and altitude (in terms of pitch, roll and yaw) affects inherent alignment between a template and the image data. Different recognition schemes are sensitive in varying degrees to these alignment and scaling errors.

The types of ground control points to be recognized have an obvious impact upon the size of the template (or for non-template based schemes the complexity of descriptors) required. Possibly not quite as obvious is the relationship between the types of ground control points and radiometric band selection.

Radiometric errors (noise and bias) have varying effects on the different classification schemes. The interplay between geometric and radiometric fidelity has led to some attempts to enhance the ground control point recognition process by effecting edge enhancement (or sharpening) prior to the recognition process[1] with an impact upon computational load.

The two obvious tasks of identifying ground control points in the imagery and assigning a geometric location to the point have not been treated in the literature.

Normally, "success" is reported in terms of recognition of a given portion of a prescribed set of ground control points[2, 3] without specifying the precision with which the registration was effected, or the frequency of detecting false control points.

Any errors in the recognition process will be manifested in the geometric correction function computed by the system. The failure to detect a control point can result in the following:

- The accuracy of the correct function may be reduced due to reduction in the order of the correction polynomial
- In hopes of preserving the order of the correction polynomial, the system may search for additional control point(s).

The other class of error of false recognition of a control point results in a spurious geometric correction function. Reported succes with cloud tracking[4] must be examined in the context of acceptable error in that application.

A4.3 MANUAL TECHNIQUES

The technique for recognizing and locating ground control points which was operationally employed at the ERTS/GDHS was basically a manual system. The system has been closed out except for periodic use for system calibration since the ERTS MSS bulk imagery meets the precision imagery accuracy requirements. The system was described by Tom Mackin,[5] the CSC Manager of Quality Control

at GSFC. The system which will be described here is that developed for the Canadian Remote Sensing Centre for handling ERTS data.[6] This is apparently very similar to that ultimately used by GSFC. The automatic system which was initially developed for GSFC for ERTS will be described in a subsequent section.

A schematic diagram of the Canadian system is shown in Figure A4-2. Using ephemeris and calibration data, the computer calculates corrections to be applied during the recording process. The output of the image recorder is processed, enlarged and presented to an operator on one of two stages of a digitizer. A topographic map is placed upon the other stage. The digitizer records the map coordinates at reference points. The geographic coordinates of the center and corners of the image are "known" from ephermeris and attitude information.

The operator has a list of control points which should be visible in the imagery and which are indicated on the map. Selecting a control point on the map, he digitizes the associated coordinates. He then recognizes the control point in the enlarged imagery and digitizes the associated plate coordinates. The computer can then calculate the difference between the true coordinates of the control point and the coordinates implied by the imagery and navigation base. This difference, with others selected from the image, serves as the basis for the correction polynomial.

A4.4 OPTICAL CORRELATION

The principles of optical correlation can be seen in an example of the superposition of two identical photographic transparencies. As a beam of light is projected through the sandwiched transparencies, the amount of light passing through a differential aperture is determined by the product of the transmissities of the two transparencies at each superposed point. The total energy transmitted is proportional to the integral of the products of the transmissities over the total aperture. The maximum amount of light will be transmitted when the transparencies are exactly in register. A systematic measurement of the transmitted light over a range of relative displacements maps out the auto-correlation function for the range. Two slightly different transparencies of the same scene so treated yield the cross-correlation function.

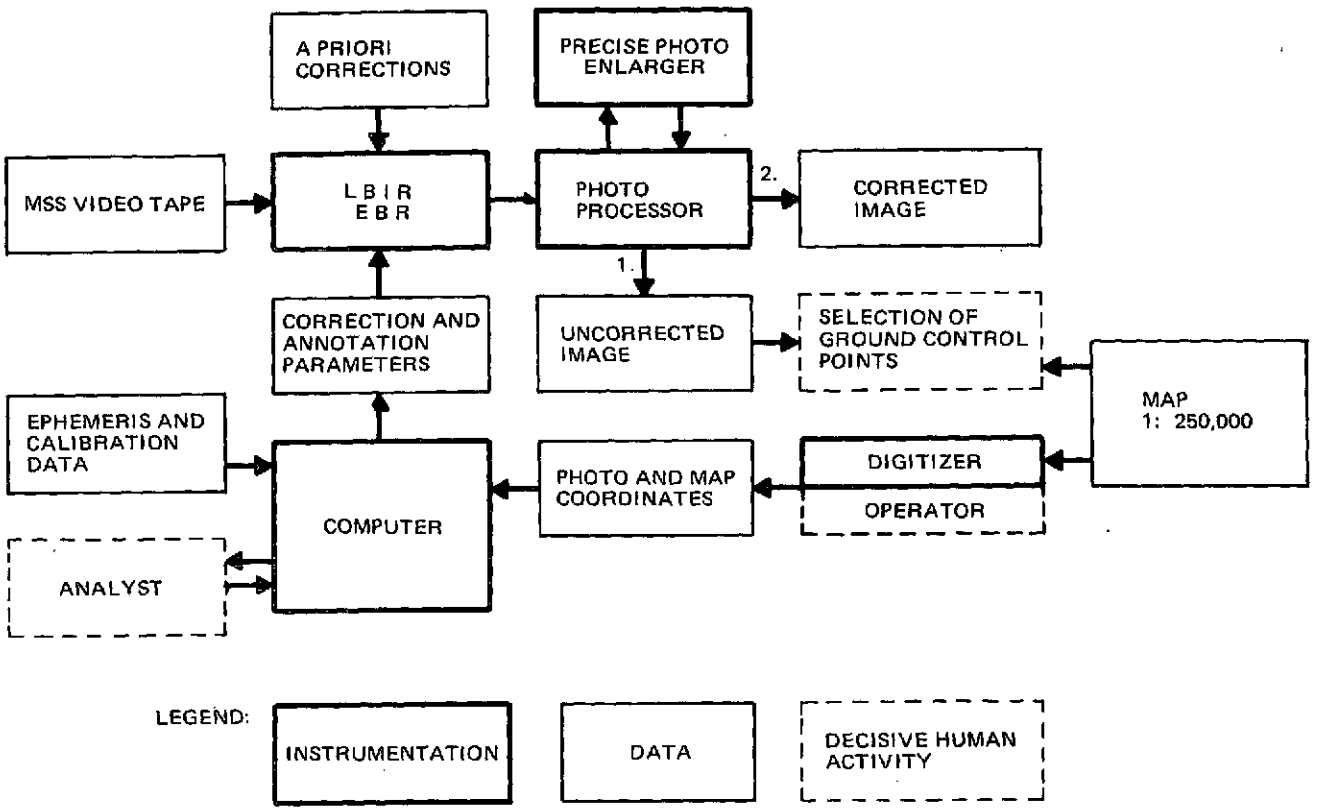

A7-10

Fig. A4-2 Flow Chart of Precision Processing

An optical correlation system was developed for ERTS for the recognition of ground control points.[7, 8] In this system, the operator placed ERTS bulk images on one illuminated stage of a two stage system. A plate with a chip containing a desired control point cut from a transparency was placed on the other stage. Using ephemeris data to determine the approximate location of the control point in the imagery, the system used a scanning device to effect the optical correlation process.

A4.5 TEMPLATE MATCHING TECHNIQUES

A corollary to the optical ground control point recognition scheme previously discussed is to represent the optical mask by a digital pattern (template) to calculate a measure of the correlation between the template and input imagery data.

Three template matching schemes are likely candidates:

- Direct digital correlation
- Two dimensional discrete Fourier transforms
- Sequential Similarity Detection Algorithms (SSDA).

The first two techniques can be considered to be functionally equivalent (i.e., they both obtain a correlation coefficient at every candidate point in the image). The SSDA's accomplish the same result; every candidate point is considered, but if prior to exhaustively calculating a measure of correlation at each point, the trend indicates poor correlation, the process moves to the next candidate point.

The application of transforms other than the Fourier transform has been suggested by numerous authors.[9, 10, 11] In particular, the Walsh/Hadamard and Haar transforms have been suggested because of the relative simplicity compared to the Fourier case. The Walsh/Hadamard transform has been used with success in character recognition, where relative alignment and scale can be controlled. However, Silverman[12] observes that the simpler transforms do not possess the formal correlation property. The variations in practical applications of remote sensing due to ephemeris, pointing and seasonal changes suggest that the use of template matching techniques is tenuous at best; therefore, the use of transforms which degrade correlation is not usually advised.

The basic problem solved by all of the techniques is shown schematically in Figure A4-3.

The template T of dimension n x n (square assumption is not necessary) is to be comared with scene S. From limits associated with ephemeris and pointing accuracy, it is determined that the upper left (1, 1) point of the template can be associated with any point in the m x m subregion S' with upper left-hand corner coordinates (α, β). As T moves parallel with the borders of S' the region bounded by (α, β), (α, β + m + n - 2), (α + m + n - 2, β + m + n - 2) and (α + m + n -2, β) is

covered. The complexity associated with relative rotations between the template and the scene is easily seen. It presently appears to be the case that any relative rotation (or even shifts) would require the introduction of a resampling algorithm for each discrete possible rotation.

The direct correlation technique is implemented by moving the template to a given point in S' and computing the correlation coefficient in the following manner. Rewriting the two-dimensional array T (i, j) $1 \leq i, j \leq n$ as a one dimension array results in T (k) where $k = n(i - 1) + j$. Similarily S'' $(\eta, \xi), (\alpha \leq \eta \leq \alpha + m + n - 2,$ $\beta \leq \xi \leq \beta + m + n - 2)$ can be rewritten as S'' (k) with $k = n(\eta - \alpha) + (\xi - \beta + 1)$.

The (square of the) correlation coefficient associated with the (η, ξ) point in S'' can be written as

$$\varphi^2(\eta; \xi) = \frac{\left(\sum_{k=1}^{n^2} T(k)\, S''(k)\right)^2}{\sum_{k=1}^{n^2} (T_k - \mu_T)^2 \sum_{k=1}^{n^2} (S''_k - \mu_{S''})^2}$$

where μ_T is the mean data value of T and $\mu_{S''}$ is the mean data value over S''.

In the case of direct correlation φ must be calculated at each of the n^2 points of S'.

The numerator of φ^2 can be calculated with the aid of the discrete Fourier transform. The computations associated withthe Fourier transform technique are complex (both in degree and type). However, once Fourier transforms calculated on the basis of the template augmented with 0's to the dimension of S'' and S'' itself are available the correlation coefficients associated with the template referenced to every point within S' can be calculated directly with a sequence of matrix multiplications.

The Sequential Similarity Detection Algorithm in a simple form moves the template to each reference location, but instead of computing the correlation coefficient, the algorithm accumulates the sum of the absolute value of the differences

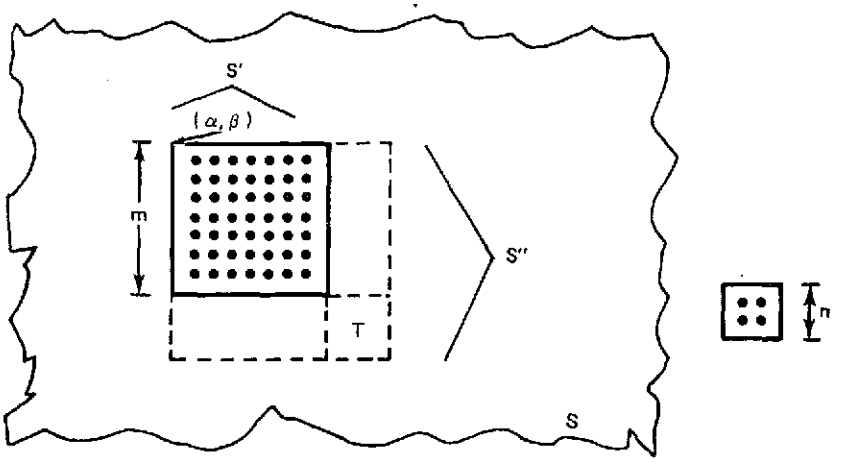

A7-43 **Fig. A4-3 Basic Template Matching Problem**

between corresponding points (either directly or normalized by the means of the sample points within the template and the scene).

As each set of corresponding points is differenced and accumulated into a running sum, the accumulated value is checked against a constant threshold. If the threshold is exceeded, the number of points accumulated prior to exceeding the threshold and the reference point are stored. The underlying assumption is that the point of which the largest number of differences are formed prior to the accumulated sum exceeding the threshold is the point of true registration.

The SSDA approach has been used with good results,[13] but much room for further research exists. The reported uses of SSDA have made use of random search techniques within the mask, and systematic search schemes have been suggested.[14] The threshold used (adaptive or constant) is a current research topic. Reference 14 summarizes the open questions relevant to SSDA's (many of which are common to the other template matching techniques). The topics are:

- Seasonal Effects - how long a GCP can be used with reliability
- Feature Characteristic - what type and spatial characteristics of a feature make it "best" and what are the optimum sizes of the search and window areas

- Spectral Band - what band is best for what class of GCP and least sensitive to uncontrolled variables
- Parametric Selection - what are the best values for the threshold sequence, etc.
- Attitude/Altitude Effects - what is the sensitivity of the SSDA algorithm to effects which change the relative geometry of the search and window areas.

A comparison of direct, Fourier transform correlation (implemented with a Fast Fourier Transform (FFT) algorithm) and an SSDA using an adaptive threshold is presented in Table A4-1. This table is based upon Reference 3. The FFT as the search area S' approaches 8 mi sq (assuming EOS resolution of 90 ft) is an order of magnitude improvement over direct correlation in computational speed but the storage requirement is increasing by the square of the increase in search area size. The SSDA is always at least an order of magnitude faster than the FFT with the basic storage requirements identical to direct correlation.

Table A4-1 Techniques vs Processing Time and Storage Requirements

AGGREGRATE SEARCH AREA (S'), mi^2	SIZE OF TEMPLATE (m), mi^2	DIRECT CORRELATION		FFT		SSDA (b)	
		EQUIVALENT ADDS	WORKING STORAGE[1]	EQUIVALENT ADDS	WORKING STORAGE (a)	EQUIVALENT ADDS	WORKING STORAGE
2	0.5	3.1×10^7	NEGLIGIBLE	2.2×10^7	1.6×10^4	4.1×10^5	NEGLIGIBLE
4	0.5	1.6×10^{-8}	↓	1.0×10^8	6.4×10^4	5.0×10^6	↓
8	0.5	7.5×10^8		4.4×10^8	2.6×10^5	3.2×10^7	
2	1.0	5.6×10^7		1.9×10^7	1.6×10^4	2.2×10^5	
4	1.0	4.9×10^8		1.0×10^8	6.4×10^4	6.5×10^6	
8	1.0	2.6×10^{-9}	↓	$4.x \times 10^8$	2.6×10^5	2.0×10^7	↓

(a) STORAGE FOR TEMPORARY ARRAYS IN ADDITION TO DATA
(b) ADAPTIVE THRESHOLD

A7T-9

The following list of arguments is presented as the case for limiting consideration of template matching techniques to the SSDA's.

- First, in the range that the application of the FFT exhibits the strongest argument in terms of computational speed as a choice over direct correlation (large search area) the core requirement rapidly becomes intractable

- The SSDA is (theoretically and practically) as good as exhaustive direct correlation[3, 13] which is functionally identical to the FFT
- The SSDA's (and direct correlation) are functionally simple
- Integer arithmetic can be used with the SSDA
- As the SSDA research continues, and if a judicious structuring[3] of the algorithm is made at the outset, changes can be easily incorporated.

This one template matching technique is not a base endorsement of this class of ground control point location techniques. The problems introduced by rotation may or may not be severe. Although this problem is mentioned in some of the literature, it is usually given short shrift with statements to the effect that "it can be considered, but this paper will ignore the problem." However, if the need for resampling suggested earlier is borne out, the rotation problem is probably the driver in consideration of the techniques.

Part of the reason for recommending the SSDA was precisly related to this tone of caution. The use of the FFT would require considerable investment in terms of analysis for efficient implementation and hardware. The SSDA is a low-risk (in a cost sense) technology item since, if template matching techniques prove to be not feasible, relatively little expenditure of software development or hardware has been made.

The point made earlier concerning the distinction between recognizing and locating GCP's is worthy of further emphasis. Considering only the single effect of seasonal variability, it would appear to be highly probable that a template matching technique would be subject to at least a one pixel error in registering the reference point. The likely requirement is for one pixel adjustment accuracy. The effect of a one pixel error in registration for a GCP is manifested throughout the image by the correction polynomial. This could be a case of flagging a problem which in reality does not exist. However, there is no definitive evidence that absolute registration with real data can be accomplished with high reliability.

A4.6 CLUSTER BASED SYSTEMS

The template matching techniques discussed require the availability of the radiant energy measured for each pixel. Another approach to the problem of recognizing ground control points is to categorize all elements within the boundary of and identifiable feature as being identical and to base GCP recognition on spatial characteristics of the feature. A number of techniques are presently used in multi-spectral, unsupervised classification and can be termed clustering techniques. An example of clustering techniques[15] is the following:

The process used two parameters, C and R, which determine when to merge existing clusters into the same class and when to begin new clusters. The first data point determines a cluster with a mean equal to the sample value and weight of one. Each subsequent sample point is assigned to the nearest mean (which is within R), the new mean is computed and the weight of the cluster is incremented by one. The new mean is then compared with other means and if it is within C of any other mean the two clusters are merged into one, and the mean and weights are updated. A second pass is made through the data and each sample point is assigned to a cluster. During this second pass the outlines of region of connected pixels belonging to the same cluster can be developed.

Techniques have been developed to extract borders directly without processing interior points, thus in effect creating clusters. The techniques are based upon the recognition that significant shapes within an image are often noted by drastic transition in brightness from pixel to pixel. The most common approach to detecting an edge element is to apply a differential operator such as the Laplacian or squared gradient to the data. If an edge element is detected then a border tracing technique such as that developed by Mason and Clemens can be used.[16] This technique effectively "walks" around the border turning left after a cluster point is found and right when background is encountered. The edge extraction techniques have received considerable attention in the pattern recognition literature related to recognition of

printed characters against a white background. However, these techniques would appear to be plagued by low contrast situations often associated with natural landmarks.

Beaudet[17] proposed an algorithm for coding a scene which is amenable to either clustering techniques or edge extractors. This approach in effect is a method for doing template matching where the template is described as a sequence of binary numbers. The technique is subject to the problems of orientation encountered with other template matching schemes. However, Beaudet's conjector that outlines are less sensitive to seasonal and agricultural changes then the interior of a region is probably correct. Any number of recognition schemes can be based upon a knowledge of the clusters within a search region. The area, length of perimeter, ratio of area to perimeter length, existence of sharp breaks on the perimeter have all been suggested as basically reliable identifiers. Class comparisons between a template and scene clusters based upon the respective data statistics have merit for further considerations. The primary advantage of descriptive identifiers is that problems associated with orientation and seasonal changes can be nonexistent. However it must be emphasized that the use of clustering techniques for recognition of ground control points must be considered only as a conjecture.

A4.7 ARTIFICIAL LANDMARKS

Many of the problems (seasonal variation, relative rotations, etc) encountered in attempting to recognize natural landmarks and engineering features can be avoided through the use of artificial landmarks. Lasers and other active systems have been suggested for this purpose. However, a low-cost reliable passive artificial landmark has recently been demonstrated by Evans.[18]

In his experiment, Evans used a 22 in. diameter vanity mirror positioned to reflect the sun toward a satellite during a pass. With very crude equipment (the mirror was mounted on an oil drum filled with water in a frame allowing azimuth and elevation adjustments) the image from the sun saturated a single resolution

element in all four bands of ERTS MSS during four of six attempts. The failures were due to the small mirror and very crude approximations of the relative position of the satellite during the passes. Increasing the mirror to 2 x 6 ft. would virtually assure acquisition even with Evans' approximations of satellite positions.

A4.8 REFERENCES

A4.8.1 Specific Citations

1. Anuta, P. E., "Spatial Recognition of Multispectral and Multitemporal Digital Imagery Using Fast Fourier Transform Techniques", IEEE Transactions on Geoscience Electronics. V GE-8. October 1970.

2. Bernstein, R., "Results of Precision Processing (Scene Correlation) of ERTS-1 Images Using Digital Processing Techniques", Volume 1, Proceedings of Symposium on Significant Results Obtained from the Earth Resources Technology Satellite - 1, New Carrollton, Maryland, March 5-9, 1973.

3. Barnea, D., Silverman, H., "A Class of Algorithms for Fast Digital Image Registration", IEEE Transactions on Computers, V C-21, No. 2, February 1972.

4. Smith, E., Phillips, D., "Automated Cloud Tracking Using Precisely Aligned Digital ATS Pictures", IEEE Transactions on Computers, V C-21, No. 7, July 1972.

5. Telephone Conversation with Tom Mackin, 20 August 1974.

6. Kratky, V., "Precision Processing of ERTS Imagery", Proceedings of the 1971 ASP-ACSM Fall Convention, San Francisco, California, September 7-11, 1971.

7. Webber, D., "Optical Processing in a Data Handling Facility", TRW IOC 7538-7-001, 2 May 1972.

REFERENCES (Cont)

8. Forrest, R., "Geometric Processing of ERTS Images", Bendix Research Laboratories, Report 70-342, Southfield, Michigan.

9. Carl, J., Hall, C., "The Application of Film and Transforms to the General Classification Problem," IEEE Transactions on Computer, July, 1972.

10. Andrews, H., Computer Techniques in Image Processing, Academic Press, New York, 1970.

11. Huang, T., Schreiber, W., Tretiak, O., Lecture Notes in Image Processing, Massachusetts Institute of Technology, 1971.

12. Silverman, H., "On the Uses of Transforms for Satellite Image Processing", Proceedings of the Seventh International Symposium on Remote Sensing of the Environment, The University of Michigan, Ann Arbor, May 17-21, 1971.

13. Markarian, H., Bernstein, R., Ferneyhough, D., Gregg, L., Sharp, F., "Implementation of Digital Techniques for Correcting High Resolution Images", Proceedings of the 1971 ASP-ACSM Fall Convention, San Francisco, California, September 7-11, 1971. Also see Reference 1.

14. Nagel, R. Rosenfeld, "Ordered Search Techniques in Template Matching", Proceedings of the IEEE, February 1972.

15. Detchmendy, D., et al, "Algorithm Simulation Test and Evaluation Program", TRW 20029-H170-R0-00, April 16, 1973.

16. Mason, S., Clemons, J., "Character Recognition in an Experimental Reading Machine for the Blind", Recognizing Patterns, MIT Press, 1968.

17. Beaudet, P., "Rapid Alignment Algorithm for Successive ERTS Images, CSC Briefing, Silver Spring, Maryland.

18. Evans, W., "Marking ERTS Images with a Small Mirror Reflector", Photogrammetric Engineering, June 1974.

A4. 8. 2 General References

Andrews, H., Tescher, A., Kruger, R., "Image Processing by Digital Computer", IEEE Spectrum, July, 1972.

General Electric Company, Definition of the Total Earth Resources System for the Shuttle Era, An Assessment of the State of the Art, September 26, 1973.

Goodman, J., Introduction to Fourier Optics, McGraw-Hill, New York, 1968.

Andrews, H., Mathematical Techniques in Pattern Recognition, Wiley-Interscience, New York, 1972.

Nagy, G., "Digital Image Processing Activities in Remote Sensing for Earth Resources", Proceedings of the IEEE, V 60, No. 10, October, 1972.

A5 LEVEL I PROCESSING

A5.1 INTRODUCTION

In considering the Level I processing, it was assumed that all three Thematic Mapper (TM) approaches would produce a linear scan, where the peak departure from linearity was a small fraction of a pixel. For the Hughes' TM approach, this precise linearity implies a compensator within the instrument to linearize the motion of the oscillating mirror. Our most recent information, however, indicates that even with such compensation, the Hughes' approach will yield a departure from linearity that is as large as 0.5 percent. Such a value results in a 15 pixel lag or lead during the "slow" and "fast" portions of the TM scan, respectively, which must be corrected during the Level I processing (line "stretching"). This appendix describes the one-dimensional interpolator which is used in the line stretcher. Alternatives for interpolation and evaluation of several of the simpler configurations is included. We have assumed for this discussion that an equal-angle (EA) resampling clock is available on the ground having been derived from the scan-error data sent from the spacecraft.

A5.2 BASIC INTERPOLATION PROBLEM

The basic problem is shown in Figure A5-1. In Figure A5-1(a), we sketch the path taken by the scanner during one complete west-to-east sweep. The actual motion of the scanner departs from a linear function of time so that $d\theta/dt$ is not constant. Nevertheless, samples of the detector output voltages are taken at uniformly spaced time increments spaced T seconds apart (typically, T is 6.6 μ seconds). The actual samples of the detector output are depicted in the upper part of Figure A5-1(b). Below this, we show the equal-angle resampling pulses. The objective of the interpolation process is to generate samples at the resampling instants rather than at the positions where the samples were actually taken. In general, this process requires the generation of "new" or interpolated samples which are some function of the original samples.

It should be emphasized at this point that we are interested in interpolating a stream of continuous picture samples "on-the-fly"; that is, the input stream is clocked in at a certain rate to the interpolator and we are supplied with a resampling clock which is close to, but does not coincide exactly with, this input clock. This creates a slightly different situation than one would ordinarily associate with the interpolation process. Note in Figure A5-1(c), the two types of situations that can occur if one utilizes a simple resampling of the original data according to the resampling clock. At the top of Figure A5-1(c), the resampling (EA) clock has a period slightly longer than T. We assume that the true samples are "held" until the next resampling pulse arrives at which time the sample is supplied to the output. If no resampling pulse occurs before the next input sample arrives, then that particular input sample is never supplied to the output. This occurs in the case of sample "d" in the upper figure which is skipped and does not appear in the output. In the lower part of Figure A5-1(c), we see the opposite situation where the resampling clock period is $T - \epsilon$ seconds. Here occasional samples are duplicated in the output as shown again by sample "d" in the example.

A5.3 SOME SIMPLE INTERPOLATION ALGORITHMS

An improvement to the straightforward EA resampling is to provide intermediate samples which the resampling clock can supply to the output. Such an approach, in effect, provides interpolated values at equally spaced intervals between the true samples so that the resampling clock can select one of these values to supply at the output rather than one of the original samples. If the resampling pulse occurs near the end of an intersample interval T, it would be better to supply an interpolated sample to the output rather than the sample that was held from the beginning of the interval. This approach shows Figure A5-2(a), where we now assume that the original picture material was a sinusoidal brightness pattern at some frequency f_p which is $\ll$ the sampling frequency $f_s = 1/T$.

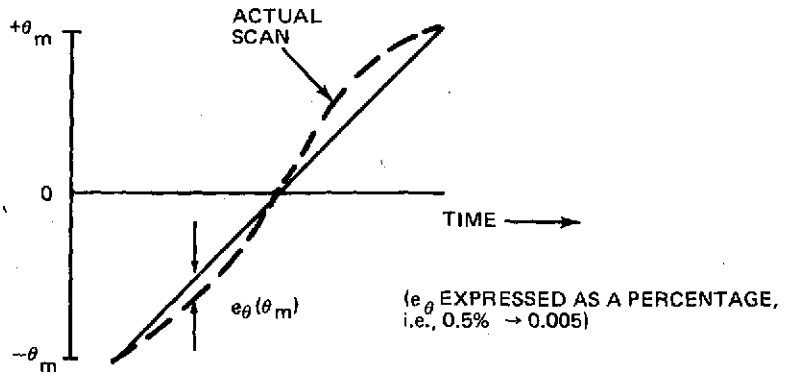

a. SCANNER TRAVEL DURING ONE SWEEP

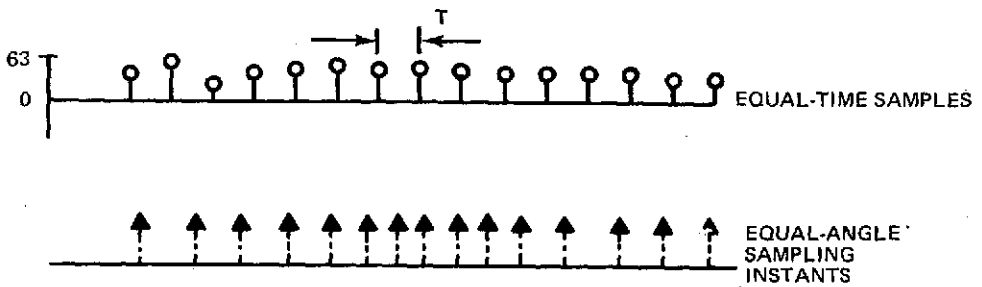

b. RELATIONSHIP BETWEEN ORIGIONAL ET SAMPLES AND THE EA RESAMPLING CLOCK

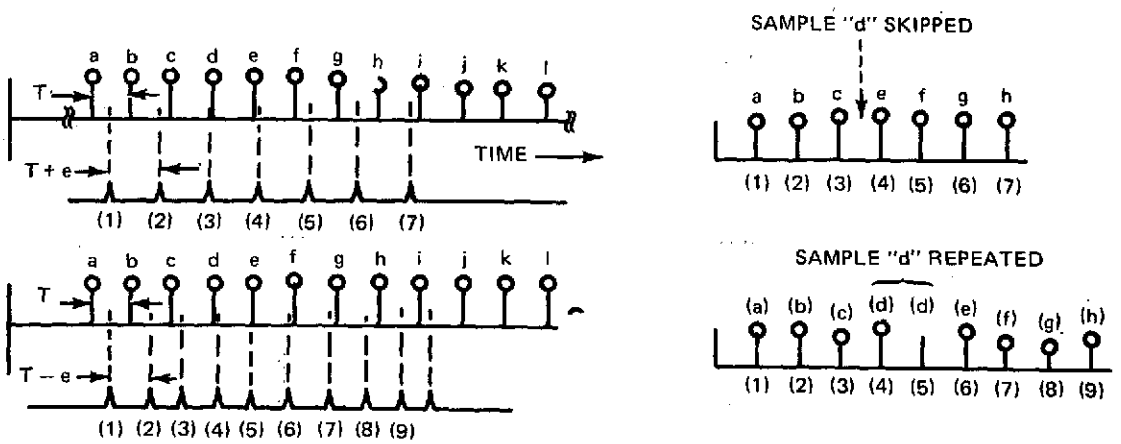

c. DIRECT RESAMPLING WHEN EA CLOCK HAS PERIOD T ± e

Fig. A5-1 Basic Equal-Time (ET) and Equal-Angle (EA) Sampling

The basic interpolating idea (Figure A5-2(a)), is to generate M interpolated values equally spaced between the original ET samples. Each of these values is computed as a function of 2N true samples which range $\pm$ N samples from the intersample interval of interest. For example, a single interpolated sample I_{bc} is shown between true samples b and c; thus M = 1. This sample could be formed from only samples b and c (N = 1), from a, b, c and d (N = 2), or from higher order combinations of the true samples.

The simplest possible interpolator (M = 1, N = 1) is shown in Figure A5-2(b). In this case, a clock at twice the ET sample rate is derived and alternating samples or zeroes are supplied to three delay stages. At a particular instant of time we show samples a and b as residing in the outer stages with a zero in the center stage. At this position, an interpolated sample $i_{ab} = 1/2a + 1/2b$ is computed and sent to a storage register. At each cycle of the 2 ET clock, a flip-flop enables either the true sample or the interpolated sample (alternately) to be supplied to the output when the EA sampling pulse appears. Since the EA clock drifts slowly with respect to the ET clock, the output will be made up of periods when only true samples are supplied, followed by intervals of interpolated samples, and so on.

Figure A5-2(c), shows a slightly more complicated version of A5-2(b) where 4 input samples are used to produce a single interpolated sample using, for the point between b and c

$$i_{bc} = 9/16\ (b + c) - 1/16\ (a + d)$$

Note that this interpolator still operates at a rate of twice the ET clock.

Figure A5-2(d), shows an interpolator in which 3 points are interpolated between each true sample (M=3), (N=1). This device operates at 4 times the ET clock rate so that the sequency a, 0, 0, 0, b, 0, 0, 0, c, ... are entered into the delay stages. Three interpolated samples are produced between a and b spaced at intervals T/4, T/2, 3T/4 in the interval T. These are made available at the output in sequence where only one is selected when the EA sampling clock arrives.

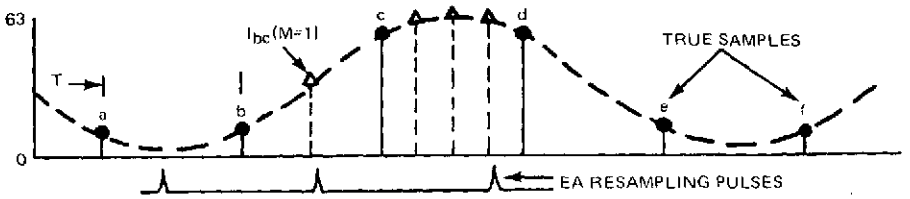

a. OPTIONS FOR INTERPOLATION BETWEEN POINTS a, b, c, d, e, f

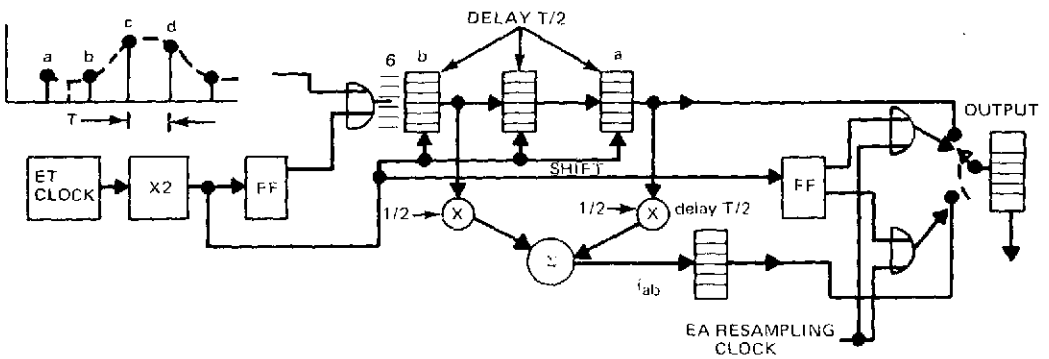

b. TWO-POINT INTERPOLATOR WITH M = 1, N = 1

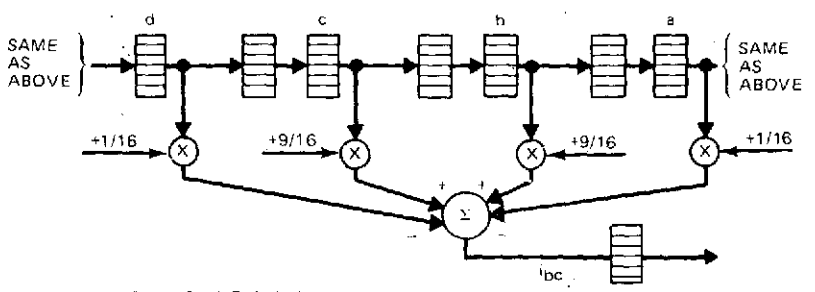

c. FOUR-POINT INTERPOLATOR WITH M = 1, N 2

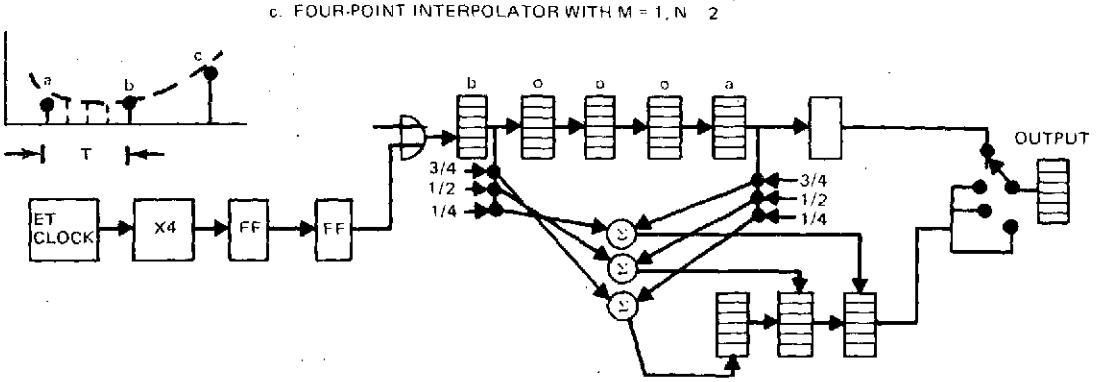

A7-12

d. TWO-POINT INTERPOLATOR WITH M = 3

Fig. A5-2 Simple Interpolators

A5.4 EVALUATION OF INTERPOLATION ALGORITHMS

To evaluate the interpolation algorithms as well as direct EA resampling, we will retain the assumption that the input picture material (i.e., the "ground truth") is a sinusoidal pattern of brightness values as shown at the left of Figure A5-3. If we assume an ideal optical system with no bandwidth limitations, we can represent a set of samples of the ground truth as:

$$P(kT) = V_p \sin\left[2\pi k\, f_p/f_s + \phi\right] \tag{1}$$

where

- V_p - is the peak value of the sinusoidal picture information
- f_p - is the "frequency" of the picture material
- f_s - is the sampling frequency (1/T)
- ϕ - is an arbitrary initial phasing of the picture material with respect to the start of scan
- k - is a time index that ranges from 0 to $(K_m - 1)$ as K_m samples are taken in the angular interval $-\theta_m$ to $(+\theta_m - \Delta\theta)$

Equation (1) assumes a linear correspondence between time and angle, that is, if the scanning starts at t_o, we can represent discrete time as

$$\text{Time} = t_o + kT;\ k = 0, 1, 2, \ldots (K_m - 1) \tag{2}$$

and for a linear angular scan, discrete angle becomes

$$\theta(kT) = -\theta_m + k\,\frac{(2\theta_m)}{K_m}$$

or defining $\Delta\theta \equiv 2\theta_m/K_m$

$$\theta(kT) = -\theta_m + k\Delta\theta;\ k = 1, 2, \ldots (K_m - 1) \tag{3}$$

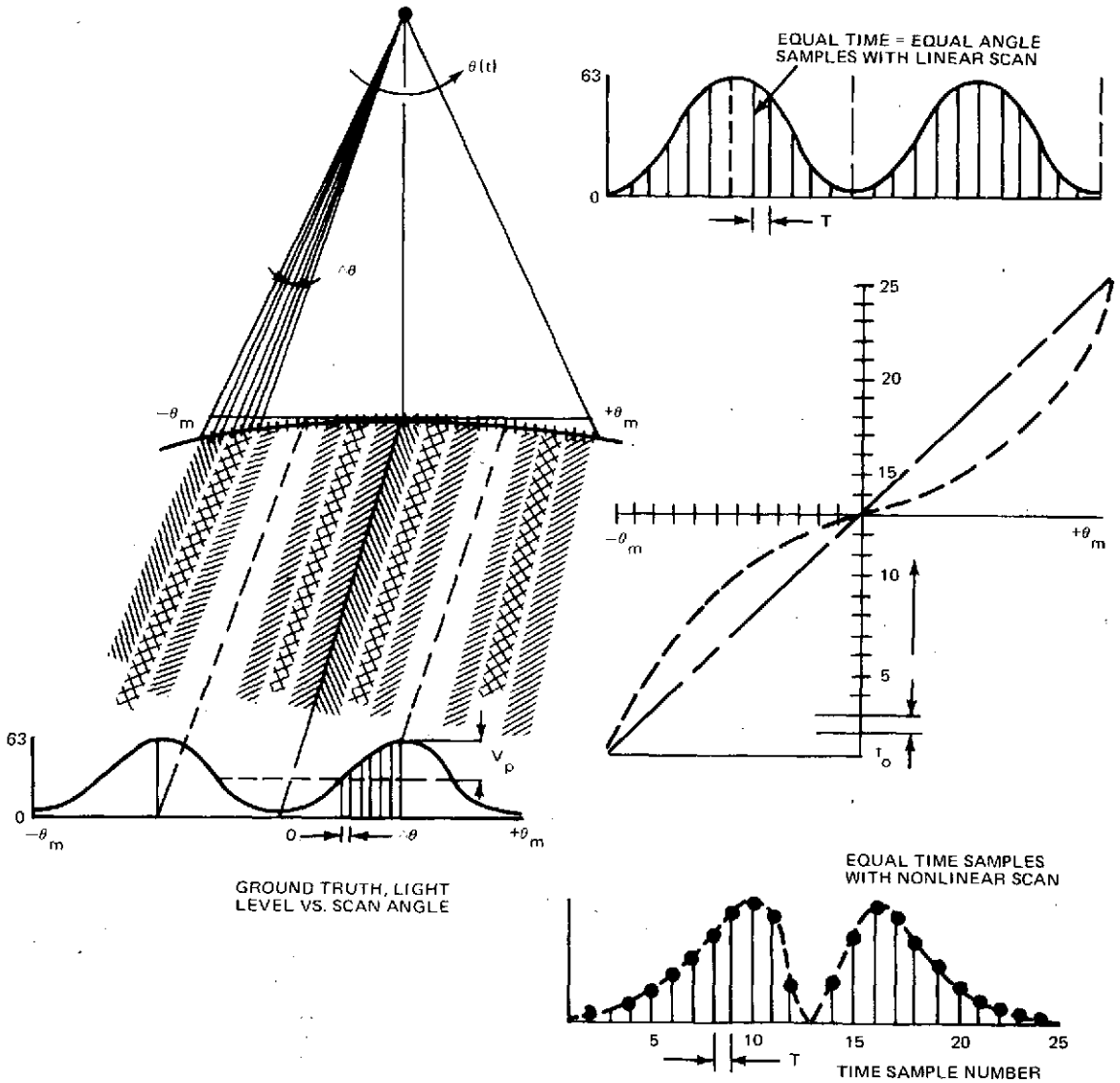

A7-13 **Fig. A5-3 Assumed Sinusoidal Ground Truth and Resulting Samples for Nonlinear Scanning.**

For the linear scan, therefore, we can relate time t_o to angle $-\theta_m$ and, at each step, the angle is incremented by $\Delta\theta$ and time by T so that k serves as a common index for both time and angle. With the nonlinear scanner, angular motion is not a linear function of time and we cannot use the same time index in both (2) and (3). If we represent the nonlinear angle scanning as

$$\theta(\ell T) = -\theta_m + e\Delta\theta - e_\theta \theta_m \sin(2\pi\ell / K_m) \tag{4}$$

where

ℓ - represents the index of the nonlinear angle steps; $\ell = 0, 1, \ldots\ldots (K_m - 1)$

e_θ - represents the magnitude of the peak scan nonlinearity expressed as a fraction of θ_m (i.e., 0.5% nonlinearity gives $e_\theta = 0.005$)

Combining (1) and (4), we can rewrite the samples actually taken by the sensor as

$$P'(\ell T) = V_p \sin\left\{2\pi f_p/f_s\left[\ell - \frac{K_m}{2} e_\theta \sin(2\pi\ell/K_m)\right] + \phi\right\} \tag{5}$$

which is simply a phase modulated version of the original sinusoidal image data.

The objective of the interpolation-resampling procedure is to estimate P(kT) in (1) from $P'(\ell T)$ in (5) making use of a resampling clock derived from (4). If the resampling clock is derived at the ground without error, then the error between the desired output sample (the EA samples) and the available samples (the ET samples) for straightforward resampling can be computed as:

$$e_k = P(kT) - P'(\ell T) \quad k = 0, 1 \ldots (K_{max} - 1) \tag{6}$$

where ℓ is the largest integer such that the argument in (5) is less than the argument in (1). These errors can then be summed over all K_{max} output samples to determine mean and mean-square values.

In Figure A5-4, we plot the ratio of rms error to peak sinusoidal level as a function of the ratio f_p/f_s. These results show that error, expressed in decibels, is approximately a linear function of log f_p/f_s, rising at 6 dB/octave. The error is relatively insensitive to the degree of scan nonlinearity which is primarily due to the fact that the resampling clock is derived at the ground without error. If one considered the errors incurred in deriving this EA clock, it is expected that the radiometric errors would be larger for the larger scan nonlinearity (i.e., the servo bandwidth must be wider to track, without appreciable lag, the larger phase deviation).

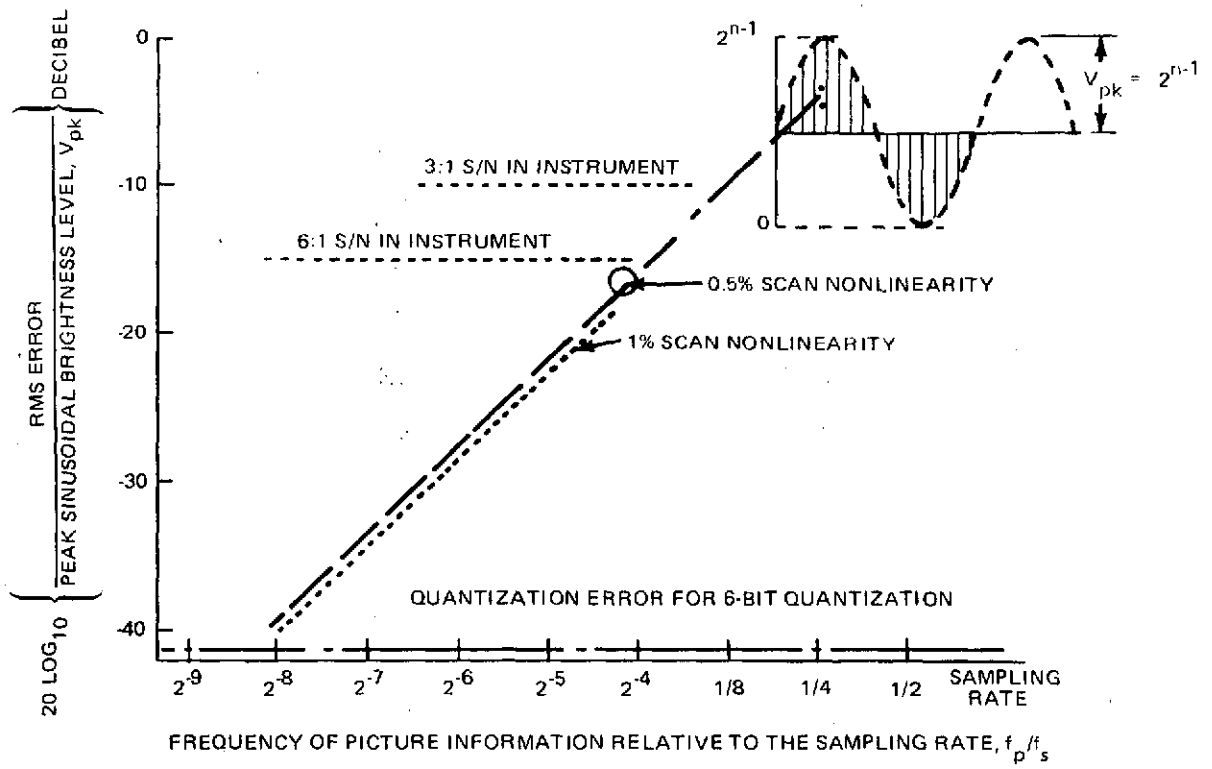

A7-14 **Fig. A5-4 RMS Resampling Error Relative to Peak Sinusoidal Pciture Data for Straightforward Equal-Angle Resampling with No Interpolation**

A conclusion from Figure A5-4 is that straightforward resampling does not preserve the radiometric accuracy of the instrument for the high-frequency picture information ($f_p/f_s > 2^{-4}$ to 2^{-3} depending on the S/N ratio of the instrument).

By using a simple 2-point interpolator, rms error is reduced by 6 dB, as in Figure A5-5, so that the ratio f_p/f_s for which a particular radiometric accuracy is maintained is increased by an octave.

A four-point interpolator has also been evaluated which obtains an interpolated point i_{bc} (see Figure A5-2a) as

$$i_{bc} = 9/16\,(b+c) - 1/16\,(a+d) \qquad (7)$$

The ratio of root-mean-square error to peak picture information for the four-point interpolator is also plotted in Figure A5-5. This configuration gives less than a 0.5 dB improvement over the 2-point interpolator.

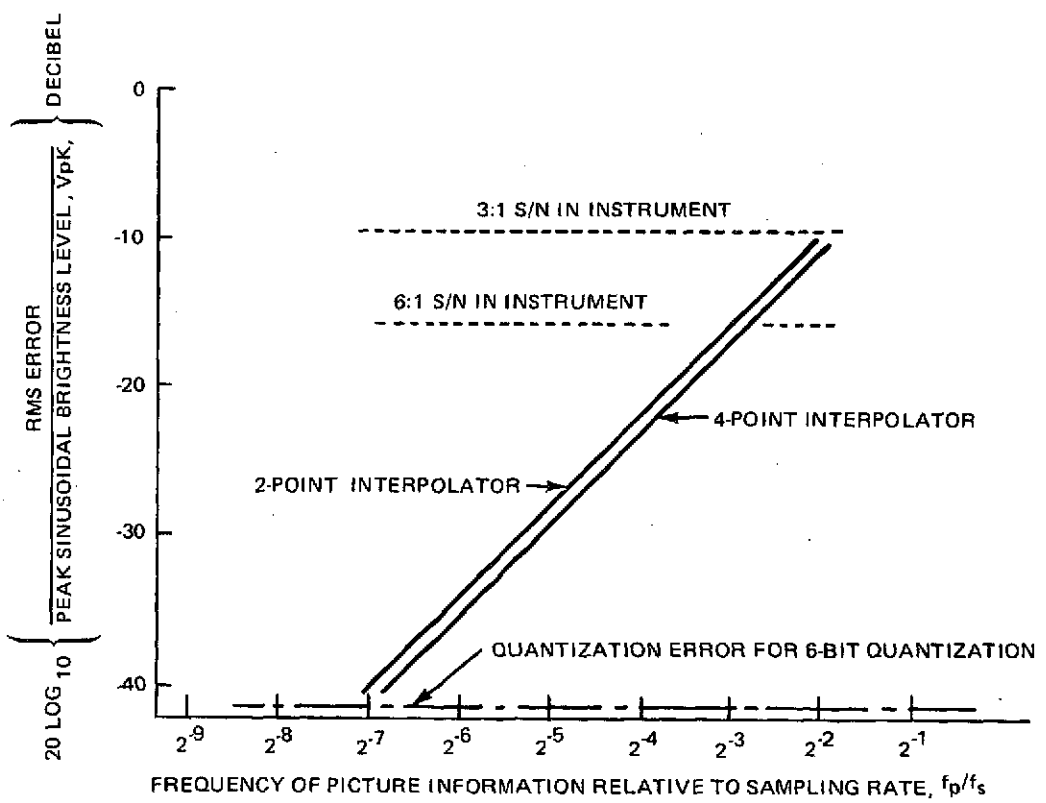

A7-15

Fig. A5-5 RMS Resampling Error Relative to Peak Sinusoidal Picture Data – Two-Point and Four-Point Interpolators

A5.5 CONCLUSIONS

It appears that a simple 2-point interpolator, which operates at twice the basic sampling rate, is desirable to preserve radiometric fidelity when resampling the TM data to correct for scan nonlinearity. The additional improvement by utilizing a more complex 4-point interpolator is very small.

It is suspected that additional improvement would be obtained by computing three points (equally spaced) between each original sample. However, the interpolator must now operate at 4 times the original sample rate.

The question of correlation between successive errors has been neglected in this treatment. Since the error pattern tends to be periodic for periodic picture material, the effect of errors could be more objectionable than the rms error values would indicate.

The derivation of the equal-angle resampling clock has also been neglected here. Simulation of the error signal formation (in S/C), scan-to-scan jitter, and ground PLL acquisition and tracking would be required to investigate this problem thoroughly. Actually, jitter in the EA clock could, if not too large, improve the situation by reducing the periodicity in the error patterns. Of more concern is the ability of the loop to acquire and track the nonlinearity without initial transients or significant lags.

A6 CENTRAL DATA PROCESSING - IMPLEMENTATION CONCEPT

A6.1 INTRODUCTION

The main function of the Central Data Processing Facility (CDPF) is to digitally process the instrument data prior to production of output products (digital & photographic). This processing, described in the report proper, consists of three "levels" - Level I involving radiometric data corrections, Level II including geometric data corrections, Level III utilizing ground control points (GCP's) for best accuracy. Three implementation approaches were considered for this activity - general purpose digital machines, special purpose processors, and an Associative Array Processor (STARAN by Goodyear). These are described in some detail. Since the largest task, by far, in the CDPF is the Level II & III processing, the concepts were primarily focused on these activities. Level I activities are treated separately (Appendix A5) and can be summarized as follows:

- Extract and format scene identification and other annotation data for input to ISS and archive
- Invert the calibration data for use as a radiometric correction table
- Perform the radiometric correction table lookup on the pixel data
- Extract timing data, compute interpolation coefficients, and perform linear interpolation for line rectification
- Perform overall control of the Level I process.

Figure A6-1 shows an overall block diagram of the CDPF. Data received from the primary ground station or via the TDRSS is provided to the CDPF in the form of an acquisition high density data tape. This tape is read by a playback unit and the data fed through a decommutator and interface unit at the input of the CDPF. The data then goes directly into the Level I processing system. The output of the Level I process is stored in the archive and is retrived when required for processing by the Level II & III

processing system. The Level II & III output is also stored in the archive and is retrieved when required for generation of digital or photographic user products. The overall CDPF operates under the control of the ISS.

A6.2 LEVEL II & III PROCESSING

Level II processing basically involves three steps: (1) transformation of the desired output grid format, which is usually a UTM map projection, into the scanner coordinate system; (2) computing the exact coordinates of the desired output pixels with respect to the data taken by the scanner; and (3) interpolating between the line-rectified samples, as necessary, to produce the elements in the output image. This step assumes that Level I processing has been performed, if necessary, to yield an orthogonal array of original samples.

Level III processing differs from Level II only in step (1) above where ground control points are located in the image data first so as to provide a more accurate location of the intersections of the output grid lines. The basic steps in the Level II processing are shown conceptually in Figure A6-2.

The objective in step (1) above is to precisely locate the intersections of the output grid lines (lines of latitude and longitude on a UTM projection) in terms of the line and pixel number of the array of scanner data. This procedure requires several coordinate transformations and makes use of the best available estimates of S/C ephemeris and attitude. Since it would be impossible to locate each output pixel in this manner, the image is subdivided (say into 20-40 North-South and East-West lines) to give a set of approximately 1000 grid line intersections. These grid line intersections define a set of approximately 1000 output blocks which are small enough (possibly 5 km by 5 km square) that lines and columns of output data can be considered as linear over these small regions. With the linear assumption, the computation of the exact coordinates of each output pixel is relatively simple, and can be performed recursively requiring only a few machine operations per point. Furthermore, the coordinate computations serve for all bands, since the detectors in the different spectral bands are precisely registered.

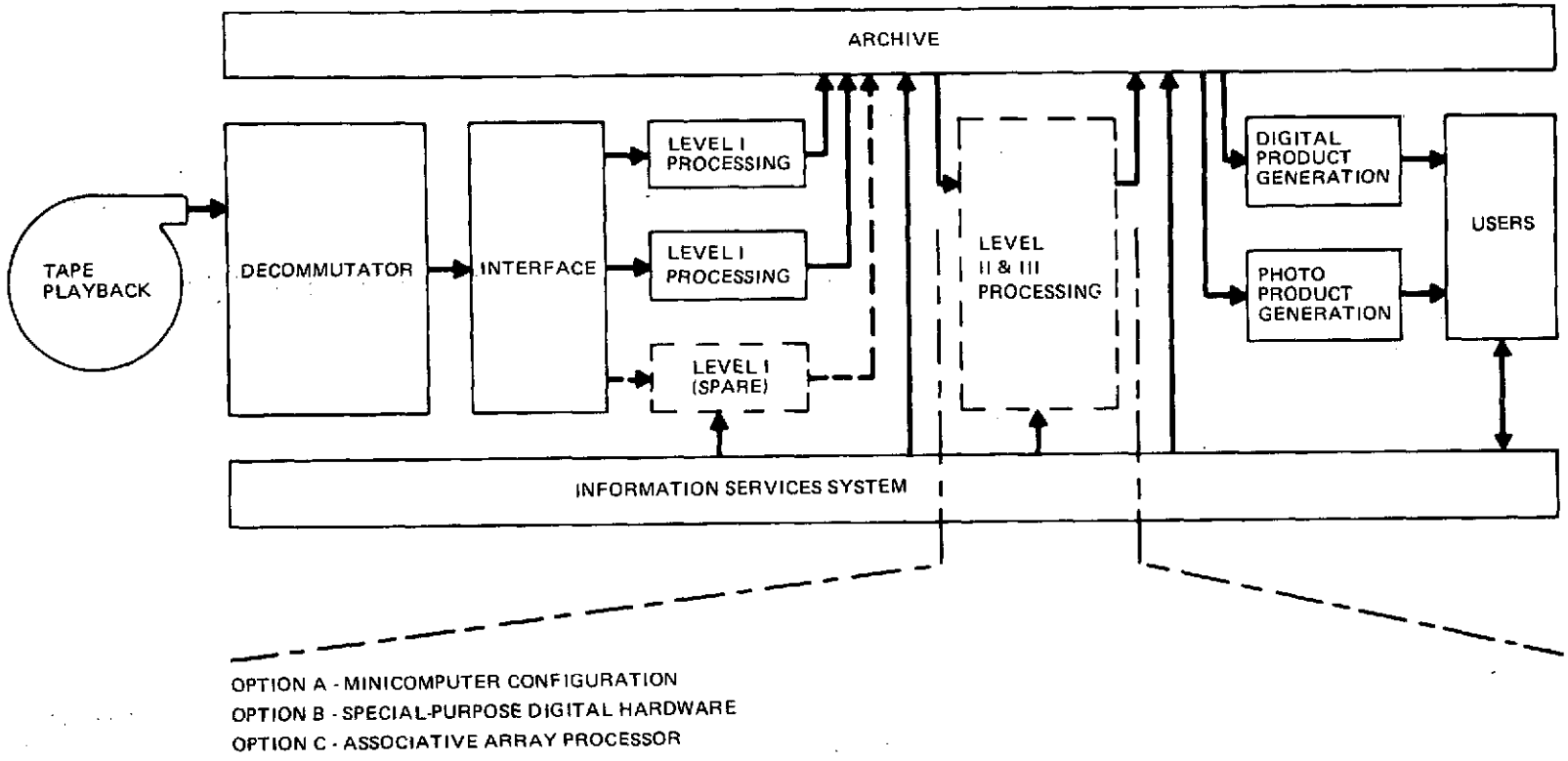

Fig. A6-1 CDPF — Alternative Configurations

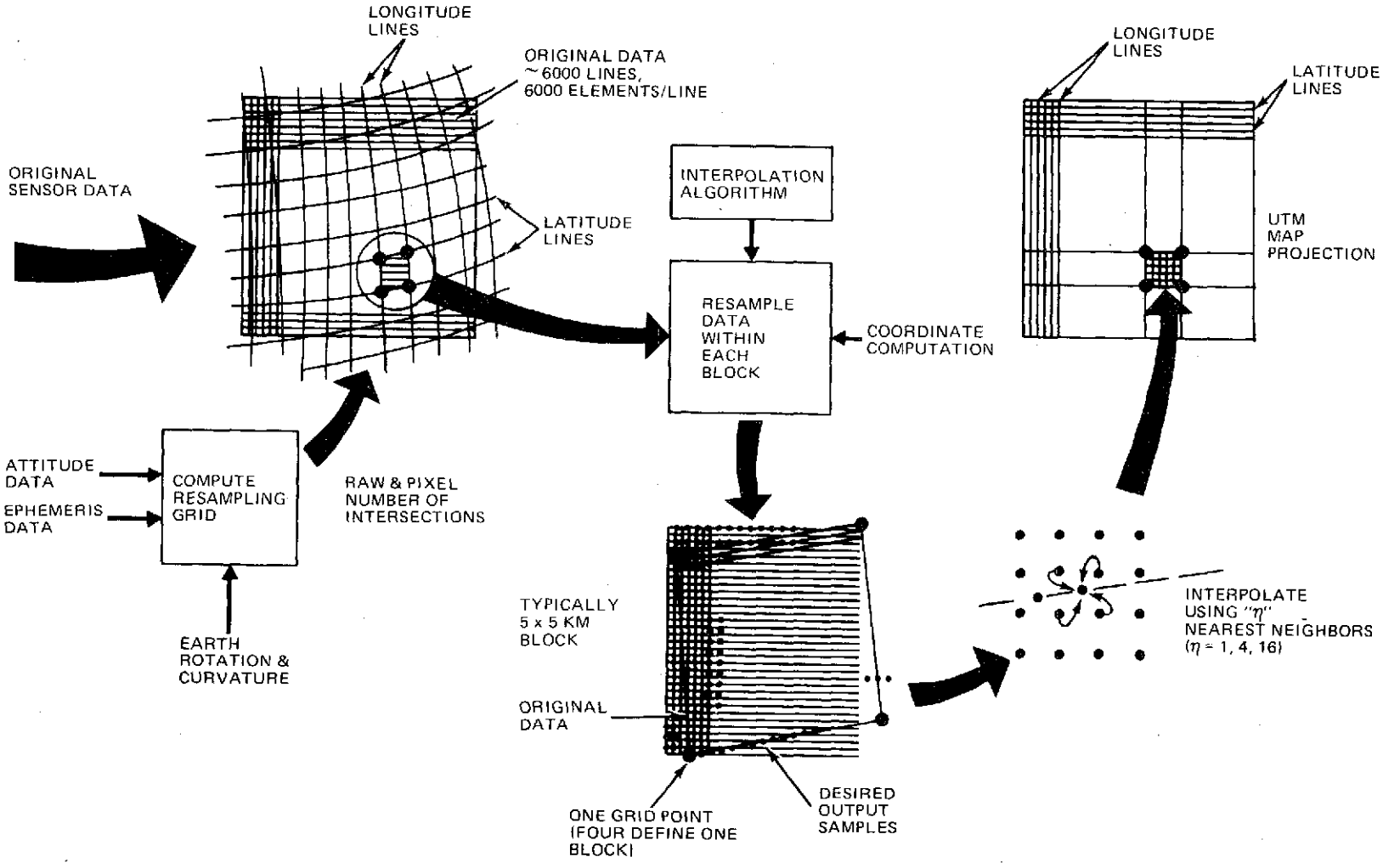

Fig. A6-2 Basic Steps in Level II Processing

The total number of machine operations required for the Level II processing can be summarized by the relationship

$$O_{II} = N_{GP} O_{GP} + N_p/b\, O_c + N_p O_i \qquad (1)$$

where

O_{II} is the number of machine operations (equivalent integer adds) required for Level II processing.

N_{GP} is the number of grid line intersections (grid points) to be located in the scene.

O_{GP} is the number of machine operations to locate one grid point.

N_p is the total number of pixels in a scene

b is the number of bands per scene (6-1/9)

O_c is the number of machine operations for coordinate computation

O_i is the number of machine operations required to interpolate each output point.

Since N_p is approximately $3x10^8$, the third term in (1) dominates the other two. For example, if $N_{GP} = 10^3$ (resampling over 6 km blocks), and $O_{GP} = 10^5$, we have

$$O_{II} = 10^8 + 4.7x10^7\, O_c + 3x10^8\, O_i \qquad (2)$$

Since O_c is less than 10 machine instructions and O_i ranges from 10 (nearest neighbor interpolation) to 60-80 instructions (cubic convolution), (2) is determined almost entirely by the last term.

The absolute accuracy of the image data produced by the Level II processing is limited by the ephemeris and pointing (attitude) data which is made available for the grid computation. Generally, errors in these data will limit the absolute geometric accuracy of pixel location in the output images to several hundred meters.

To improve the absolute geometric accuracy of the TM images, additional processing can be performed to locate areas in the digital image data -- referred to as ground-control "points" -- for which latitude/longitude coordinates are known precisely. Level III processing, therefore, differs from the Level II processing only in the fact that GCP location is performed first to allow more precise location of the resampling grid points in the input data.

GCP location can be accomplished by either manual or automatic means and it is likely for EOS that the process would be automated. Appendix A4 treats this subject in detail. We can estimate the impact of GCP location on the overall processing load by writing the total number of machine operations for Level III processing as

$$O_{III} = O_{II} + N_{GCP}\, O_{GCP} \frac{\text{machine operations}}{\text{scene}} \qquad (3)$$

where

O_{II} is the number of machine operations per scene from (2)

N_{GCP} is the number of GCP's found per scene (ranges from less than one to several)

O_{GCP} is the number of machine operations required to locate one ground-control point

The number of operations per GCP is a function of the algorithm used for automatic location, the size of the original search area, and the size of the control point itself. If we normalize O_{GCP} by $3x10^8$ (number of pixels/scene), we can summarize the equivalent number of machine operations per pixel required to locate one GCP in the TM image as shown in Figure A6-3. For direct correlation, the equivalent processing load can become large if the search area exceeds an 8 x 8 km square; here, the equivalent number of instructions exceeds one and the processing is no longer negligible compared to coordinate computation and interpolation. For other algorithms, however, specifically the sequential search procedure (Sequential Similarity Detection Algorithm, SSDA) and correlation using the (Fast Fourier Transform), FFT, the operations are negligible compared to the other processing that must be performed on the image data.

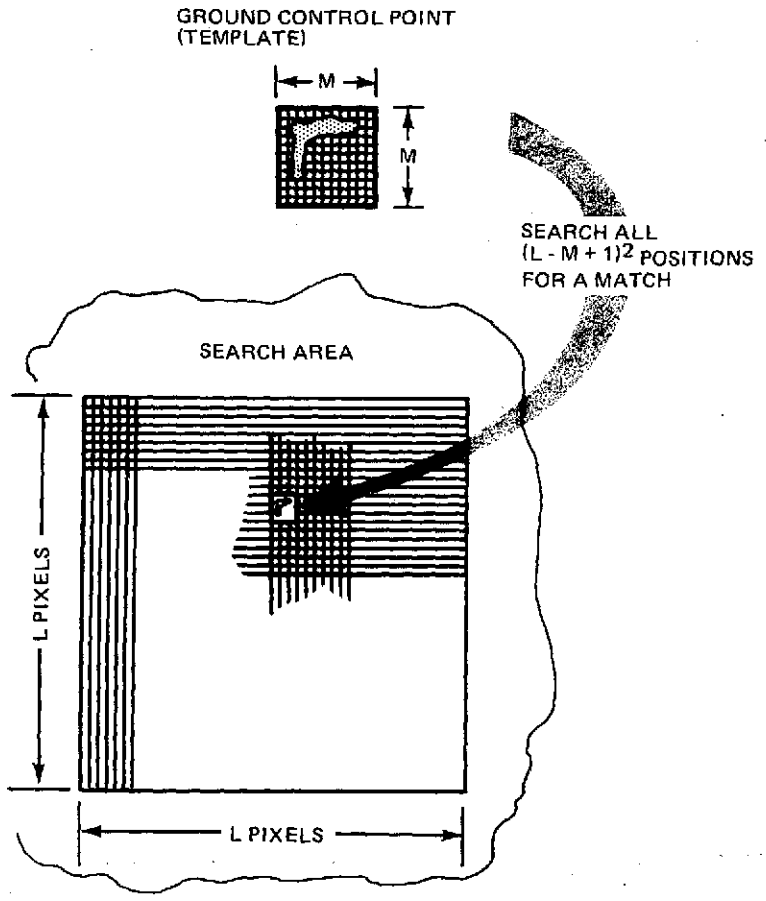

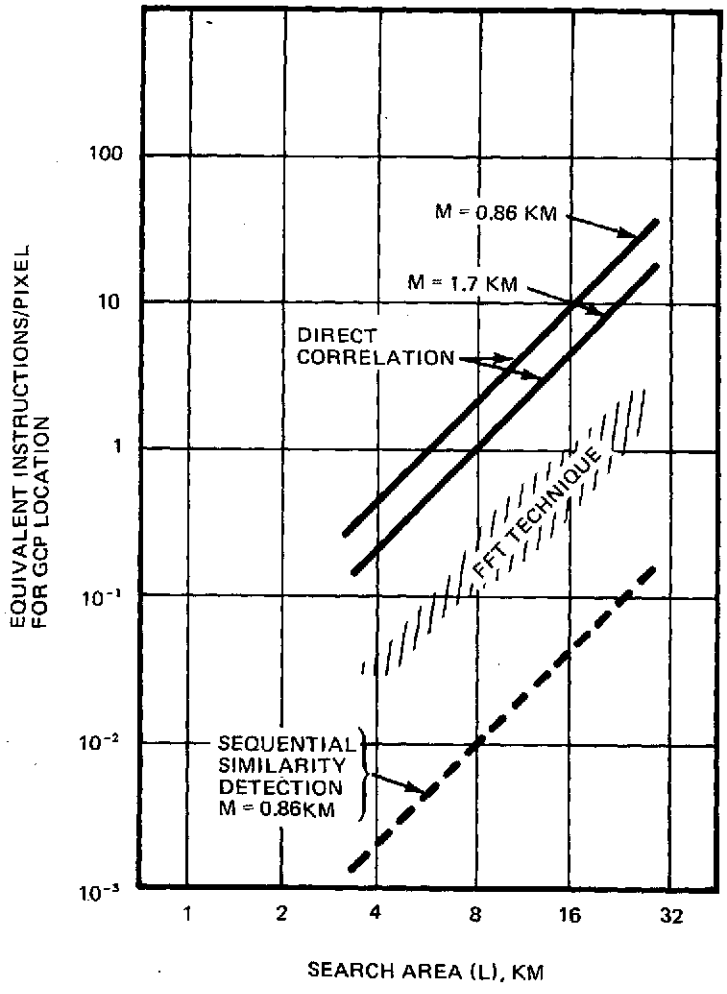

Fig. A6-3 Summary of Machine Operations Required for Ground-Control Point Location

For automatic GCP location to be feasible, therefore, algorithms other than direct correlation must be used. Also, search areas must be kept reasonably small (implying a precise attitude control system). If these conditions are met, the location of ground control points can be implemented with little impact on the throughput of the system.

Three options were considered for the Level II/III processing and are described in detail in the following sections:

1. A concept based on the use of a multiprocessor configuration of conventional, general-purpose minicomputers.
2. A concept based on using special purpose hardware for those functions requiring high throughput.
3. A concept based on an unconventional general purpose processor (the Goodyear STARAN) having special architecture that provides parallel processing for appropriately organized data.

A6.3 GENERAL PURPOSE GROUND PROCESSING SYSTEM

One general purpose processor approach involves the use of multiple configurations of minicomputers throughout the system design. Advantages to this approach include:

- The minimum load system involves no excessive hardware or development costs.
- Additional capability may be added with relatively small cost increments.
- Much of the system may be developed with a minimum of hardware.
- Most of the system hardware consists of proven components.
- The resulting system is sufficiently modifiable to permit redesign of the system or a shift in processing characteristics.

- The multiplicity of components permits a relatively low cost inventory of spares.
- The multiple configuration approach automatically provides several levels of performance degradation.
- Specially designed hardware components may be incorporated into the system as they are designed and developed with less modification or system interference.

Among the disadvantages of this approach are the following:

- The costs for maximum loads is essentially a linear extension of the minimum system cost.
- The throughput of software controlled processors is probably less than the potential throughput of hardwired systems.

A6.3.1 LEVEL I PROCESSING

Investigations were made for the processing loads involved with the Level I processing assuming a specific hardware configuration currently available. These studies indicate that the Level I processing is dominated by the radiometric correction function and the line stretching function. These two functions accounted for more than 99 percent of the total Level I processing. The requirement for the minimum system load of twenty TM scenes per day is for a Level I processing capability of nearly three million instructions per second. The specific processor used for evaluation is capable of approximately 1.6 million instructions per second. Two such processors are capable of handling the complete Level I task.

A6.3.1.1 ACQUISITION - LEVEL I INTERFACE

The data rates during the actual data acquisition by the primary ground stations requires special high speed recording devices. Eventually the data must be input to a computer which can reformat for archiving, and perform some of the corrective functions. The input to this system must be at a rate that is consistently slower than the worst case processing rate or the input must be start-stop controllable in manageable portions of data.

In the minimum system each byte or pixel must be processed in approximately 4 microseconds for Level I corrective functions. This includes the processing plus input and output transfers and controls, editing, formatting, and all other overhead. For the maximum system the equivalent performance period shrinks to approximately 200 nanoseconds per byte.

This multi-mini-configuration system assumes that the acquired data has been played back, edited and formatted, and recorded on an efficient computer compatible magnetic tape. The best current example of such a medium is the IBM 6250 bpi tape and the 3420-8 tape drive. Other comparable alternatives should be available within the implementation time frame. The drives provide a maximum instantaneous transfer rate of 1.25 megabytes per second which support a maximum average rate of approximately 1 megabyte per second.

The editing and reformatting functions could be combined with the Level I processing provided some means of controlling the acquisition tapes can be devised and interfaced with a conventional processing system. This would increase the processing load on the Level I configurations thus decreasing the throughput per configuration and increasing the number of configurations required for the total system. Whether this approach is cost effective depends on the costs of the assumed alternatives.

A6.3.1.2 CALIBRATION DATA INVERSION

The data which is received from the satellite for sensor calibration purposes indicates the current response of a specific detector to a known source. The data which must be tabled for lookup correction of actual data pixels is the true stimulus or source value which would cause the detector to indicate a pixel value. The calibration data must thus be "inverted" before use on the pixel data. The location in the table must correspond to the received or input pixel value and the contents of the table or the table entries must correspond to the known source values.

A6.3.1.3 LEVEL I RADIOMETRIC CORRECTIONS

The radiometric correction function is second only to the line stretching function in processing load during the Level I processing. (This function could also be implemented in special purpose hardware controlled by a minicomputer.) It is possible to combine the radiometric correction function with the line stretching function and thus reduce the processing overhead. However, corrected values would have to be "looked up" twice rather than once. The overall optimum is to perform the functions separately. This function is also sensitive to the sequence in which the pixel data is processed. If each line of pixel data is corrected at one time before proceeding to the next line, the sequence is not compatible with the acquisition sequence. If the data is corrected in a sequence close to the acquisition sequence, then many tables must be available simultaneously, since each line in each band of a scan must be corrected by a unique table of 128 values.

A6.3.1.4 LINE STRETCHING FUNCTION

This is the single most time consuming function performed during Level I processing by the general purpose configuration. Performance could be improved with the implementation of special purpose hardware (hybrid system) which could be interfaced to the minicomputer. Increased throughput could reduce the number of configurations required for large loads. This improvement would be limited by the input and/or output rates obtainable from the configuration. Provided the special hardware could support the processing, two or more minicomputers could share the hardware for the line stretching function while maintaining independent and parallel streams of input data and output data to the archive devices. This function is also sensitive to the sequence in which the input pixel data is processed. If the data is processed one line at a time, the interpolation coefficients must be saved for subsequent lines or else the identical coefficients would have to be recomputed. If the data is processed in the acquisition sequence, the coefficients need be saved only for the single pixel on each output line rather than the entire scan. The actual interpolation function must be performed uniquely for each output pixel in either case.

A6.3.2 LEVEL II/III PROCESSING

A6.3.2.1 GENERAL

Figure A6-4 shows the Level II/III GP processing configuration considered.

The processing of scene data through the Level II/III functions is triggered by reading a product data record received from the Information Management system. This record includes all the control and support information which is unique to the specific request. It contains data which limit the desired scene and identify the archive data which are required as input for processing.

In Level II processing ephemeris and attitude data are read from the input peripheral. Then, using the date and time information plus the scene limits, a set of interpolated satellite positions and attitudes are computed.

Although it is intended to maintain a satellite attitude as precisely as attitude measurement will permit, it is considered highly desirable that attitude measurements be returned to the ground with the sensor data. The availability of this data would serve to confirm the performance of the attitude control system or possibly support the location of sensor data in the event of malfunction between attitude measurement and attitude control.

In the Level II/III process, each product scene is divided into scene sections by a set of grid points. The purpose of the sectioning of the scene is to permit precise location of the pixel data without performing a very complex transformation of data for each output pixel point. This is accomplished by precisely locating each of the grid points and then using simple algorithms for the location and resampling of pixel data within each section.

The set of grid points for the desired product scene must be determined or generated in terms of the output coordinate system (UTM or equivalent geographic coordinates).

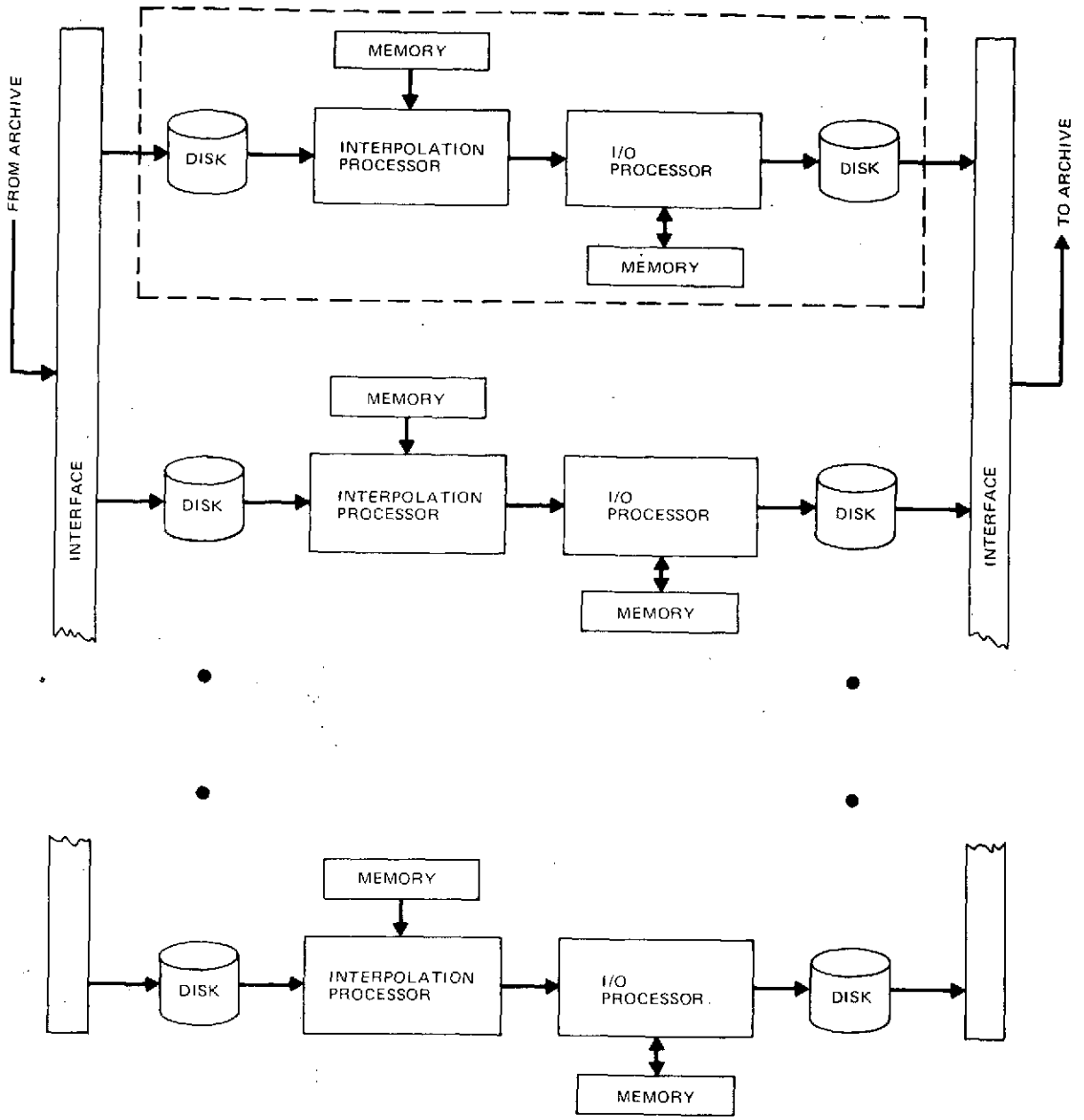

- BASIC MODULE PROCESSES 5 SCENES/DAY
- FOUR BASIC MODULES PROCESS 4×10^{10} BITS (20 TM SCENES) PER DAY

7-51, 7-58
7-104, A7-28

Fig. A6-4 Option A – Minicomputer Configuration

Then, for each section, the appropriate satellite position and attitude data must be determined. This data must be used in conjunction with the geometry and timing of the scanning function to compute the line-pixel coordinates of each of the grid points. Although the location of pixels along each line is dependent on the scanning process and timing, the line rectification performed in the Level I process places the pixels on a uniform rectangular grid, and then the effects of scan nonlinearities and timing within the scan line need not be considered in Level II/III.

In addition to computing the line-pixel coordinates of each of the grid points defining the scene sections, it is necessary to compute interpolation coefficients and resampling control parameters for each section. The interpolation coefficients vary from output point to output point and from line to line so that first and second differences of the various coefficients must be determined.

Regardless of the sequencing of data for archive purposes, the input to Level II or Level III processing is taken in blocks. The block size is reflected through a blocking factor K which indicates the number of input lines in a block and the portion of pixels from each of those lines which is included in a block. The blocking factor is used to control the balance between the amount of output buffer space required and the amount of access delay time involved with the data output. This relationship is dependent on the angle between the scanning or input lines and the geographic or output lines. The upper left-hand block is used first and the sequence of blocks proceeds vertically down the scene. The second pass of the resampling process uses the second column of blocks, etc., until K passes have been completed.

The uniqueness of the transformations between coordinate systems at this stage of processing suggests that blocks be sized to correspond with the number of lines per scan, provided it does not cause excessive access delay problems.

Although specific relationships will depend on more detailed knowledge of processing requirements, sensor instrument selection and details, and specific hardware selection, the bound on system throughput due to disk access delays is proportional to K, the blocking

factor, and inversely proportional to the sine of the scanning angle relative to the geographic line. The relationship involves the number of pixels per image and the amount of storage available or required for output buffers.

The main effect of blocking is to reduce the amount of memory required for output buffers and to reduce the number of disk accesses required to output the complete scene. It is only necessary to keep the disk access and transfer time down to the time required for actual processing of the resampling algorithm. The selection of the algorithm and the efficiency of its implementation thus impacts the blocking-memory-throughput relationship.

A6.3.2.2 ARCHIVE INTERFACE FOR LEVEL II/III PROCESSING

The staging of data in the Level II/III system is related to the block size which is required in the archive medium. For many of the potential archive systems considered the large block size is related to the relative storage efficiency of the archive medium. If the block size could be reduced to a manageable number of bytes the data staging problem could be alleviated. The prime archive candidate considered required a block size of 130,000 bytes. As a result, any computer configuration which interfaces with the archive system must have a very large memory available for buffer space or must be buffered from the archive system by an intermediate peripheral. The only way to avoid these two alternatives would be to process the data in the sequence in which it is received and at the average rate of transfer.

The general purpose system considered here uses intermediate peripherals to isolate the user configuration from the archive system. This is done at the expense of using many peripheral devices and controllers.

An additional approach considers the use of magnetic tape for the input medium to Level II/III processing, offering two possibilities for hardware configurations. One is the switchable tape system between the archive system and the processing system, plus an additional switchable tape system for interface between the processing and the tape

copying/formatting system. The other possibility is to use a single switchable tape system between the archive and processing systems and produce the output tapes onthe same system to be manually transferred to the tape processing system for copying and formatting.

The recommended system uses two independent tape systems to eliminate the need for manual handling of the data tapes.

A6.3.2.3 HARDWARE/SOFTWARE CONFIGURATION

The various functions which must be performed have been evaluated for the specific processors included in the configuration. The resulting configuration could process approximately five scenes per sixteen hour day. using the bilinear interpolation algorithm. Use of a simpler algorithm would not significantly reduce the processing time unless more memory were added to the configuration to proportionately reduce disk output time. Use of a more complex algorithm would increase processing time and allow longer disk output time and thus require less storage. Another alternative for a more involved algorithm would involve the use of an additional processing mimicomputer and dividing the resampling algorithm processing load.

For purposes of load evaluation, it was assumed that ten sets of satellite position and attitude data would be required, that second degree interpolation between the archive supplied points would suffice, and that a minimum of three sets of ephemeris data spaced sixty seconds in time and five sets of attitude data spaced ten seconds in time would be required to support the interpolation process.

The general purpose processor design proposed for the Level II/III processing system involves the pairing of a high speed processor for execution of the resampling algorithm and an I/O processor to control the disk output and the associated large memory required for output buffers. Interfaces with other systems are through a switchable tape system to the archive system and a second switchable tape system to a tape processing system. Interface with the information management system is through a communication line

controller for control and status information transfer. Much of the hardware cost is in the peripheral storage which is required for system interfaces or for the extremely large quantity of data which must be handled simultaneously.

Tables A6-1 and A6-2 show the estimated machine language instructions required for each of the processors. The same figures also show the corresponding estimates for manning of the software development through unit test. Table A6-3 shows the aggregate estimates for Level II software development through system test and integration.

Table A6-1. STAGE II SOFTWARE (I/O Processor)

	Man Months	Instr.
Resampling Intercomputer Interface Driver and Handler	2	100
System Bootstrap System Loader System Takedown System Restart	3	400
Configuration Verification Status Report Diagnostic Support Package	1	200
Working Disk Driver and Handler	4	600
Extended Memory Support Package	1	100
Output Line Buffer Assignment and Control	4	400
Working Disk Scene Read Back Control Scene Line Output Routine	2	200
Totals	17	2000

Table A6-2. STAGE II SOFTWARE

(Resampling Processor)

	Man Months	Instr.
Stage II Processing Control System Bootstrap System Loader System Takedown Routine	5	400
System Restart Routine Configuration Verification Status Report Diagnostic Support Package	3	300
System Input Device Driver and Handler	8	600
Magnetic Tape Driver (6250) and Handler	4	200
IMS Intercomputer Interface Driver and Handler	4	300
I/O Intercomputer Interface Driver and Handler	2	100
Ephemeris Data Conversion and Interpolation Package	4	300
Attitude Data Conversion and Interpolation Package	2	100
UTM to LP Coordinate Determination and Transformation[(a)]		
Grid Section Interpolation Coefficient, Boundary Test and Control Data Determination	8	400
Pixel Data I/O Buffer Control	4	400
Resampling Parameter Control	2	100
Resampling Algorithm	2	100
Product Control	1	100
Scene Read Back and Output	1	100
Line Format and Sequence Processing	2	200
Totals	52	3700

[(a)] Not Determined

Table A6-3. STAGE II SOFTWARE

	Man Months
Direct Software Production	69
Contingent Software and Debug Support	24
Subsystem Test and Integration	12
System Test and Integration	6
Total (Direct)	111

A6.3.2.4 OUTPUT PRODUCT TAPE PROCESSING

The input for this system is the processed scene data as generated by the Level II or Level III processing systems. The data is input from a high speed, high density magnetic tape unit. The output is to be formatted according to predetermined formats and/or sequences which are made available to users. The tapes produced are generally computer compatible tapes of specified standard densities.

This system could also handle any special formatting or tape preparation for input into the photo processing system and to produce limited or selected hard copy of image data values or line printer produced mappings of limited areas.

A single configuration appears capable of handling the full load for the minimum twenty scenes per day.

A6.4 SPECIAL PURPOSE PROCESSOR (SPP)

This section describes a special purpose hardware processor design for Level II/III processing. State-of-the-art digital techniques were used to achieve the highest degree of picture resolution at a maximum throughput on a cost effective basis. The special purpose hardware is capable of processing video data from the minimum system up to 400 scenes in a 16 hour day. The system is modularized and is configured to process individual scenes whose parameters include:

- Scene size - 185 km x 185 km
- Bands per scene - 6 visible bands (VB)
  1 infrared band (IRB)

- VB resolution element - 27m x 27m picture cell (pixel)
- IRB resolution element - 81m x 81m pixel (P)
- Pixel resolution - 8 bits (b), 1 byte (B)

Provisions provide three selectable interpolation algorithms accordant with video resolution and throughput requirements as follows:

- Cubic interpolation (CC) - highest accuracy, lowest throughput
- Bilinear interpolation (BI) - medium accuracy, medium throughput
- Nearest neighbor interpolation (NN) - lowest accuracy, highest throughput.

The processor is a special purpose hardware design optimized for video (pixel) interpolation using CC. To achieve a design throughput goal of 400 scenes per day the video data rate must be greater than 2×10^6 pixels per second. The design uses 7 video interpolators, one per band.

A6.4.1 FUNCTIONAL OPERATION

A Special Purpose Video Processor (SPVP) is depicted in Figure A6-5. The functions of each SPVP's functional block are:

(a) Master Process Controller (MPC)

- Control the input and output density digital tapes - IHDDT, OHDDT
- Synchronize the SPP's Input Controller (IC) and Output Controller (OC) with the IHDDT and OHDDT, respectively
- Transfer scene blocks of raw pixels from Raw Band Storage (RBS) to a Working Block Memory (WBM)
- Transfer scene block grid coordinates from the Grid Computer (GC) to the SPP's Video Coordinate Computer (VCC)
- Supervise the SPP's Video Interpolators (VIs) including interpolation algorithm selection - CC, BI and NN
- Transfer scene blocks of interpolated pixels to Interpolated Band Storage (IBS)

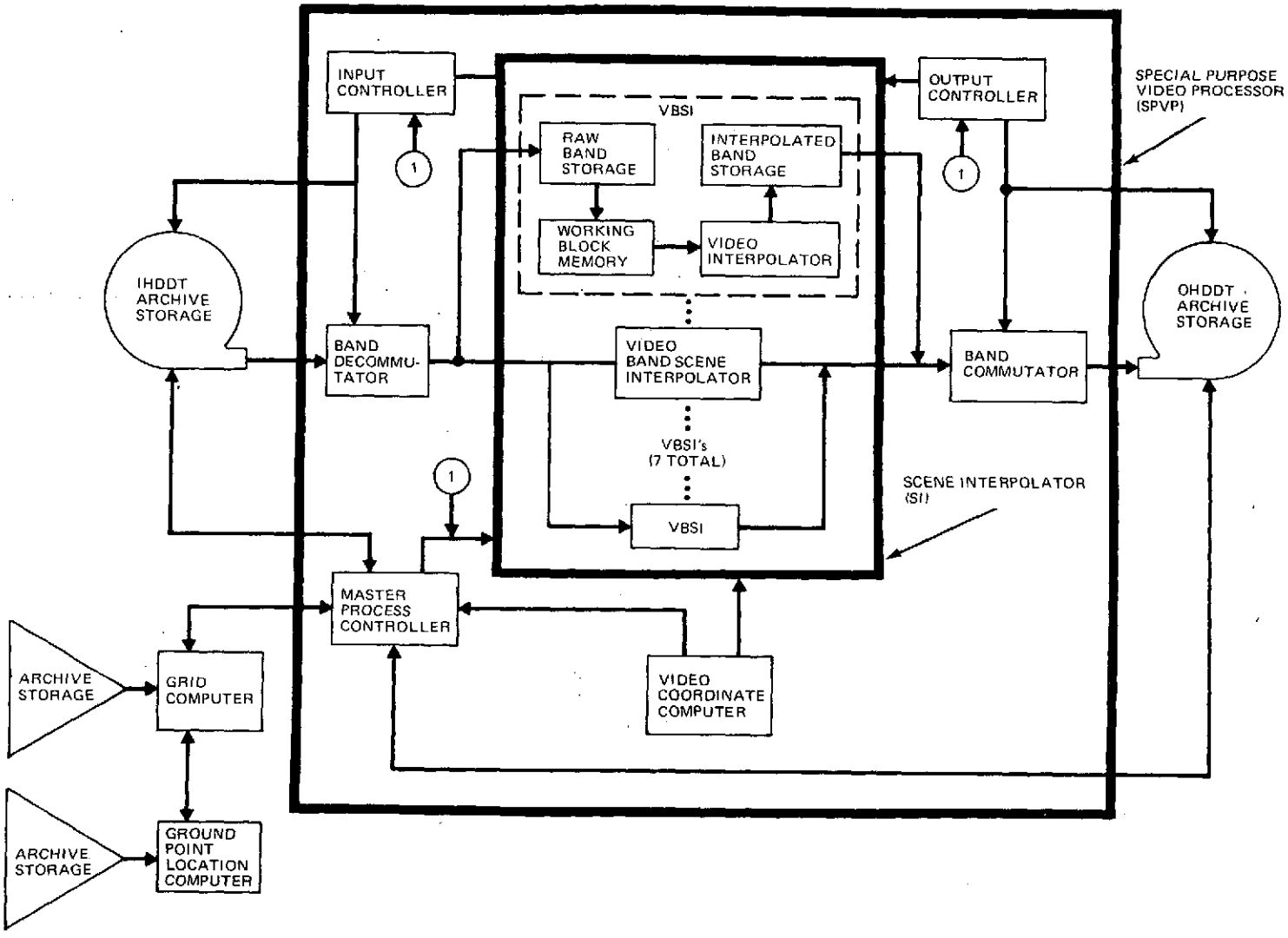

A7-29 **Fig. A6-5 EOS Special Putpose Video Processing System (Ground Point Location, Grid Computation, Video Interpolation, Archives)**

- Transfer pixel coordinates from the VCC to the VIs
- Inform the OC of the desired record format - Band Sequential (BS), Line Sequential (LS) or Pixel-Interleaved (P-I)

(b) Input Controller (IC)

- Supervise the Band Decommutator (BD) according to the playback format - Natural Pixel-Interleaved (NP-I)
- Transfer raw band scenes from the BD to RBS, including header data
- Inform the MPC of a raw band scene transferral completion
- Supply control signals to IHDDT and BD.

(c) Output Controller (OC)

- Supervise the Band Commutator (BC) in accordance with the desired format (BS, LS or P-I)
- Transfer interpolated band scenes from the IBS to the BC, including scene identification and header data
- Inform the MPC of an interpolated band scene transferral completion
- Supply control signals to OHDDT and BC.

(d) Band Decommutator (BD)

- Decommutate, at a IHDDT control rate, scene data (natural pixel-interleaved format) into 7 bands which include: 6 raw visible bands, 1 raw infra-red band, plus scene header data.

(e) Band Commutator (BC)

- Commutate 7 bands at a OHDDT control rate into scenes accordant with the desired format (BS, LS or P-I). Each output scene includes: 6 interpolated visible bands, 1 interpolated infra-red band, and header data.

(f) Video Coordinate Computer (ICC)

- Supply each video interpolator (VI) per video band scene interpolator (VBSI) with coordinates of each pixel within a scene block

- Inform the MPC when more scene block grid coordinates are needed.

(g) Video Band Scene Interpolator (VBSI)

- Provide double buffer storage (RBS) for 2 raw band scenes
- Provide a double buffer working block memory (WBM) for continuous pixel interpolation
- Provide a video interpolator (VI) capable of interpolation in accordance and with CC, BI or NN at a maximum daily throughput of 400 scenes
- Provide double buffer storage (IBS) for 2 interpolated bands.

(h) Scene Interpolator (SI)

- Interpolate one band out of each EOS scene, at a throughput rate of 400 scenes per day per interpolation algorithm. Requires 7 VBSI's for the 7 bands in a scene.

Although not part of the SPP, Figure A6-5 depicts 4 other functional blocks. These include:

(i) Grid Computer (GC)

- Retrieve necessary data from archive storage to compute the scene grid
- Compute SPP's scene resampling grid for the following video processing types:

  Type II - utilizes UTM coordinates
  Type III - utilizes data from GPLC.

- Supply scene block grid coordinates to the VCC
- Inform the SPP that the scene grid is ready.

(j) Ground Point Location Computer (GPLC)

- Retrieve necessary data from archive storage to compute scene ground control points (GCP)
- Supply GC with ground control points (GCPs) in computing scene resampling grid for Type III video processing.

C-2

(k) Input High Density Digital Tape (IHDDT)

- Playback 400 raw EOS scenes (maximum) retrieved from archive storage under the control of the MPC and IC
- Data format is natural pixel-interleaved, byte and bit serial at a rate compatible with a 400 scene per day throughput.

(l) Output High Density Digital Tape (OHDDT)

- Record 400 interpolated EOS scenes for archive storage under the control of the MPC and OC
- Data format is determined by the MPC (BS, LI or P-I), byte and bit serial at a rate compatible with a 400 scene per day throughput.

A6.4.2 TYPICAL SCENE INTERPOLATION

Each interpolated scene is related to a raw scene as depicted in Equation 1-1 and Figure A6-6.

$$IS = RS\ (\sin \alpha + \cos \alpha)^2 \qquad (1\text{-}1)$$

where

IS = interpolated scene

RS = raw scene

α = S/C tilt angle

Archive tapes are obtained to compute a resampling grid for Type II or Type III processing.

Type II - interpolation to a resampling grid computed with UTM projection coordinates, longitude and latitude

Type III - interpolation to a resampling grid computed with ground control point templates

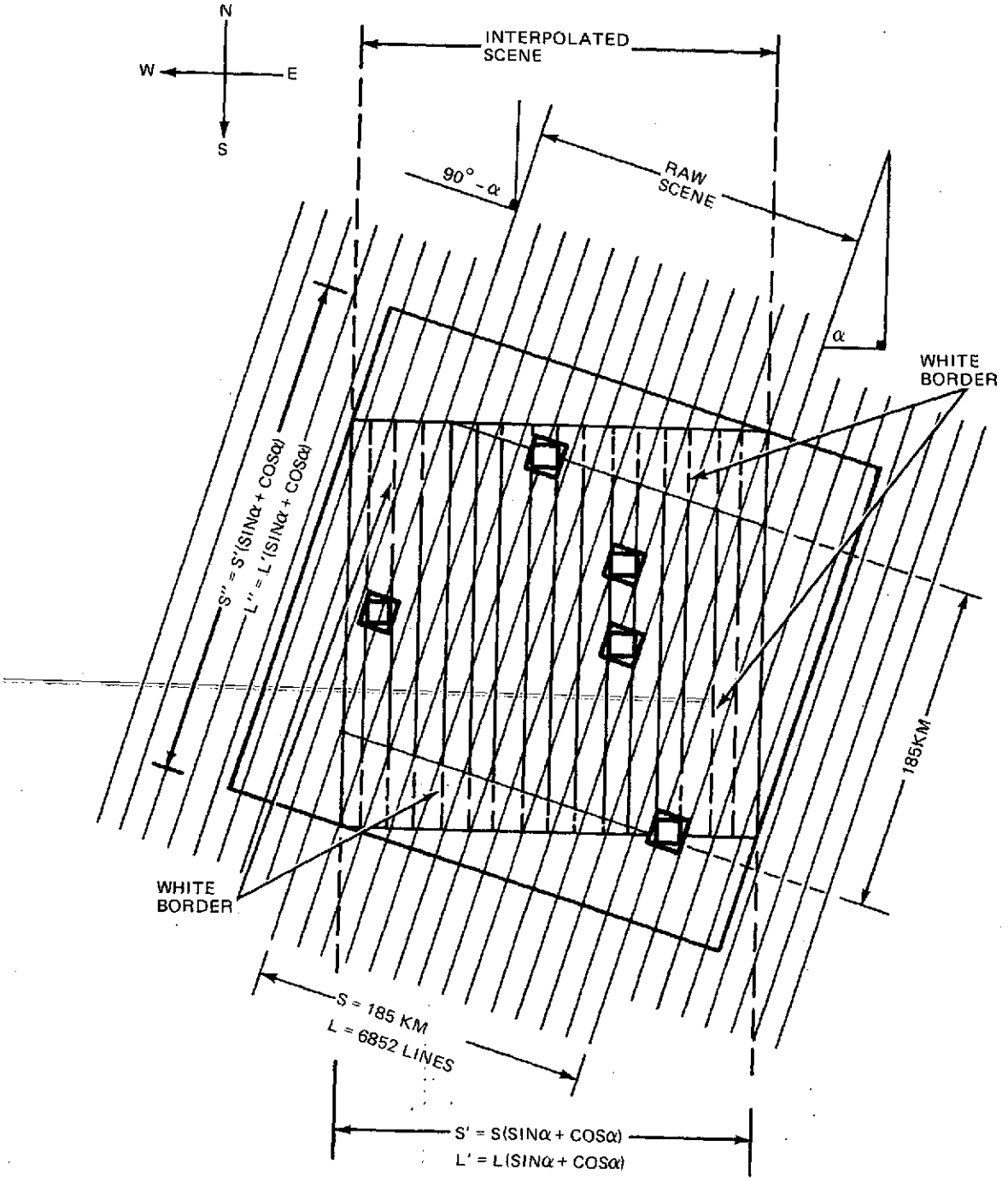

A7-30 **Fig. A6-6 Superimposed Scene Picture (Raw Scene, Interpolated Scene, Spacecraft Tilt Angle, Scene Blocks)**

Figure A6-7 shows a timing diagram for an SPP. Having computed a resampling grid for n EOS scenes, time ($T_{IRS1} - T_o$), the Grid Computer (GC) informs the Special Purpose Processor (SPP) that it is ready to supply scene block grid coordinates. The MPC starts the IHDDT, synchronizing the IC with the IHDDT, time T_{IRS1}. The IC, providing the tape control signal, proceeds to supervise the transferral, time ($T_{IRS(n)} - T_{IRS(n-1)}$), of 7 raw bands (6 visible bands and 1 infrared band) per EOS scene from the BD to RBS, supplying n raw bands for each video band scene interpolator. Upon the first EOS raw scene transferral completion, time T_{IRS2}, the IC informs the MPC to begin scene interpolation. The MPC then proceeds to supervise scene interpolation, time ($T_{VIRS(n)} - T_{VIRS(n-1)}$), producing n interpolated bands per video band scene. EOS scene interpolation, 7 bands simultaneously, is accomplished in terms of small scene blocks. (See Figure A6-6). The MPC supervises the raw block transferrals (RBS to WBM), the Video Interpolator (VI) and the interpolated block transferrals (PI to IPS). Upon the first interpolated EOS scene transferral completion time T_{VIRS2}, the MPC starts the OHDDT, synchronizing the OC with the OHDDT times T_{OIS1}. The OC, providing the tape control signal as well as the begin header data, proceed to supervise the transferral, time ($T_{OIS(n)} - T_{OIS(n-1)}$), of 7 interpolated bands per EOS scene from IBS to the BC, supplying n interpolated bands from each video band scene interpolator for a OHDDT record. Each EOS interpolated scene, 7 bands, is recorded with the MPC's desired format (BS, LS or P-I), including scene identification. At time T_{F+2} the OC inserts the end header data and informs the MPC that the interpolation cycle of n scenes is complete. The MPC then rewinds the OHDDT and IHDDT. Once the rewind process is complete, the MPC turns off the tape drives and signals that it has completed the present EOS scene interpolation request.

A6.4.3 THROUGHPUT VERSUS INTERPOLATION ALGORITHM

Cubic Convolution

Individual pixel interpolation is accomplished in accordance with Equation 1-2, whose geometrics are depicted in Figure A6-8(c).

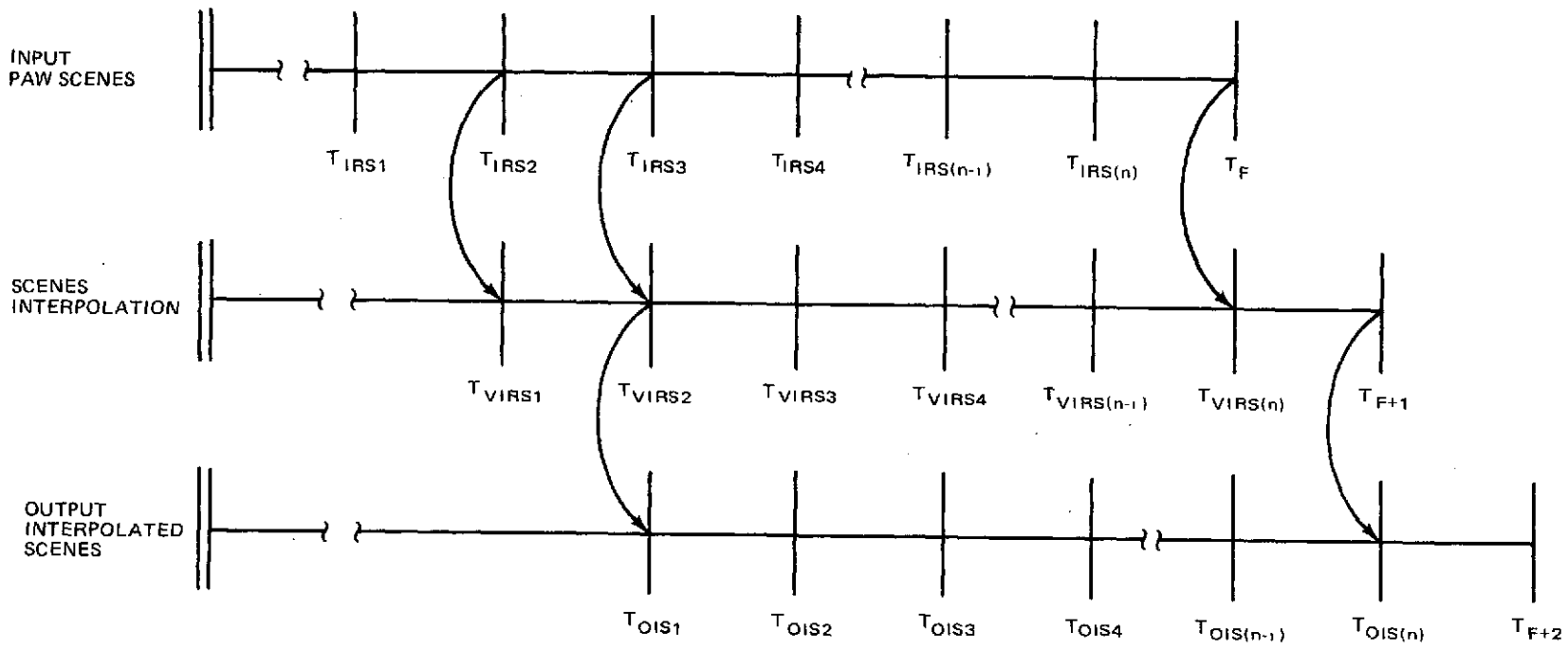

- **CONSTRAINTS:**

  $T_{IRS(n)} - T_{IRS(n-1)} \geqq T_{VIRS(n)} - T_{VIRS(n-1)}$
  $T_{IRS(n)} - T_{IRS(n-1)} \geqq T_{OIS(n)} - T_{OIS(n-1)}$
  $T_{VIRS(n)}$ FOLLOWS $T_{IRS(n)}$
  $T_{OIS(n)}$ FOLLOWS $T_{VIRS(n)}$

- **DEFINITION:**

  $T_{IRS1} - T_O$ = GRID COMPUTION TIME
  $T_{IRS(n)} - T_{IRS(n-1)}$ = RAW SCENE INPUT TIME
  $T_{VIRS(n)} - T_{IRS(n-1)}$ = RAW SCENE VIDEO INTERPOLATION TIME
  $T_{OIS(n)} - T_{OIS(n-1)}$ = INTERPOLATED SCENE OUTPUT TIME

  } WHERE n = 1 THRU 400

Fig. A6-7 Special Purpose Processor Top-Level Timing Diagram (Scene Inputting, Interpolation, Outputting)

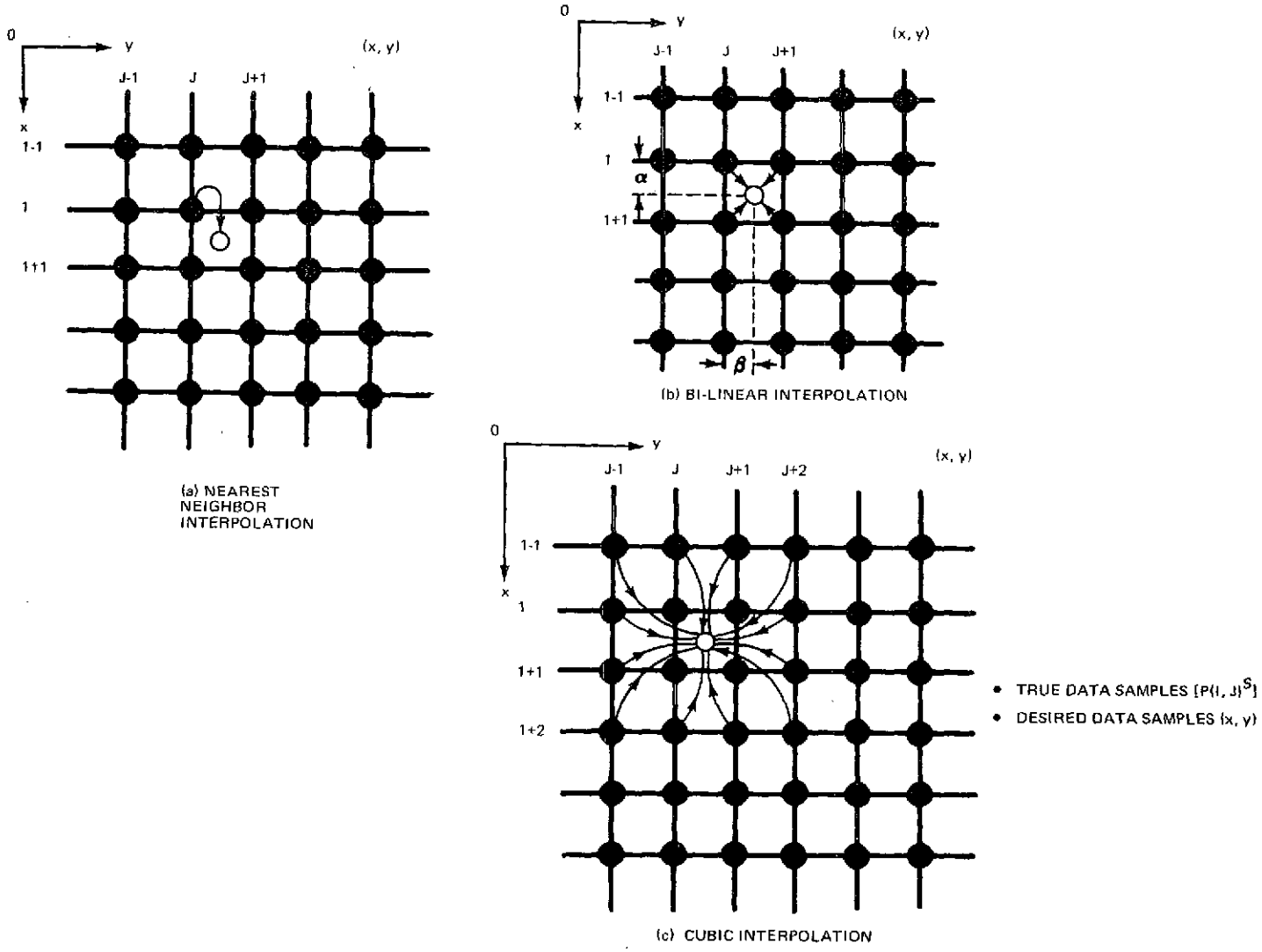

(a) NEAREST NEIGHBOR INTERPOLATION

(b) BI-LINEAR INTERPOLATION

(c) CUBIC INTERPOLATION

Fig. A6-8 Geometries for Various Interpolations Algorithms

$$IP = \sum_{i=1}^{i=16} NP_i \left[\frac{\left(\frac{\sin X_i}{X_i}\right)\left(\frac{\sin Y_i}{Y_i}\right)}{16} \right]$$

$$= \sum_{i=1}^{i=16} \frac{(NP_i)(S_i)}{16} \qquad (1\text{-}2)$$

where

IP = interpolated (desired) pixel at coordinate location (x, y)

NP_i = known (true) pixel at coordinate location (J, I)

X_i = x coordinate distance (normalized to $\pm$ 2) from IP to NP_i

Y_i = y coordinate distance (normalized to $\pm$ 2) from IP to NP_i

$S_i = \left(\frac{\sin X_i}{X_i}\right)\left(\frac{\sin Y_i}{Y_i}\right)$, With each distribution in terms of x and y distances ($\pm 2\pi$ radian maximum) is normalized for +1.0, -0.2, relevant to distribution centers $\left(\frac{\sin x}{x} = 1, \frac{\sin y}{y} = 1\right)$ being positioned at IP. Figure A.6-9 depicts $\frac{\sin x}{x}$ or $\frac{\sin y}{y}$ distribution curves for three conditions, median ($\pm 3\pi/2$), -2 extreme ($-\pi$, $+2\pi$) and -2π extreme (-2π, $+\pi$).

Each video interpolator utilizes IP coordinates supplied by the video coordinate computer (ICC) to calculate X_i, Y_i distances and NP_i locations. These calculated values are converted to memory addresses to retrieve S_i from a weighted product table and NP_i from the Working Block Memory (WB). A 16 product accumulated sum is kept, which when divided by 16 results in an interpolated pixel, IP.

Bilinear

Individual pixel interpolation is accomplished with Equation 1-3, whose geometrices are depicted in Figure A.6-8(b). Each

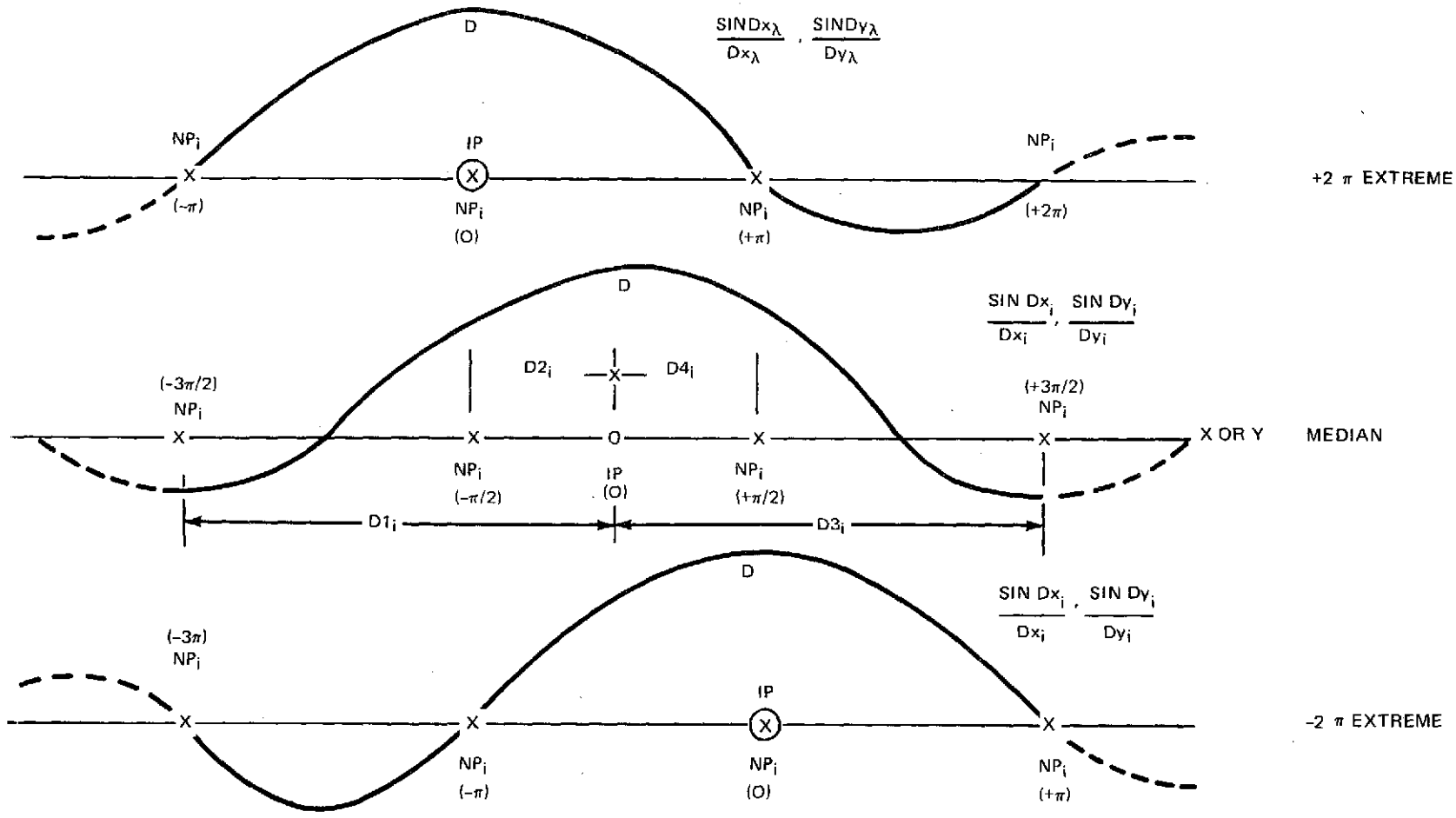

NOTE: (1) CENTER OF DISTRIBUTION CURVES POSITIONED AT THE CENTER OF THE PIXEL TO BE INTERPOLATED, ±1 NORMALIZATION)

(2) D = DISTANCE

Fig. A6-9 Normalized $Sinx_i$, $Siny_i$ Distribution Curves

$$IP = \sum_{i=1}^{i=4} NP_i \left[\left(X_i \right) \left(Y_i \right) \right]$$

$$= \sum_{i=1}^{i=4} NP_i \left(D_i \right) \qquad (1\text{-}3)$$

where:

IP = interpolated (desired) pixel at coordinate location (X, Y)

NP_i = known (true pixel at coordinate location (J, I)

X_i = absolute x coordinate distance (normalized to +1, +0) from IP to the mirror image of NP_i

Y_i = absolute y coordinate distance (normalized to +1, +0) from IP to the mirror image of NP_i

D_i = (X_i) (Y_i) product normalized to +1, +0.

Each Pixel Interpolator utilizes PI coordinates supplied by the ICC to calculate X_i, Y_i distances on NP_i locations. These calculated values are converted to memory addresses from a weighted product table and NP_i from the WBM. A 4 product accumulated sum is kept, resulting in an interpolated pixel, PI.

Nearest Neighbor

Individual video interpolation is carried out with the geometrics as illustrated in Figure A6-8(a). Each video interpolator utilizes IP coordinates supplied by the VCC to calculate, first, the nearest NP_i pair in the x direction and then the nearest NP_i per NP_i pair in the y direction. The final comparison results in an interpolated pixel, PI.

The SPP's design is configured for a maximum 400 scene throughput with the cubic convolution algorithm. This present throughput, governed by the speed of pixel interpolation, could be theoretically increased by a factor of 4 and 16 for bilinear and

nearest neighbor interpolation, respectively. That is, the BL requires 4 multiply operations and the NN requires none as opposed to 16 for the CC. Although present integrated device technology is available for a VI design with faster interpolation rates, the required data transferral rates from RBS to WBM and PI to IBS to achieve the higher throughputs cannot be obtained with the present state of bulk or random access memory device technology, unless parallelism is employed within a VBSI's design. Deployment of one VI and multiple RBS, WBM and IBS running in parallel is the only way to achieve the possible higher throughput rates. Relevant to the BI and NN, this parallelism would significantly add to a VBSI's cost as well as the SPP's overall cost.

A6.4.4 INTERPOLATED SCENE RECORD

An interpolated scene record is related to a raw scene as depicted in Equation (1-2), Paragraph A6.4.2, and derived from the geometrics of Figure A6-6. Each interpolated scene is square, S/C tilt angle removed, consisting of the interpolated raw scene (185 km^2) plus a white border. In order to interpolate, other than a white border, adjacent east-west and north-south scene data is required as depicted by $S'' = S'(\sin \alpha + \cos \alpha)$ where S' is the interpolated scene plus the white border. Due to the fact that there will never be any east-west and at times no north-south scene data beyond the 185 km^2 raw input scene area, it is proposed to square-up an interpolated scene by adding a white border. This white border, including a spelled out scene identification number within said border, will lend itself to an easier procedure for joining multiple scenes. It will also simplify the SPP's MPC and OC complexity with regard to scene interpolation as well as to pixel format records, BS, LS and P-I.

Scene interpolation is accomplished in terms of small scene blocks. Several of these scene blocks are shown in Figure A6-6. Each outer block represents the necessary raw pixel data to interpolate a complete inner block, where each inner block is composed of fractional bands and lines of equal pixel counts. Within an inner block the

dark area indicates interpolated pixels with the blank area being white in the absence of raw pixel data. Due to the lack of raw pixel data, band lines approaching the white border will be interpolated by the BL and NN as opposed to CC interpolation. This is desired because of the necessary interpolation geometrics (see Figure A6-8) where CC, BL and NN required minimum pixel samples of 16, 4 and 2, respectively.

A6.4.5 FOUR HUNDRED SCENES THROUGHPUT

In order to achieve a daily 400 scene throughput goal, the interpolation process is continuous until n raw scenes have been transformed to n interpolated scenes. That is, the IHDDT and OHDDT, once started, will run continuously until the interpolation request is complete.

To ensure no loss of data, each storage area (RBS, WM and IBS) per video band scene interpolator is double buffered and every functional process and/or transferral within the SPP is phase timed with the 400 scenes throughput - approximately 2×10^6 interpolated pixels per second.

It will be necessary to double buffer the IHDDT and OHDDT tape drives. If this is not done, the design throughput goal will be reduced by the human operation factor of tape replacement. Utilization of two tape drives would give the operators 9 tapes to replace timed with Equation (1-4).

$$T_R = T_n = (n)\,(T_s) \tag{1-4}$$

where

T_R = tape replacement time

n = number scenes per tape

T_n = time to interpolate n tape scenes

T_s = time to interpolate one scene = $\frac{16 \text{ hours}}{\text{scene throughput}}$

An assumption of 10 DOS scenes per tape (n = 10, T_s = 144 sec) leaves approximately 24 minutes for tape replacement. The MPC will utilize an audible alarm to acknowledge when interpolation is complete for each EOS scene tape. This will occur after the rewind process; however, at no time will the MPC cease EOS scene interpolation.

A6.4.6 THROUGHPUT VERSUS MODULARIZATION

The SPP's design utilizes several modules for supervising data transferral and video process control. These modules are required for interpolation of one or simultaneous multiple EOS band scenes and include:

- Master Processor Control (MPC)
- Input Controller (IC)
- Output Controller (OC)
- Band Decommutator (BD)
- Band Commutator (BC).

However, a reduction in video band scene interpolators (VBSI) can be realized but at the expense of scene throughput as depicted by Equation (1-5) and Table A6-4.

$$S_T = n(S_7/7) = (n)(\frac{400}{7}) \qquad (1\text{-}5)$$

where

S_T = Scene throughput

S_7 = Scene throughput with 7 VBSI

n = number of VBSI = (1/4, 1/2, 1, 2, 3, 4, 5, 6, 7)

A reduction in the number of VBSIs results in slightly more expensive MPC, BC, IC, OC, BD and OHDDT modules. This additional cost amounts to a fractional cost of one VBSI. The more complex OHDDT system will utilize one additional OHDDT for buffer purposes. As depicted in Table A6-4 an x quantity of IHDDT and OHDDT passes (that is, multiple tape playbacks) will be required per scene tape for complete

Table A6-4 THROUGHPUT VERSUS VBSI's

VBSI[a] (n)	Daily Throughput EOS Scenes	IHDDT/OHDDT Passes (x per Scene Tape)
7	400	1
6	342	2
5	285	2
4	228	2
3	171	3
2	114	4
1	57	7
[b]1	28	14
[c]1	14	28

[a]VBSI = Double Buffered (RBS, WBM, IBS)

[b]VBSI = Single Buffered (RBS, IBS), Double Buffered (WBM) = 1/2 VBSI

[c]VBSI = Single Buffered (RBS, WBM, IBS) = 1/4 VBSI

interpolation of n EOS scenes. For each tape pass the SPP will interpolate bands per available VBSIs. The MPC will supervise each pass, decommutating/commutating EOS band scenes and ping-ponging two OHDDT's in a fashion where one OHDDT will be in a playback mode, supplying previously interpolated bands, and the other OHDDT will be in a record mode, receiving both past and present interpolated bands. The present interpolated bands will be supplied by the available VBSIs. Upon initiating each EOS scene tape interpolation, the first tape pass will utilize a blank OHDDT to record available VBSI scenes. Thereafter OHDDT ping-pong operation will be utilized until interpolation of each EOS scene tape is complete.

Further cost reduction can be realized when a SPP is configured with one VBSI. Each RBS and IBS module per VBSI is double buffered to achieve 400 scenes throughput. Utilization of single buffered storage as opposed to double buffered storage for one complete VBSI will result in a slightly more complex MPC, BD and BC module in addition to that already stated for the IC, OC and OHDDT modules. A single buffered

RBS and IBS configuration ($^{(a)}$VBSI) will necessitate the interpolation of every other band per EOS band. This results in a scene throughput of approximately 28 scenes per day. The SPP's functional operation as described for a complete (double buffered) VBSI applies to a single buffered $^{(a)}$VBSI (1/2 VBSI). Additional cost reduction beyond a $^{(a)}$VBSI can be realized when a $^{(a)}$VBSI is configured with single buffered WBM ($^{(b)}$VBSI). System complexity for a $^{(b)}$VBSI is the same as for a $^{(a)}$VBSI except for the fact that every fourth band will be interpolated with 28 tape passes required per interpolated EOS scene tape. The daily throughput for a SPP configured with a $^{(b)}$VBSI is approximately 14 scenes.

A6.4.7 THROUGHPUT VERSUS COST

Tables A6-5 through A6-8 depict cost-throughput relationship relevant to a SPP design for interpolation in accordance with the CC, BL and NN, including selection of the desired scene format for a OHDDT record - BS, LS and P-I. The costs in the four tables are relevant to a S/C angle (α) = 12^{o} maximum. For larger S/C angles the cost will be increased by a factor approximately equal to $(\sin\alpha + \cos\alpha)^2$.

Each table represents a SPP configuration as follows:

Table A6-5 (Configuration No. 1, $\alpha = 12^{o}$)

RBS and IBS - fastest access time

RBS and IBS - moderate physical size

WBM - ultra fast access time

Table A6-6 (Configuration No. 2, $\alpha = 12^{o}$)

RBS and IBS - fastest access time

RBS and IBS - large physical size (4 times configuration No. 1)

WBM - ultra fast access time

Table A6-7 (Configuration No. 3, $\alpha = 12^{o}$)

RBS and IBS - fast access time

RBS and IBS - moderate physical size

WBM - fast access time

Table A6-5 CONFIGURATION NO. 1 - THROUGHPUT VERSUS COST
(Tape System, SPP, 9 Throughputs, $\alpha = 12^{o}$)

SPP Functional Modules	Cost Versus Throughput ($ x 10^3) EOS Scenes								
	400	342	285	228	171	114	57	28	14
MPC	225	225	225	225	225	225	225	225	225
IC	150	150	150	150	150	150	150	150	150
OC	150	150	150	150	150	150	150	150	150
BD	20	30	30	30	30	30	30	30	30
BC	20	45	45	45	45	45	45	45	45
VCC	125	125	125	125	125	125	125	125	125
	n = 7	n = 6	n = 5	n = 4	n = 3	n = 2	n = 1	n = 1/2	n = 1/4
nVBSI	12,399	10,676	9,149	7,521	5,664	4,518	2,717	2,112	1,815
Archive	Tape Systems External to Special Purpose Video Processor (SPP)								
IHDDT	450	450	450	450	450	450	450	450	450
OHDDT	300	450	450	450	450	450	450	450	450
Total Cost	Summation of Above								
	13,839	12,301	10,774	9,146	7,289	6,143	4,342	3,737	3,440

Table A6-6 CONFIGURATION NO. 2 - THROUGHPUT VERSUS COST
(Tape System, SPP, 9 Throughputs, $\alpha = 12^{o}$)

SPP Functional Modules	Cost Versus Throughput ($ x 10^3)								
	EOS Scenes								
	400	342	285	228	171	114	57	28	14
MPC	225	225	225	225	225	225	225	225	225
IC	150	150	150	150	150	150	150	150	150
OC	150	150	150	150	150	150	150	150	150
BD	20	30	30	30	30	30	30	30	30
BC	20	45	45	45	45	45	45	45	45
VCC	125	125	125	125	125	125	125	125	125
	n = 7	n = 6	n = 5	n = 4	n = 3	n = 2	n = 1	n =1/2	n = 1/4
nVBSI	10,333	8,902	7,472	6,328	4,826	3,825	2,298	1,906	1,609
Archive	Tape Systems External to Special Purpose Video Processor (SPP)								
IHDDT	450	450	450	450	450	450	450	450	450
OHDDT	300	450	450	450	450	450	450	450	450
Total Cost	Summation of Above								
	11,773	10,527	9,097	7,953	6,451	5,450	3,923	3,531	3,234

Table A6-7 CONFIGURATION NO. 3 - THROUGHPUT VERSUS COST
(Tape System, SPP, 9 Throughputs, $\alpha = 12^{o}$)

SPP Functional Modules	Cost Versus Throughput ($ x 10^3)								
	EOS Scenes								
	400	342	285	228	171	114	57	28	14
MPC	225	225	225	225	225	225	225	225	225
IC	150	150	150	150	150	150	150	150	150
OC	150	150	150	150	150	150	150	150	150
BD	20	30	30	30	30	30	30	30	30
BC	20	45	45	45	45	45	45	45	45
VCC	125	125	125	125	125	125	125	125	125
	n = 7	n = 6	n = 5	n = 4	n = 3	n = 2	n = 1	n = 1/2	n = 1/4
nVBSI	15,073	12,967	11,040	9,036	6,968	4,839	2,709	2,151	2,053
Archive	Tape Systems External to Special Purpose Video Processor (SPP)								
IHDDT	450	450	450	450	450	450	450	450	450
OHDDT	300	450	450	450	450	450	450	450	450
Total Cost	Summation of Above								
	16,513	14,592	12,665	10,661	8,593	6,464	4,334	3,776	3,678

Table A6-8 CONFIGURATION NO. 4 - THROUGHPUT VERSUS COST
(Tape System, SPP, 9 Throughputs, $\alpha = 12^{o}$)

SPP Functional Modules	Cost Versus Throughput ($ x 10^3)								
	EOS Scenes								
	400	342	285	228	171	114	57	28	14
MPC	225	225	225	225	225	225	225	225	225
IC	150	150	150	150	150	150	150	150	150
OC	150	150	150	150	150	150	150	150	150
BD	20	30	30	30	30	30	30	30	30
BC	20	45	45	45	45	45	45	45	45
VCC	125	125	125	125	125	125	125	125	125
	n = 7	n = 6	n = 5	n = 4	n = 3	n = 2	n = 1	n=1/2	n=1/4
nVBSI	13,243	11,396	9,551	7,978	6,063	4,222	2,334	1,966	1,868
Archive	Tape Systems External to Special Purpose Video Processor (SPP)								
IHDDT	450	450	450	450	450	450	450	450	450
OHDDT	300	450	450	450	450	450	450	450	450
Total Cost	Summation of Above								
	14,683	13,021	11,176	9,603	7,688	5,847	3,959	3,591	3,493

Table A6-8 (Configuration No. 4, $\alpha = 12^{o}$)

RBS and IBS - fast access time

RBS and IBS - large physical size (4 times configuration No. 3)

WBM - fast access time

Configuration No. 3 and No. 4 are presently off-the-shelf available. Configuration No. 1 and No. 2 are anticipated in 6 to 12 months. WBM byte cost for configuration No. 1 and No. 2 is approximated as twice that for configuration No. 3 or No. 4.

Relevant to the four configurations the conclusions are:

- Higher data transfer rate - lower cost (Configuration No. 1 and No. 2)
- Physically larger disk configuration - lower cost (Configuration No. 2)

A6.4.8 VIDEO BAND SCENE INTERPOLATOR (VBSI)

The present state-of-the-art for digital device technology has dictated simultaneous interpolation of 7 bands for every EOS scene interpolation.

A6.4.8.1 VBSI DESCRIPTION

A typical VBSI is depicted in Figure A6-10. These modules include:

RBS

- Double buffered band disk 1 (BDIA, BDIB)
- Double input buffer 1 (IBIA, IBIB)
- Double output buffer 1 (OBIA, OBIB)

WBM

- Double buffered video interpolation memory (VIM1, VIM2)

VI

- Video interpolator

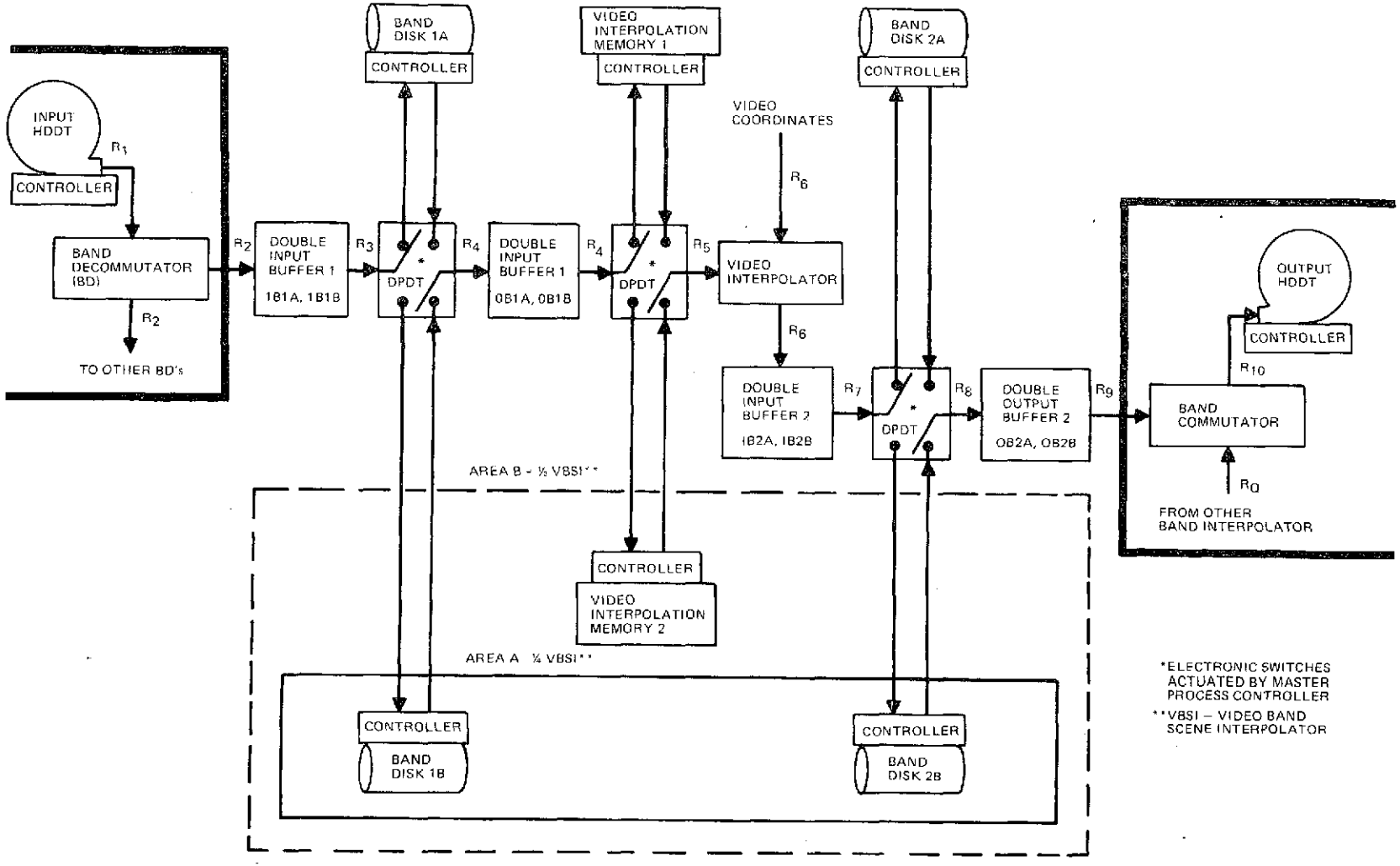

Fig. A6-10 EOS Special Purpose Video Band Scene Interpolator (Pixel Interpolation, Formatting, Routing and Storage)

IBS

- Double buffered band disk 2 (BD2A, BD2B)
- Double input buffer 2 (IB2A, IB2B)
- Double output buffer 2 (OB2A, OB2B)

A SPP can be configured with seven or as little as one complete VBSI, resulting in a cost reduction but with regressive scene throughput.

A6.4.8.2 TYPICAL VBSI OPERATION

Figure A6-11 is a VBSI timing phase diagram. For a 100 percent video interpolation efficiency (no loss of data) each VBSI must meet the following timing constraints.

$$*T_{IRBS(n+1)} - T_{IRBS(n)} \geq T_{A(n)} + T_{B(n)} + T_{c(n)}; n \geq 2$$

$$T_{A(n)} = T_{VIM(n)} - T_{VIM(n-1)}; n \geq 2$$

$$T_{B(n)} = T_{VI(n)} - T_{VI(n-1)}; n \geq 2$$

$$T_{C(n)} = T_{TIBS(n)} - T_{TIBS(n-1)}; n \geq 2$$

$$**T_{A(n)} \leq T_{B(n)}; n \geq 2$$

$$**T_{C(n)} \leq T_{B(n)}; n \geq 2$$

$$*T_{OIBS(n)} - T_{OIBS(n-1)} \leq T_{IRBS(n+2)} - T_{IRBS(n+1)}; n \geq 2$$

$T_{STX(IHDDT)}$ initiates T_{IRBSI}

$T_{IRBS(n+1)}$ initiates $T_{VTM(n)}$; $n \geq 1$

$T_{VIM(n)}$ initiates $T_{VI(n)}$; $n \geq 1$

$T_{VI(n)}$ initiates $T_{TIBS(n)}$; $n \geq 1$

$T_{IRBS(3)}$ initiates $T_{STX(OHDDT)}$

---

*Relevant to bands

**Relevant to blocks

$T_{IRBS(n+2)}$ initiates $T_{OIBS(n)}$; $n \geq 1$

T_F initiates T_{IR}

Upon receipt of status from the Grid Computer (GC) that a resampling grid is complete the master process controller (MPC) starts the input HDDT, synchronizing the IHDDT with the input controller (IC), time $T_{STX(IHDDT)}$. At time $T_{IRBS(1)}$ the first of n raw bands, one of 7 per EOS scene supplied by the band decommutator (BD), is received for storage, input buffer No. 1 (IB1A, IB1B) connected to band disk 1A (BD1A) and output buffer No. 1 (OB1A, OB1B) connected to band disk 1B (BD1B). At time $T_{IRBS(s)}$, the second of n raw bands is received for storage, IB1A and IB1B connected to BD1B and OB1A and OB1B connected to BD1A. This raw band input sequence is continued for n bands, with each raw band, odd-even, being inputted in the same manner as the first-second, respectively. For each time, $T_{IRBS(n)}$, that a new raw band is inputted IB1A and IB1B bounces in a ping-pong fashion to either BD1A or BD1B. Time, $T_{IRBS(n)} - T_{IRBS(n-1)}$ represents the time to input a complete raw band set for 185 km^2.

Upon the transferral completion of the first raw band set, time T_{IRBS2}, the first interpolation of n raw bands is initiated, time $T_{VTM(1)}$, $T_{VI(1)}$ and $T_{TIBS(1)}$. Each interpolation is accomplished in terms of small square blocks where each block is equal to (y) number of fractional band lines, each line being of equal pixel counts. Depending upon the band being interpolated, raw blocks are transferred from either BD1A or BD1B to the video interpolation memory, VTM1 and VTM2. The first block is transferred to VTM1, OB1A and OB1B connected to VTM1 and the video interpolated (VI) connected to VTM2. The second block is transferred to VTM2, OB1A and OB1B connected to VTM2 and the VI connected to VTM1. This block transfer sequence (OB1A and OB1B) ounces in a ping-pong fashion between VTM1 and VTM2 for each block and is continued for (n) (x) blocks per n bands, with each block, odd-even, being transferred in the same manner as the first-second, respectively. Time, $T_{VTM(n)} - T_{VTM(n-1)}$, represents the (x) blocks transferral time for a band set retrieved from either BD1A or BD1B.

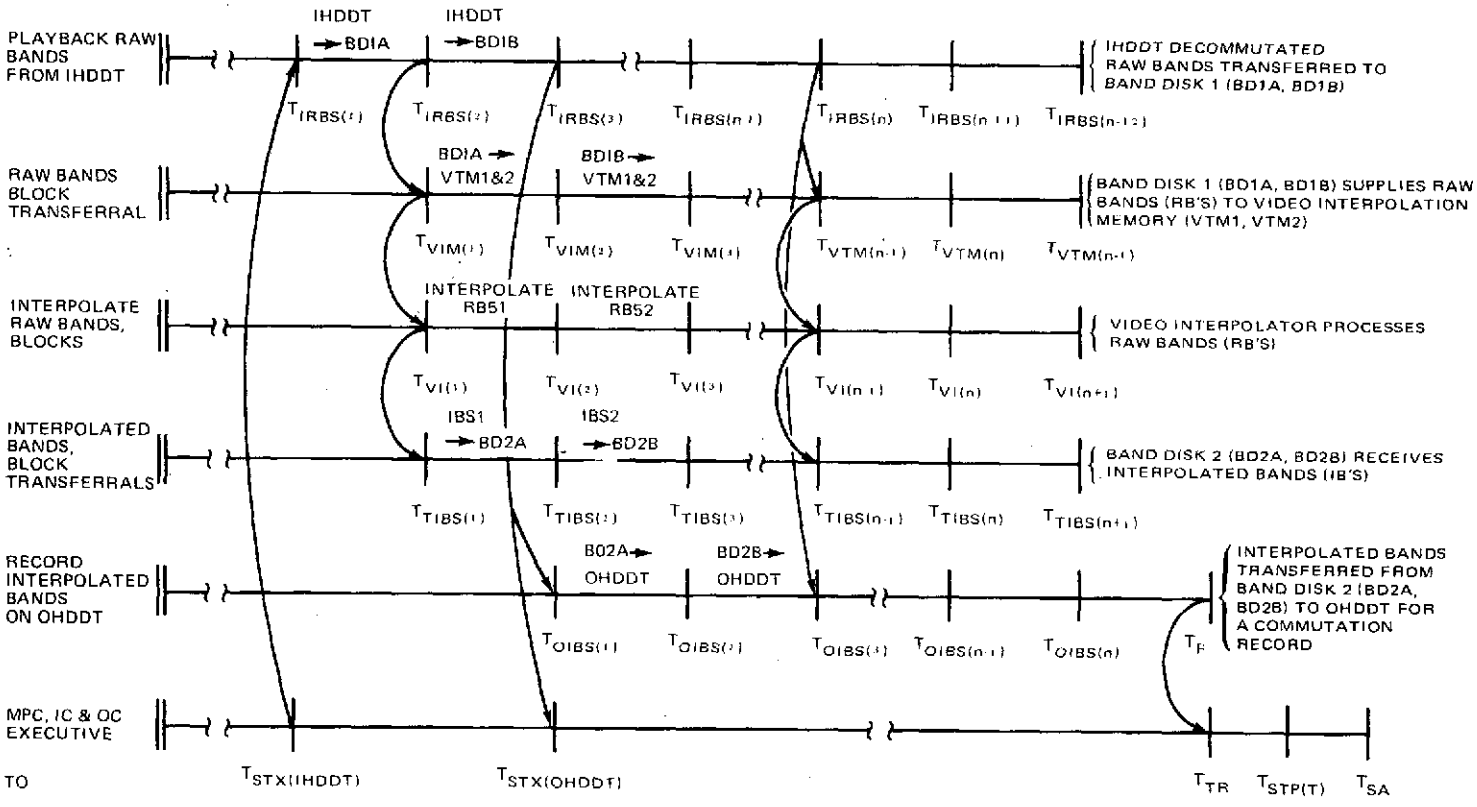

Fig. A6-11 VBSI Timing Phase Diagram (Band Scene Inputting, Inteppolation, Outputting)

With the first block available, the VI accesses VTM1, interpolating this block. Upon completing interpolation of the first block, the VI accesses VIM2, interpolating the second block. This interpolation sequence is continued with the VI bouncing in a ping-pong fashion between VIM1 and VIM2, interpolating (n) (x) blocks per n bands. $T_{VI(n)} - T_{VI(n-1)}$ represents the time to interpolate (x) blocks of a band set retrieved from either BD1A or BD1B.

Depending upon the bands being interpolated, each interpolated block is transferred to either band disk 2A(BD2A) or band disk 2B(BD2B). The odd interpolated bands are transferred to BD2A, input buffer 2 (IB2A, IB2B) connected to BD2A and output buffer 2 (OB2A, OB2B) connected to BD2B. The even interpolated bands are transferred to BD2B, IB2A and IB2B connected to BD2B and OB2A and OB2B connected to BD2A. This interpolated band input sequence is continued for n bands with the IB2A and IB2B bouncing in a ping-pong fashion to either BD2A or BD2B. Time $T_{TIBS(n)} - T_{TIBS(n-1)}$, represents an interpolated band set (small blocks) transferral time.

With the first interpolated band in BD2A, time $T_{IRBS(3)}$, the MPC starts the output IHDDT, synchronizing the OHDDT with the output controller (OC), time $T_{STX(OHDDT)}$. At time T_{OIBS1}, the first interpolated band, one of 7 per EOS scene supplied to the band commutator (BC), is outputted for a OHDDT record. In a ping-pong fashion OB2A and OB2B bounces between BD2A and BD2B supplying odd and even interpolated bands, respectively. For each time, $T_{OIBS(n)} - T_{OIBS(n-1)}$, one interpolated band is outputted for a total of n bands per n EOS scenes. Seven interpolated bands (one per VBSI) are commutated into one EOS scene. Relevant to n EOS scenes, 7 bands per EOS scene are outputted accordant with the desired format (band sequential, line sequential or pixel-interleaved) for a OHDDT record.

At time T_F, with the last interpolated band in the OHDDT record, the MPC initiates a OHDDT and IHDDT rewind, time T_{TR}. At time $T_{STP(T)}$, with the tape rewind complete, the MPC stops both tapes, time $T_{STP(T)}$ and follows with an audible alarm, time T_{SA}, indicating that the present EOS scene interpolation request is complete.

A6.4.9 EQUIPMENT DESIGN CONSIDERATION

A6.4.9.1 THROUGHPUT REQUIREMENTS

All data formatting and transferral will be controlled by a master process controller, an input controller and an output controller in a manner to allow a video interpolator to process incoming pixels at 100 percent efficiency. This results in maximum system throughput based on the pixel interpolation rate.

Table A6-9 gives the required video interpolation rates (video data rate) to achieve a throughput design goal of 400 scenes a day for the cubic convolution algorithm. Utilization of one video interpolator per one scene (6 VB plus 1IRB) is presently beyond the state of art with respect to both cost and technology.

Table A6-9 REQUIRED VIDEO DATA RATES

Pixels Interpolated Per a 16 Hour Day	Pixel Interpolation Rate	Pixel Interpolation Time
400 visible bands	32.64×10^4 Pps	3.063 μsec pP
400 infrared bands	3.64×10^4 Pps	27.462 μsec pP
400 scenes	199.48×10^4 Pps	0.501 μsec pP

As depicted in Equation 1-6 a cubic algorithm requires at a minimum, 16 multiplications, 15 additions and 1 division. Utilization of a pipeline state-of-the-art

$$IP = \sum_{i=1}^{i=16} \frac{NP_i \left(\frac{\sin X_i}{X_i} \cdot \frac{\sin Y_i}{Y_i} \right)}{16} \qquad (1\text{-}6)$$

interpolator operating at a single maximum multiplication time of 0.125 μsec would at best result in a pixel interpolation time of 2.0 μsec. This processing time is approximately a factor of 4 slower than the required 0.501 μsec for a 400 scene throughput. However, Table A6-9 gives rise to the utilization of 7 such interpolators, one per band, to meet the scene throughput goal. This leaves approximately 30% for processing overhead (memory read cycles) which will realistically be necessary for a 400 scene throughput goal.

A VB interpolator for the IRB at a 1/9 $\left(\frac{3.063\ \mu sec}{27.462\ \mu sec} = 1/9\right)$ throughput efficiency is also used. Excess master controller time will be used to handle status data.

A6.4.9.2 IHDDT REQUIREMENTS

Compatibility with the throughput design goal dictates the IHDDT data rate to be ≥18.2784 mbps. The IHDDT data format shall be as shown in Figure A6-12, bit serial and byte serial with 8 bits per byte.

Two IHDDT will be required, both servoed together and under the control of the master process controller (MPC). The MPC will bounce in a ping-pong fashion between each IHDDT, supplying the maximum of 400 continuous EOS scenes.

A6.4.9.3 BAND DECOMMUTATOR REQUIREMENTS

Throughput compatibility dictates the decommutated data rate to be ≥ 2.6112 mbps or 326.4 kBps. The data format will be bit parallel and byte serial with 8 bits per byte. With reference to Figure A6-12, the decommutation of the 6 visible bands (VB) will result in pixel data, the one IR band will result in its pixel data as well as all status data. The IR band interpolator will utilize its excess processing time to transfer status, in between pixel interpolation, from band disk 1 to band disk 2, supplying commutation inputs (status and interpolated IRB) for an OHDDT record.

For a standard SPP configuration (7 VBSI) the band decommutator (BD) will be hard wired for channel (6 VB and 1 IRB) decommutation. With a reduced configuration, (1 through 7 VBSI, 1/2 VBSI or 1/4 VBSI) channel decommutation will be supervised by the MPC.

A6.4.9.4 INPUT BUFFER REQUIREMENTS

Raw EOS scene data supplied by the band decommutator (BD) is received at an asynchronous rate with respect to band disk 1 (BD1A, BD1B) control (clock) signal. This asynchronism will require a double buffer, input buffer 1 (IB1A, IB1B) to synchronize data transferrals, BD to BD1A or BD1B.

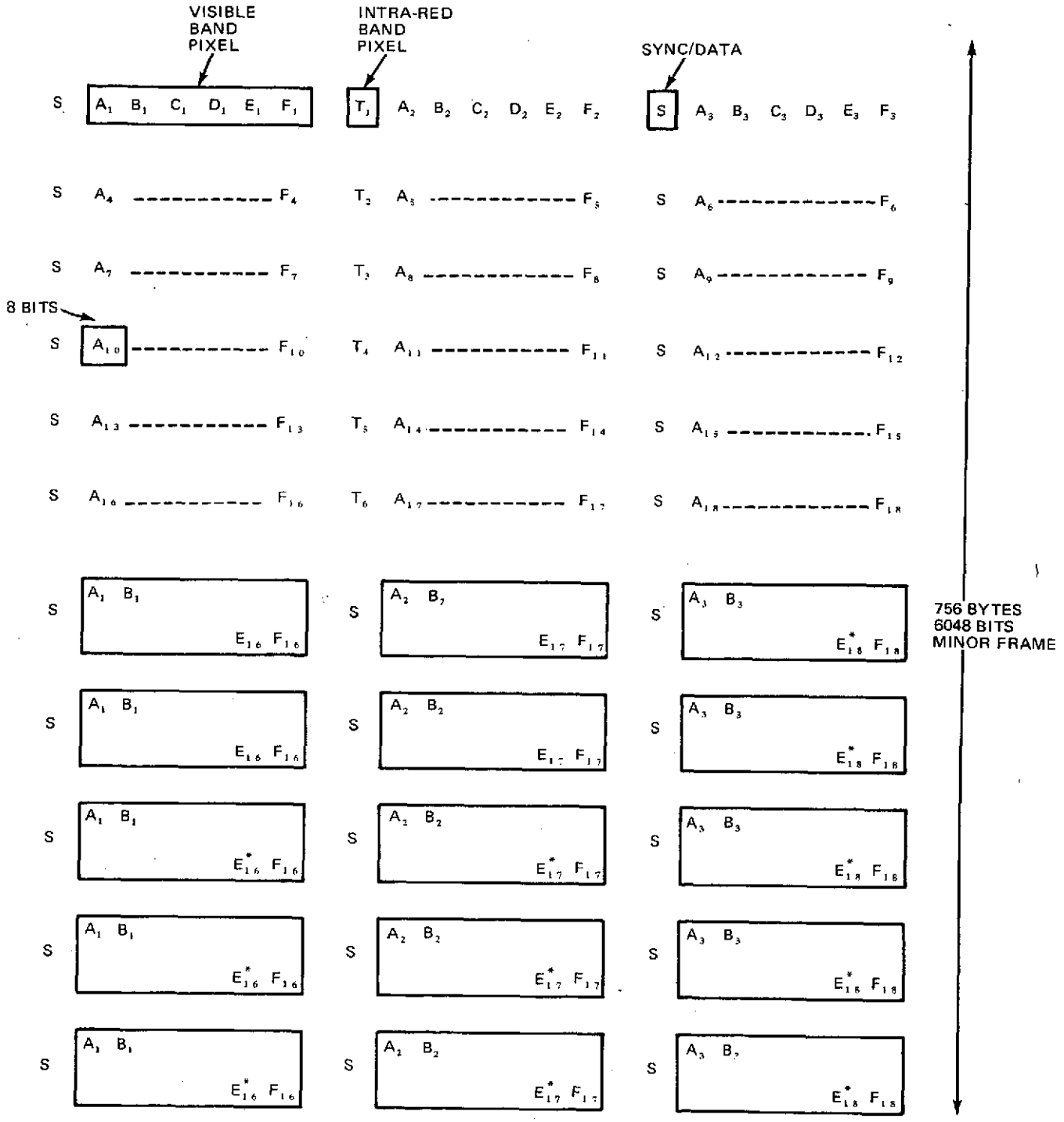

Figure A6-12 IHDDT Data Format for One Minor Frame (Natural Format, Pixel-Interleaved, BIT Serial, BYTE Serial)

With reference to Figure A6-10, the input controller (IC) will transfer BD data to IB1A at a rate equal to R2 while the data from the other buffer, IB1B, is being transferred into a disk track, BD1A or BD1B, at a rate equal to R_3. On the next input cycle data will be loaded into IB1B and read from IB1A. For each input cycle the roles of IB1A and IB1B will be reversed in a ping-pong fashion, continuing in this sequence for as long as the BD supplies data.

To assure no loss of BD data each transfer to band disk 1 (BD3A or BD1B) will be in a burst fashion. That is, R_3 will be much greater than R_2, with the average buffer read rate being equal to the write rate, R_2. The write rate is fixed in accordance with a 400 scene throughput at 326.4 kBps. Therefore, the buffer's size will be directly determined by R_3, with a faster disk resulting in a smaller buffer.

The buffer size, IB1A or IB1B, is:

$$N_B T_{BW} \geq T_{DT} = T_{DS} + N_B T_{DW}$$

where

N_B = bytes per buffer

T_{DT} = disk data transfer time

T_{BW} = time to write one buffer byte

T_{DW} = time to write one disk byte

T_{DS} = time to find disk write (sector) area

Two state-of-the-disk configurations have been investigated, one with a data transfer of 8.8 mBps (DT1 - 3600 rpm) and another at a rate of 4.4 mBps (DT2 - 1800 rpm). Utilization of the above equation results in the following buffer sizes.

$$OB1A = \frac{DT_1}{OB1B} = 6.912 \text{ kB} \qquad OB2A = \frac{DT_2}{OB2B} = 13.824 \text{ kB}$$

A6.4.9.5 BAND DISK REQUIREMENTS

Band Disk 1 data transfer rate (BD1A or BD1B) dictates the size requirement for disk input staging, IB1. This is also true for output staging and the size of the video interpolation memory (VTM). Effectively, the faster the disk, the smaller the size requirement for input/output (I/O) staging.

Standard disk systems transmit data in a bit serial fashion at a rate ≤ 10 mbps. Accordant with a 400 scene throughput, this transmission procedure is too slow for a cost effective I/O staging design. Imposing a bit parallel, byte serial transfer requirement will effectively increase the disk's data transfer rate (bit rate) by a factor of 8. Utilizing a 3 file system, reading and writing in a 1 - 2 - 3 file sequence, will result in an additional factor of 3 for a total of 24. Therefore, 3 disk files with separate controllers can be deployed for Band Disk 1, utilizing one disk surface to accommodate a bit, 8 such surfaces for a byte.

The effective disk transfer time includes the disk track's access and latency time, T_{DS}, in addition to its bit/byte data rate. The selected band disk requires a head per track, minimizing track switching (access) times and the highest possible speed of revolution (smallest latency) 30/60 rps. Disk transferrals should be in block form, utilizing track sectoring to achieve a maximum latency time of one revolution. Due to the EOS raw data format, (natural pixel-interleaved) only one byte will be disk written per control (clock) signal. Each EOS scene progressively supplies groups of 18 complete band lines (BSL). Therefore, this feature will be utilized, writing 18 BSL (≈ 6.852 kB) on a single disk track, to minimize the master process (MPC) and input (IC) controllers' design requirements. Although writing one byte per disk clock period results in a reasonable OB1 size, a simultaneous 3 byte disk write should be investigated in the future for a possible OB1 size reduction. The investigation should be conducted along the lines of an optimum raw band storage format versus block interpolation versus an interpolated band storage format, all relevant to an OHDDT record.

Use of 18 BSL per track, one byte per disk clock, results in the following requirements for a BD1A or BD1B band scene storage format.

- 18 BSL per track per 8 surfaces
- 6858 bits per track sector
- 2284 BSL per 8 surfaces per disk file
- 6852 BSL per 3 disk files.

To accommodate the S/C angle α, the present interpolation procedure requires block over-reads from the disk. Therefore, relevant to disk sectoring, the disk controller shall be capable of retrieving blocks from within one sector as well as within a maximum area of two over-lapping sectors. The disk will be addressable in the read mode beyond that of a sector.

Two state-of-the-art disks have been investigated relevant to desired band disk 1 (BD1) design requirements. Both configurations, disk type 1 (DT1) and disk type 2 (DT2) satisfy the design goals. DT2 dictates larger I/O staging size requirements as opposed to reduce needs for DT1. A VBSI configuration deploying DT1 will require semi-conductor memory whose anticipated availability will be within 6 to 18 months. The DT1 and DT2 specifications are:

DT1	DT2
8.8 mBps	4.4 mBps
3600 rpm	1800 rpm
150 kb/track	150 kb/track
128 tracks/surfaces	128 tracks/surface
1024 tracks/file	1024 tracks/file
3072 tracks/3 files	3072 tracks/3 files

A6.4.9.6 OUTPUT BUFFER REQUIREMENTS

Output buffer 1 (OB1A, OB1B) will double buffer data transfers (3 bytes, one per file) from band disk 1 (BD1A, BD1B) to the video interpolation memory. Each file control signal will be used to write bytes into the VIM. OB1A will synchronize a

file byte to a control signal edge. The second buffer, OB1B, will synchronize the OB1A byte to a memory write cycle. Each write pulse will be synchronously generated from each file control signal.

A6.4.9.7 VIDEO INTERPOLATION MEMORY REQUIREMENTS

The video interpolation memory (VIM) is sized to accommodate the following:

- Interpolation algorithm
  Cubic (CC), Bilinear (BL), and Nearest Neighbor (NN)
- S/C tile angle, α
  Present $\alpha_{max.} = 12^{o}$
- Square scene block interpolation
  Blocks composed of (x) BSL where each BSL contains (x) bytes.

The VIM will be segmented into three sections with each section receiving one group of 18 fractional band lines (FBL) per a BD1 read cycle. BD1 supplied data will be written into the VIM on a byte basis at a band disk 1 (BD1) clock rate. Utilization of a high speed disk, generating a memory write clock from the disk clock, will require a high speed VIM. Two investigated disk configurations, one with a 8.8 mBps data rate (DT1) and another with a 4.4 mBps data rate (DT2), result in minimum memory write cycles ($1/R_4$, Figure A6-10) of 114 nsec. and 224 nsec., respectively. For both configurations the VIM will require bipolar technology.

Although the VIM will be written on a block basis, the required high speed of interpolation as well as S/C angle α accommodation will dictate access on a random basis. Therefore, the VIM is a bipolar RAM. The CC interpolation, requiring the fastest access, needs an access time of $\leq$ 75 nsec.

A review of bipolar memory building elements located one element that now meets all specifications. However, meeting the 114 nsec. requirement write cycle per DT1 clock necessitates operating the bipolar memory element at the high end of its write cycle specification (minimum of 105 nsec). Within 6 to 18 months a better element is expected to be available for a DT1 configuration.

The VIM must be double buffered (VIM1, VIM2 per Figure A6-10) to achieve the 400 scene throughput. Each memory will be loaded in a ping-pong fashion from OB1, either BD1A or BD1B. Data transferrals from BD1 to VIM will be in burst fashion at rate $R_4 >> R_6$ (Figure A6-10) with the average transfer rate being equal to R_6, the rate of video interpolation. This transmission procedure will assure no loss of data.

The VIM size in accordance with Equation (1-8):

$$k N_{VIM} T_{IP} \leq T_{DT} = T_{DS} + N_{VIM} T_{DR} \qquad (1\text{-}8)$$

where

N_{VIM} = pixels per VIM

T_{IP} = time to interpolation one pixel (P)

T_{DT} = disk data transfer time

T_{DS} = time to find disk read areas

T_{DR} = time to write one disk byte (pixel) into VIM

k = block interpolation efficiency relevant to the S/C angle α, $< 100\%$

Utilization of Equation (1-8) with disk configurations DT1 and DT2 results in large VIMs (VIM1 or VIM2).

DT1	DT2
VIM 1 or 2 = 221.184 kB	VIM 1 or 2 = 580.608 kB

These VIM byte counts are probably larger than desired and should be investigated in the future for possible reduction. A reduction in S/C angle α could result in a N_{VIM} reduction proportional to k. However, at $\alpha = 12^{o}$ the N_{VIM} reduction is not worth the effort. Presently, T_{DR} is negligible and T_{DS} is kept to a minimum with employment of the fastest available disk (DT1), 3600 rpm.

A N_{VIM} reduction may be possible with an increase in memory segmenting, thereby loading the VIM on a 2 or 3 FBSL basis as opposed to the present block pro-

cedure, 54 FBSL minimum. Video interpolation will still be on a block basis, but once there is no longer any need for present FBSL, they will be replaced immediately with fresh FBSL. This progressive replacement of FBSL will result in a complete new raw scene block for interpolation immediately following the last pixel interpolation for the present block. This memory up-dating procedure reduces VIM size requirement by a factor of two, eliminating VIM1 or VIM2. However, this could present a problem relevant to determining the unique raw scene storage format required for the almost continuous FBSL output from BD1 and would probably complicate the MPC and IC design. These VIM size reduction approaches require additional study.

A6.4.9.8 VIDEO INTERPOLATOR REQUIREMENTS

Figure A6-13 depicts the required phase timing for a dual pixel interpolator. Each interpolator will share the VIM in addition to weighted intensity distribution look-up tables (S_i and D_i for CC and BL, respectively). This is depicted in Figure A6-13 as I_1AC/I_1DBL and I_2AC/I_2DBL. Each interpolator will contain a double buffer pixel holding register to achieve continuous interpolation. Thus, there will be no wait time for a memory data fetch cycle, resulting in continuous operation as illustrated for I_1PI and I_2PI.

The combined pixel interpolation rate (PIR) is given in Equation (1-9):

$$PIR = \frac{2n}{4\,K_1T + 2\,k_2T + n\,k_3T + k_3T} \qquad (1\text{-}9)$$

where:

PIR = effective VI pixel interpolation rate

$k_1 \leq k_2 \leq k_3/2$

T = time for one pixel interpolation (μsec)

n = number of continuous interpolations, $n >>> 1$

For $K_1 = k_2 = k_3/2$ and $n >>> 1$, the PIR is, in Equation (1-10):

$$PIR = \frac{n}{13T + nT} \approx \frac{1}{T} \qquad (1\text{-}10)$$

To accommodate the S/C angle α, T (μsec) in Equation (1-10) must be <3.063 μsec per VBSI. The required value of T is $\leq \frac{3.063}{1.2\,(\sin\alpha + \cos\alpha)^2}$ and for α equal to 12^{o} a realized PIR $\approx$ 552 kBps. This PIR requirement will satisfy a system design throughput goal of 400 scenes per 16 hour day.

Each pixel interpolator will be capable of interpolation with CC, BL and NN, controlled directly by the MPC. Look-up tables S_i and D_i will be addressed (two dimensional) with 12 and 10 binary encoded bits, respectively. Each ROM table output will be 8 bits binary magnitude. Required memory access time for D_i and S_i is $\leq$400 nsec. and $\leq$ 75 nsec., respectively.

A6.4.9.9 INPUT BUFFER 2 REQUIREMENTS

Input buffer 2 (IB2A, IB2B) system operation and requirements are identical to those for IB1. Relevant IB2, band disk 2 (BD2A, BD2B) replaces band disk 1 (BD1A, BD1B). In Figure A6-10, R_6 replaces R_2 and R_7 replaces R_3. The IB2 (IB2A, IB2B) write rate is fixed at 552 kBps. Therefore, the buffer's size will be governed by R_7, with a faster disk resulting in a smaller buffer. The buffer, sized in accordance with the two previously mention disk configurations, DT1 and DT2 is determined by Equation (1-7)

$$IB2A \overset{DT1}{=} IB2B = 17.408 \text{ kB} \qquad IB2A \overset{DT2}{=} IB2B = 26.112 \text{ kB}$$

A6.4.9.10 BAND DISK 2 REQUIREMENTS

Band disk 2 (BD2A, BD2B) requirements are identical, including study results, to band disk 1 except:

- 4 disk files are deployed for BD2A or BD2B
- Band lines (BSL) have a different pixel count
- A 4 byte read and write is available
- A one byte write sequence of 1-2-3-4 disk file is employed
- Disk file addressable in read/write made only for a sector.

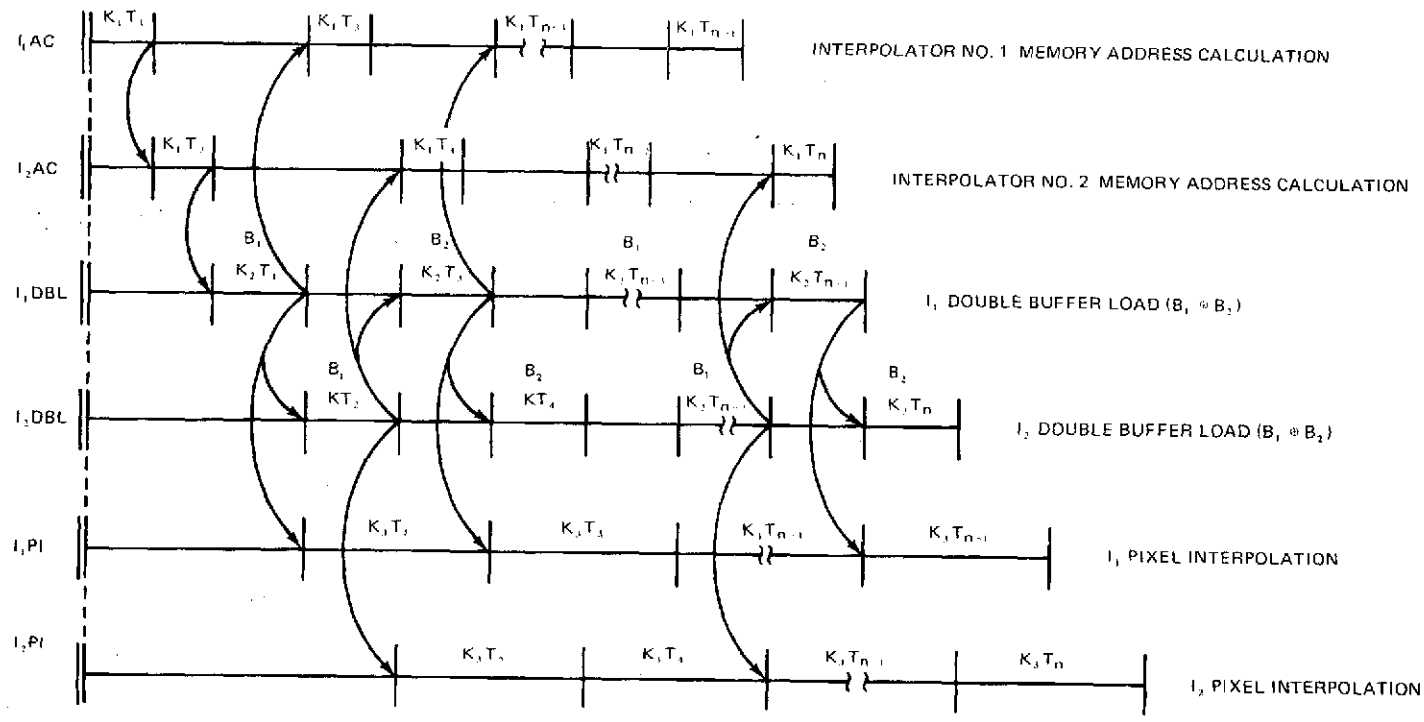

Fig. A6-13 Duel Pixel Interpolator Phase Timing Diagram (Address Calculation, Double Storage Interpolation)

Relevant to the two disk configurations, DT1 and DT2, the pixel count per BSL as well as the number of BSL per interpolated band scene is directly proportional to (sin α+ cos α) plus a reflection from band disk 1 (DT1 or DT2) to the VIM. Each interpolated BSL is calculated from Equation (1-11).

$$BSL = AN = \left[\left(\frac{185\ km}{27\ m}\right)\left(\frac{\sin\alpha + \cos\alpha}{N}\right)\right] N \qquad (1\text{-}11)$$

where:

BSL = pixel count per interpolated band line

A = highest whole number

N = pixel count for a fractional interpolated band relevant to a block size per VIM1 or VIM2.

Results of Equation (1-11) for DT1 and DT2 yields a BD2A or BD2B track allocation of 17 BSL. The total interpolated band storage format requirements for BD2 are:

DT1

- 17 BSL per track per 8 surfaces
- 8303 bits per track sector
- 2076 BSL per disk file for 3 files
- 2075 BSL per disk file for 1 file
- 8303 BSL per 4 disk files

DT2

- 17 BSL per track per 8 surfaces
- 8242 bits per track sector
- 2060 BSL per disk file for 2 files
- 2061 BSL per disk file for 2 files
- 8242 BSL per 4 disk files

BD2 size is directly proportional to the S/C tilt angle α. Reducing α could result in a 3 file system. Presently BD2B and BD2A provide storage for interpolated bands plus their white border. A reduction of BD2A or BD2B to files with storage for only interpolated video data (no white border) may be realized, but at the expense of additional cost for a MPC and IC design. This BD2 cost reduction (3 files) versus MPC/IC cost increase should be investigated further.

A6.4.9.11 OHDDT REQUIREMENTS

Compatibility with a 400 scene throughput dictates that the OHDDT data rate (R_{10}, Figure A6-10) shall be somewhat greater than the following for investigated disk configurations DT1 and DT2.

DT1	DT2
R_{10} = 26.8 mbps	R_{10} = 26.4 mbps

An EOS scene tape's anticipated capacity dictates the requirement for two OHDDTs, both servoed together and controlled by the MPC. A reduced SPP configuration for regressive throughputs that are less than 400 scenes per day will require three OHDDTs, all servoed together.

The recorded video format, whether for a reduced or maximum SPP system, will be selectable.

A6.4.9.12 BAND COMMUTATOR REQUIREMENTS

A 400 scene throughput requires the band commutator's (BC) input data rate per band (R_9, Figure A6-10) as follows:

- OHDDT, Format B & C (Line or Band Sequential)

  $R_9 = R_{10}/8$ (mBps)

DT1	DT2
R_9 = 3.35 mBps	R_9 = 3.30 mBps

- OHDDT, Format A (Pixel-Interleaved)

  $R_9 = R_{10}/56$ (mBps)

DT1	DT2
R = 478.15 mBps	R_9 = 471.74 mBps

The input data format will be bit parallel, byte serial with 8 bits per byte.

The BC will commutate 6 VB and 1 IRB with raw status data being outputted in the absence of IR data. The BC will be capable of providing one of 3 formats per EOS interpolated scene. The formats will be Band Sequential, Line Sequential and Pixel-Interleaved.

For a full (7 VBSI) SPP configuration, the BC will simultaneously commutate 7 bands per EOS scene. With a reduced SPP configuration (< 7 VBSI) the band commutator will receive present interpolated bands from available VBSIs and previous interpolated bands from one OHDDT for a commutated record onto another OHDDT.

A6.4.9.13 OUTPUT BUFFER 2 REQUIREMENTS

Output Buffer 2 (OB2A, OB2B) will synchronize band disk 2 (BD2A or BD2B) reads, providing required output staging in a manner identical to I/O staging for band disk 1 (BD1A, BD1B) and input staging for BD2.

The size requirement for OB2A or OB2B will be governed by Equation (1-12).

$$N_B T_{BR} \geq T_{DT} = T_{DS} + N_B T_{DR} \qquad (1\text{-}12)$$

where:

NB = bytes per buffer

T_{DT} = disk data transfer time

T_{BR} = time to read one buffer byte for a OHDDT record

T_{DS} = time to find disk read areas

T_{DR} = time to read one disk byte and write it in the buffer

With reference to Figure A6-10, the buffer read rate is R_9 $(1/T_{BR})$ and the buffer write rate is R_8 $(1/T_{DR})$. The read rate, R_9, is accordant with the desired EOS scene output format. R_9 represents an instantaneous read rate for formats C (pixel-interleaved), B (line sequential) and A (band sequential).

Transmitting format (C) requires R_9 to be equal to $R_{10}/56$. For two disk configurations, DT1 and DT2, the buffer size requirement is as follows:

DT1	DT2
OB2A = OB2B = 21.76 kB	OB2A = OB2B = 43.52 kB

Transmitting format (B) requires R_9 to be equal to $R_{10}/8$. However, the average read rate, R_9 (avg), is equal to $R_{10}/56$. That is, one line per band (x) is transmitted and the next line per band (x) is not transmitted until transmission is complete for 6 remaining band lines. Utilization of R_9 (avg) in Equation (1-12) results in the following buffer size requirement.

DT1	DT2
OB2A = OB2B = 33.792 kB	OB2A = OB2A = 67.584 kB

Transmitting format (A) requires R_9 to be equal to $R_{10}/8$. This results in the following buffer size requirement.

DT1	DT2
OB2A = OB2B = 143.616 kB	OB2A = OB2B = 287.232 lB

Although not a requirement, format (A) buffers will accommodate format (B) and (C), format (B) buffers will accommodate format (C) and format (C) buffers will only accommodate itself.

Format (C) and (B) buffer sizes are reasonable. However, format (A) buffer size is not desirable. Format (A) buffer is so large due to the fact that buffer bytes (pixels) are transmitted at a read rate (R_9) not much less than the write rate (R_8).

Equation (1-12) presents possibilities for a format (A) buffer size reduction. A size reduction could be achieved with a reduced T_{DS}. This is beyond the state-of-the-art for present disk technology. That is, DT1 is the fastest available disk, revolving at 3600 rpm. Therefore, a reduction in the buffer size requirements can only be realized with a reduction for T_{DR} or a increase in T_{BR}. The buffer's read rate is fixed for the 400 scene throughput requirement. Therefore, any reduction in the buffer's size must be achieved with a faster write rate ($1/T_{DR}$).

Utilization of the available 4 byte read rate for band disk 2 (BD2A, BD2B) could reduce T_{DW} (buffer write time) by a factor of 4. However, utilization of the available 4 byte read rate will require an additional analysis to determine the required interpolated scene storage format (i.e., a unique scene storage format will be required to achieve the desired reduction for T_{DR}).

A6.4.9.14 VIDEO COORDINATE COMPUTER REQUIREMENTS

The video coordinate computer (VCC) will be required to supply, in a recursive fashion, individual pixel coordinate to each (7 total) video interpolator (VI). Each video coordinate will be realized in terms of the video interpolation memory (VIM), relevant to addresses of known pixels within the memory. The video coordinates will also track each interpolated band scene line in accordance with a variable S/C tilt angle α (12^{o} max) supplied by the grid computer.

Because each VI contains a dual pixel interpolator (PI) the VCC shall supply 14 pixel coordinates, 2 per VBSI, at a rate equivalent to an EOS scene interpolation rate of 3.864 mPps (1 VI/VBSI x 7 VBSI x 552 kPps/VI = 3.864 mPps). Due to the fact that pixel coordinates will be identical for each VBSI, but different for each PI within a VI, the effective rate reduces to 552 k pixel coordinates per second (PCps). If this assumption is not correct then the rate will revert to 3.864 mPCps. Either transfer rate may dictate the use of a hardwired coordinate computer. Also, on a cost basis it may prove worthwhile to employ a hardware design as opposed to a software approach for coordinate computation. Further VCC definition analysis should solidify the most effective approach.

A6.4.9.15 SPP CONTROL REQUIREMENTS

The SPP will utilize a master process controller (MPC) to supervise video interpolation. The input of EOS raw scenes will be controlled by the input controller (IC) and outputting interpolated EOS scenes will be controlled by the output controller (OC). The OC and IC will be hardwired controllers, possibly the stored firmware type, and the MPC will most likely be a mini-computer (software type) configuration.

A6.4.10 STARAN CONFIGURATION

A6.4.10.1 PROCESSOR CHARACTERISTICS

The STARAN Associative Array Processor is a general purpose computer with special architecture oriented toward the common manipulation of tabular data. The basic concept of the machine is shown in Figure A6-14.

The Associative Processor Array (AP) is a 256 bit by 256 word array which can be divided into any number of bit fields. Each word in the array has its own processing element (arithmetic unit). Up to 32 arrays can be included in a single STARAN configuration, allowing a total of 256 bits by 8192 words. The AP's operate under the control of a memory and logic unit that contains the stored AP program. Conventional I/O, peripherals, operator interface, and utility software are provided by a sequential controller (mini-computer). High speed parallel I/O (on a bit-slice basis) can be provided by an optional interface (PIO). The PIO rate is 400 nsec per bit (in all words) or per word slice (256 bits). The output rate from the AP to the PIO is 200 nsec per bit or word slice.

For any given computation, the words are divided into bit fields under program control. Arithmetic and comparative operations are then performed on these fields simultaneously for either all words in the array or for selected words. For example, if there are 4 arrays, one arithmetic statement can be executed for a maximum of 1024 words (256 x 4) in the same time it takes for 1 word. With its multiple processing elements, STARAN processes the data of all selected words in one instruction execution.

To expedite high speed searches, the AP functions as a content-addressed (associative) memory. In a single memory access, the AP searches all content of its data file and identifies all elements that meet the specified search criteria. Execution times vary with the bit length (n) of the fields searched. Execution times for searches such as "equal to", "greater than" or "less than" range from .19 n + .73 μsec to .19 n + .82 μsec, where n is number of bits in the data field to be searched. Note that all selected words (up to 8192 depending on the number of arrays) are searched simultaneously.

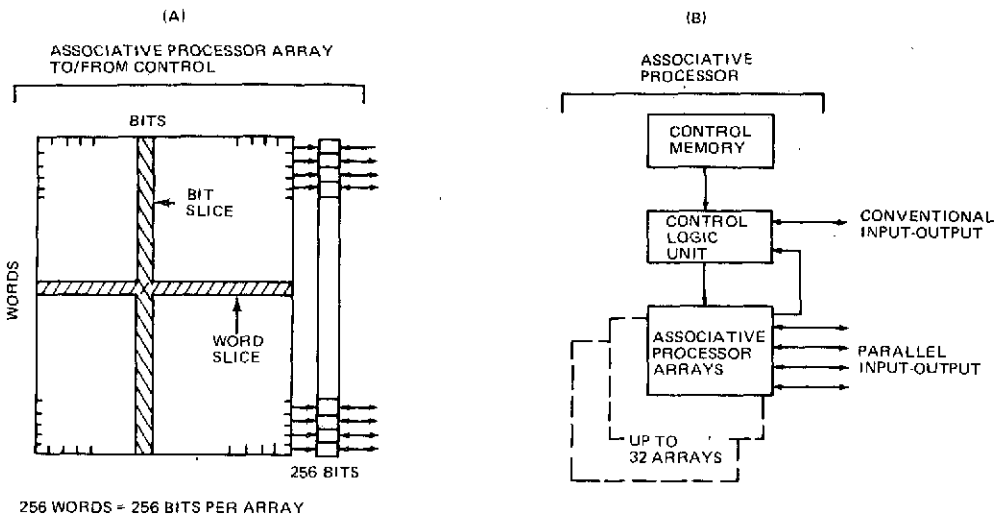

A1-38

Fig. A6-14 Associative Array Processor Concept

Selection of words in the arrays are implemented through two response store registers and one mask register shown in Figure A6-15. These registers have one bit corresponding to each word in the array (256 bits per array total). Generally, the mask selects the words for each arithmetic and/or comparative operation, and the response store tags the words that meet the specified criteria. Logical operations may be performed between these registers or with a bit column in the array to further modify the registers.

Bits in the AP array are manipulated from field to field (in each word), from bit in array to x, y or mask register and vice versa, and from field and common register to each other. For example the command ADC a, b, c adds the field a from the word plus field b from the common register and stores in field c all words which have the corresponding bit set in the mask register.

Any data stored in the AP Control Memory or to be stored there from the AP Array is transferred via the common register. The common register is the link between the AP Array and the AP Control Memory for data processing.

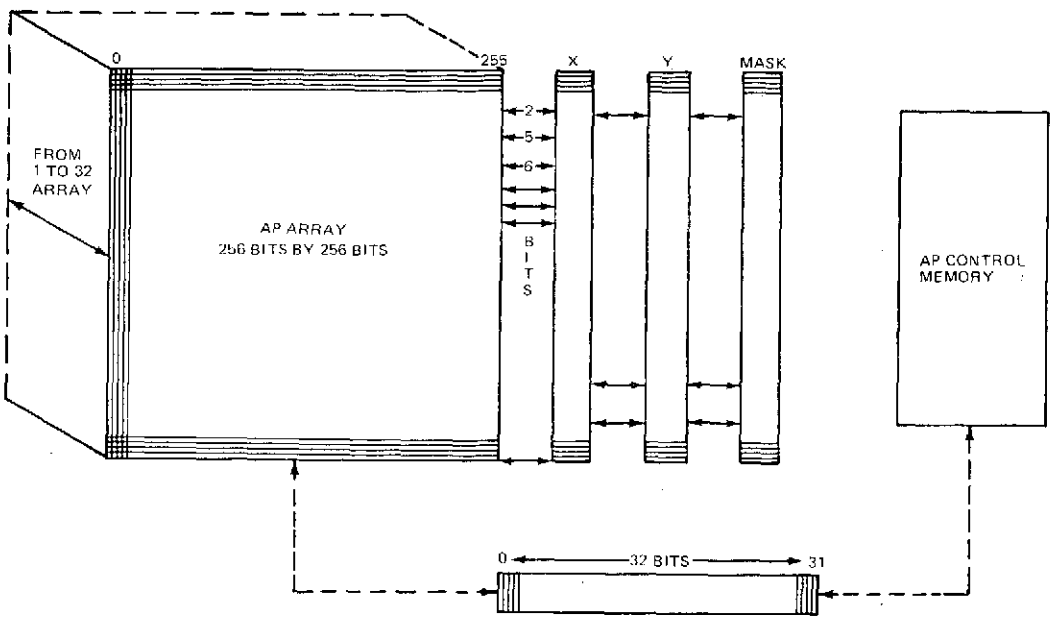

Figure A6-15 Common Register

The x and y response store registers and the mask register perform the logical operations of AND, OR, INCLUSIVE - OR, and EXCLUSIVE - OR between these registers and between register and bit field of the array. The mask register determines which words of the array are selected for operations such as arithmetic operations and move bit or move field operations.

A6.4.10.2 PROCESSING CONFIGURATION

Figure A6-16 shows a processing configuration using the STARAN AAP. Only Level II/III processing (including GCP location) was considered in the configuration design. However, it should be noted that the STARAN processor is capable of performing many other CDPF processing functions including the management of Information Services System files.

The input to the configuration is assumed to be line-rectified data resident on HDDT or in the archive. The data is loaded to a Scene Disk Bank similar to that used in the special purpose hardware configuration. The data is read from the Scene Disk Bank into a Segment Staging Memory. It is estimated that a typical Segment Staging Memory would be about 300 x 300 pixels by 7 bands.

The handling of the data is oriented toward the output lines. Thus, the input data is over-read, and the blocks loaded into the Segment Staging Memory are offset to track in stepwise fashion the angle between the input and output lines. The Segment Staging Memory is essentially the data memory for the Input Pixel Data Selection Unit, a mini or micro-computer. This data selection process represents a function that resolves a difficulty in the use of the AP for image interpolation. The problem arises because, although the AP computes the interpolated points in parallel, it would have to organize the original data points and their associated interpolation parameters serially. Such a serial procedure would be inefficient because of the architecture of the AP, and would turn to disadvantage the very features that make the AP concept attractive.

The resulting configuration is a compromise that assigns to the AP the task of performing most of the computation in parallel, while using conventional processors for the specific random access functions that are least efficient for the AP. The parallel computation performed in the AP includes the calculation of data addresses for the conventional processor. The portion of the task performed by the conventional processor is limited to the accessing of the data at the addresses supplied and some ancilliary loop control operations. An approach similar to the pixel selection is used in the selection of cubic convolution coefficients and GCP templates.

The interface between the STARAN and the various I/O and data selection processors is provided by a scratchpad array. This array is accessed by the STARAN in a bit-slice parallel mode via the parallel I/O interface. The scratchpad is accessed by the other processors in a word serial arrangement with parallel operations provided by segmentation along the lines of the STARAN structure. In its implementation, the scratchpad array is similar to a STARAN AP without the processing elements. The scratchpad serves as a queuing buffer, a storage area for intermediate results, and a speed buffer for the parallel I/O.

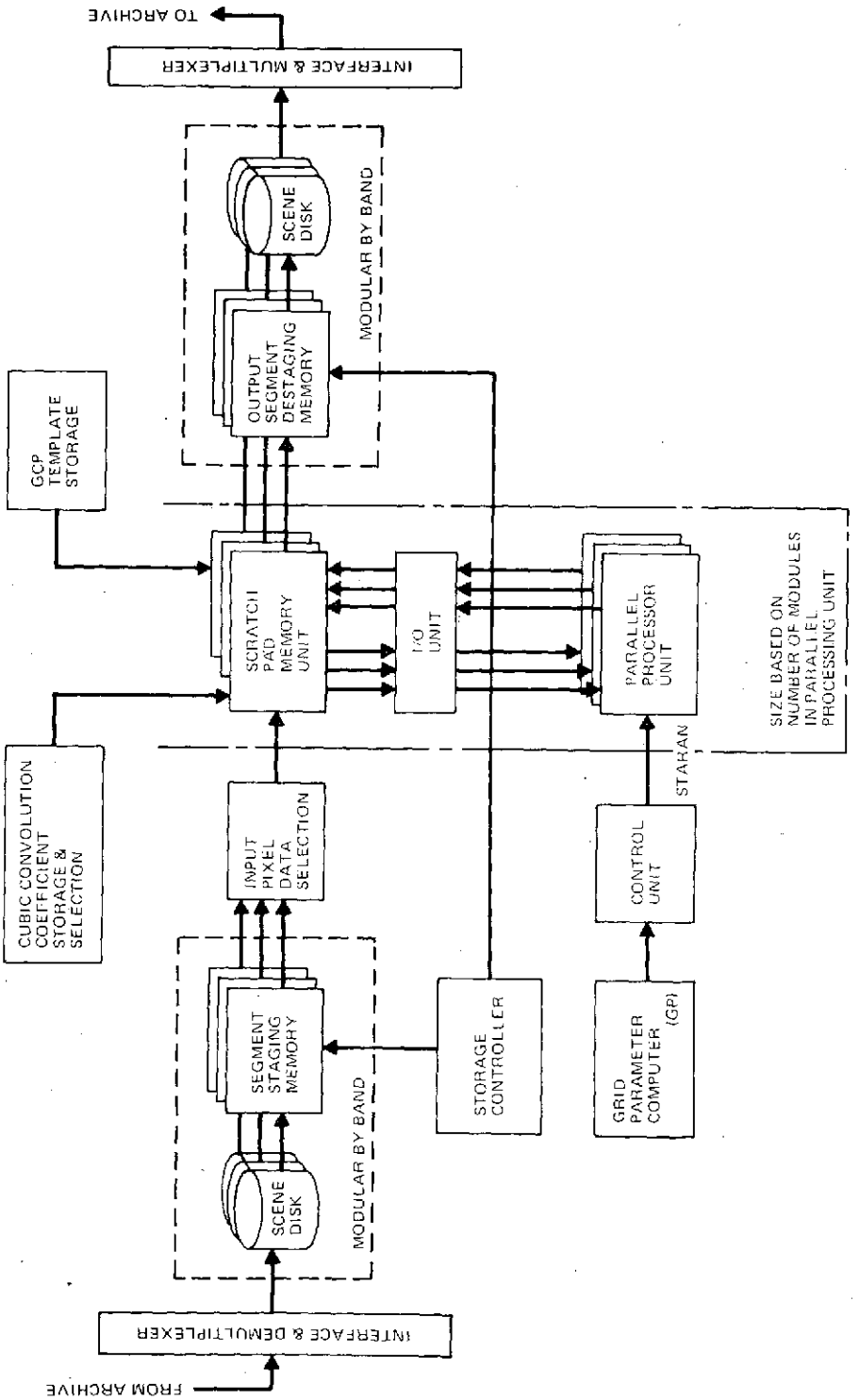

Figure A6-16 Associative Array Processor

7-53, 7-91
7-106, A7-40

The output elements of the configuration include a segment destaging memory and scene disk bank similar to the equivalent input elements.

A6.4.10.3 THROUGHPUT

The throughput of the STARAN is proportional to the number of arrays utilized. The processing takes place in a "batch mode", i.e., the STARAN handles 256 to 8192 pixels in a batch and performs all processing simultaneously. The scratchpad is sized and segmented as a double or triple buffer so that areas can be simultaneously accessed for input, output, and processing. The basic process is as follows:

(a) The STARAN performs the coordinate computation based on parameters supplied by the grid parameter computer. This may utilize fixed tables of initilaization constants stored in the scratchpad. The result of the computation is a pair of x and y coordinates for each output pixel. These coordinates take the form of an integer part and a fractional part. Based on the low data bits of the integer part, the STARAN computes the addresses of the pixel data required for the interpolation step. This will involve four values for nearest neighbor or bilinear and sixteen values for cubic interpolation. The STARAN stores the fractional parts f_x and f_y in the scratchpad array, together with the addresses of the pixel data. If cubic interpolation is being used, the STARAN also computes the addresses of the coefficients, using the fractional parts of the output pixel location.

(b) The input pixel selector unit reads the addresses of the pixel data from the scratchpad and places the pixel data values in the scratchpad. If cubic convolution is used, the coefficient selector likewise looks up and places the coefficients in the scratchpad.

(c) The STARAN performs the interpolation computation. It is most efficient to perform all bands in the same batch because of the common use of certain intermediate results. As an example, the organization of the array and scratchpad for bilinear interpolation are shown in Figure A6-17.

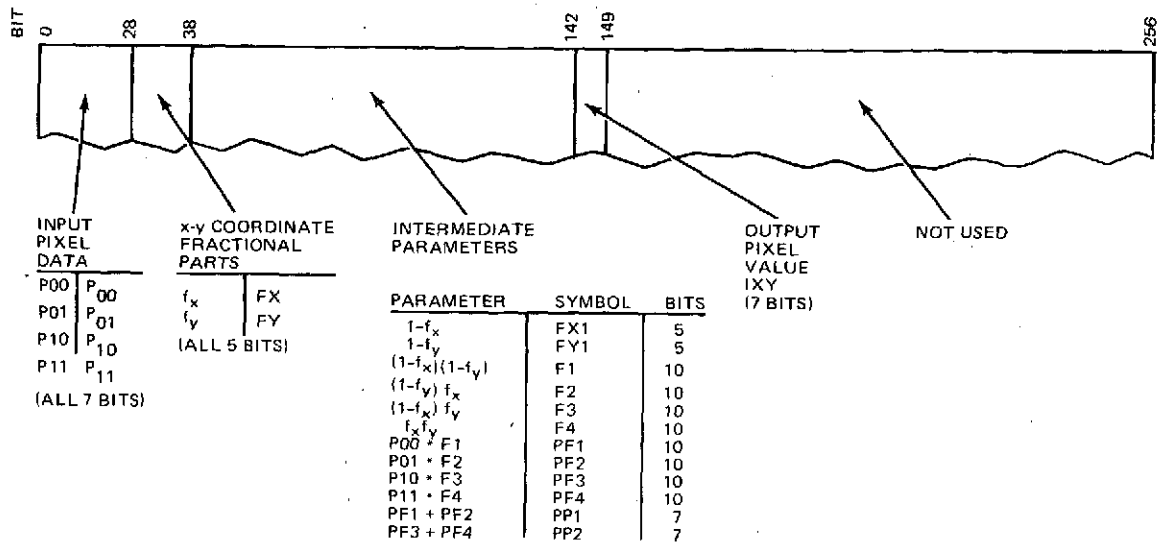

A7-41

Fig. A6-17 Associative Array Processor Variable Field Assignments

Rough timing estimates for the interpolation algorithms have been calculated assuming data alignment before entering the array. The nearest neighbor calculation senses the highest order bits of the fractional representation of the x and y coordinates. Using the four coordinates as described by Figure A6-18, the bits from x and y are compared for all coordinates using four logic instructions between bit field and mask bit. The move instructions move the bits to the output field. Based on eight bit fields, the four logic and move instructions plus input and output time take about 33.66 microseconds for 256 points per array up to 32 arrays of 8291 points.

The bilinear interpolation algorithm is based on equation

$$I_{xy} = \left[P_{00}\,(1 - f_x) + P_{01}\,f_x\right](1 - f_y) + \left[P_{10}\,(1 - f_x + P_{11}\,f_x\right]f_y$$

Since for all bands the f_x and f_y terms are the same at each point, the computations are completed for one band and then the new P values are entered for another band. The previously calculated f_x and f_y terms are not recalculated. In addition to a mask set and a load common register with 1.00 (for $1.0 - f_y$, etc.), this algorithm requires two subtracts for the initial band. Subsequent calculations for all bands

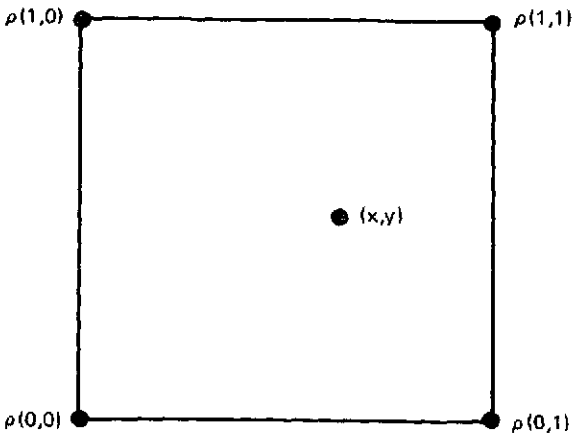

Fig. A6-18 Pixel Point Coordinate System

A7-42

include six multiply fields and three add fields. Using seven bits for each point, five for f_x and f_y, and 8 bits for I_{xy}, the computation time excluding input and output is 1548 microseconds for 256 to 8192 points for six bands. Input time via the PIO is 15.2 microseconds for 38 bits and output time is 1.6 microseconds for 8 output bits.

The remaining AP computations are the addressing and the coordinate computations. The addressing involves finding the four points P (i, nj), P (i + 1, nj), P (i, n (j + 1)) and P (i + 1, n (j + 1)), where each point is six bits. The computation for addressing (without I/O) is 130.23 microseconds for the 4 points.

$$x_i = x_0 + (\Delta_{1x} + \Delta_{2x}\, j)\, i$$

$$Y_i = y_0 + (\Delta_{1y} + \Delta_{2y}\, i)\, j$$

The calculations of x_i and y_i in the preceding equations require 4 adds and 4 multiplies for a total of 309.08 microseconds excluding I/O. Each delta is assumed 8 bits, and i and j are six bits. The initial x and y values (x_0, y_0) are assumed to be 20 bits each. Again this is for 256 to 8192 words depending upon the number of arrays. In the equation, i is the linear stretch in the x direction and j in the y direction.

For cubic convolution, the addresses of the pixels and the coefficients are calculated first in the AP array. These addresses are then entered into the scratchpad and passed to the selection units. The coefficients corresponding to the pixels and coefficients are extracted from the tables by the selection units and enter the AP through the buffered scratch area. From the scratch array the data is input in parallel through the PIO into the AP array. The cubic convolution coefficients require 16 multiply fields and 15 add fields calculations. The total time including the addressing is 7888 μsecs or approximately 7900 μsec.

Table A6-10 summarizes the steps and indicates the assembler coding used in the STARAN system.

A 400 scene per day requirement implies a processing rate that handles one pixel (all bands) in 3 μsec. Assuming 7900 μsec for cubic convolution, an 11 array STARAN configuration (7900 ÷ 3 ÷ 256) will fulfill this requirement. A 20 scene per day system requires the minimum configuration of 2 arrays.

Table A6-10 TYPICAL STARAN PROCEDURE FOR BILINEAR INTERPOLATION (6 Bands)

Step	STARAN Assembler Coding
a. Define the fields in the array to be associated with each input, output, and intermediate variable.	The program coding defines each field in a "DF" statement.
b. Define the arrays (numbered 0 to 31) to be included in the calculation.	LI, 2 AS, X'C000'
c. Set the mask to include all words in the calculation (assumes each word contains the information to calculate one output pixel, all bands).	L M
d. Read the fractional parts f_x and f_y from the scratchpad.	(Coding depends on PIO interface design)

Table A6-10 TYPICAL STARAN PROCEDURE FOR BILINEAR INTERPOLATION (6 Bands) (Cont)

Step	STARAN Assembler Coding
e. Load the value 1.00 in the common register.	LI C, 1.00
f. Compute values $1 - f_x$ and $1 - f_y$ and store in fields FX1 and FY1. The value 1.00 is contained in the common register in a field denoted "ONE".	SUBC ONE, FX, FX1 SUBC ONE, FY, FY1
g. Compute interpolation coefficients for use with pixel data. These are $f_x(1 - f_y)$, $f_y(1 - f_x)$, $f_x f_y$, and $(1 - f_x)(1 - f_y)$*.	MPF FX1, FY1, F1 MPF FY1, FX , F2 MPF FX1, FY , F3
h. Set counter for number of passes through pixel data loop. (For 6 bands loop back 5 times).	LI BL, 5
i. Begin pixel data loop. Read in values of P_{00}, P_{01}, and P_{11} for first band from the scratchpad.	LOOP (remaining coding depends on PIO interface design)
j. Multiply pixel values by coefficients and save the results in intermediates variable fields.	MPF P00, F1, PF1 MPF P01, F2, PF2 MPF P10, F3, PF3 MPF P11, F4, PF4
k. Sum the products calculated in Step (j) to compute the output pixel values IXY.	ADF PF1, PF2, PP1 ADF PF3, PF4, PP2 ADF PP1, PP2, IXY
l. Output the calculated pixel values to the scratchpad.	(Coding depends on PIO interface design)
m. Perform loop control.	BX, BL DONE, 1 BRS LOOP DONE END

* When multiplying fields the product field bits must be the sum of the bits in the multiplier and multiplican fields. For example, if FX1 and FX2 are 5 bits each F1 must be at least 10 bits. The fields may be redefined during the calculation. For example, if only 7 bits of F1 are needed for subsequent operations, not all 10 bits need be used.

APPENDIX B PROGRAM EFFECTIVENESS ANALYSIS

B.1 INTRODUCTION

The limitation of budgets available today for space payloads requires that performance analysis emphasize cost-effectiveness. Designers must now attempt to achieve the best level of performance possible within a fixed total cost constraint, and must stringently justify any increased cost for higher performance. The analysis is complicated by the potential accommodation of multiple alternative instruments aboard a given spacecraft, and by the potential servicing or retrieval of the spacecraft and instruments which will extend the observatory useful life. The success of the missi can no longer be characterized by the launching of the highest-weight, most-reliable, working spacecraft, for experience has shown that outright failure seldom occurs in orbit. More commonly, the performance of the spacecraft slowly degrades from full capability down to unacceptably low levels.

Users of orbital observatories desire high quality, long-term observation capabilities to satisfy their needs. Thus the evaluation of orbital observatories should account for the quality and quantity of the data returned, and the cost of the system. These factors depend on the state of technology and the budgeting environment. All of the performance parameters may be collected under the title "System Effectiveness", so that systems are evaluated in terms of effectiveness and cost. For the EOS System Definition Study we have built and programmed a mathematical model to compute the effectiveness of an EOS system design in achieving the EOS mission objectives.

B.2 PURPOSE OF THE EFFECTIVENESS MODEL

During the process of system design there arises three types of evaluation problems:

1. The System Optimization Problems

   Within a total cost constraint, design a system to bring about the best results by proper selection of system elements from all the potential alternates.

2. The Design/Cost Trade Problem

   In the absence of an absolute budget limit, choosing the most "cost-effective" design. That is, one that is worth its cost and has a high cost/performance value relative to the alternatives.

3. The System Effectiveness Problem

   Evaluating a particular system design with respect to its achievement of program objectives.

The EOS Effectiveness Model provides an approach to the solution of these problems. An Effectiveness Model expresses the sensitivity of system performance to changes in all hardware design parameters to the level of detail required for design discussions.

Figure B-1 shows the relation between the effectiveness evaluation and the other tasks involved in the overall EOS System design approach. In the System Definition Study system design alternatives were synthesized by accounting for both the major system options and potential budgetary levels available. These alternatives were evaluated by performing many design cost trades and the data resulting from the trades was provided as input to the effectiveness model. This data was combined in the model to provide a top level performance value for each alternate which was then combined with the cost of the alternate to provide a basis of comparison and to aid in the selection of the preferred EOS design approach.

B.3 THEORY OF EFFECTIVENESS MODELS

An Effectiveness Model methodically relates evaluating criteria, and hardware design and performance parameters to the system purpose. It calculates a single characteristic measure of the success of the alternative system designs at achieving the system objectives. It thus compares alternative designs against common standard. The measure of performance which is calculated is called the "figure of merit" or "FOM". The FOM is a dimensional, cardinal number expressing the effectiveness of a system design alternative. The effectiveness model quantifies the system performance in terms of timeliness, usefulness,

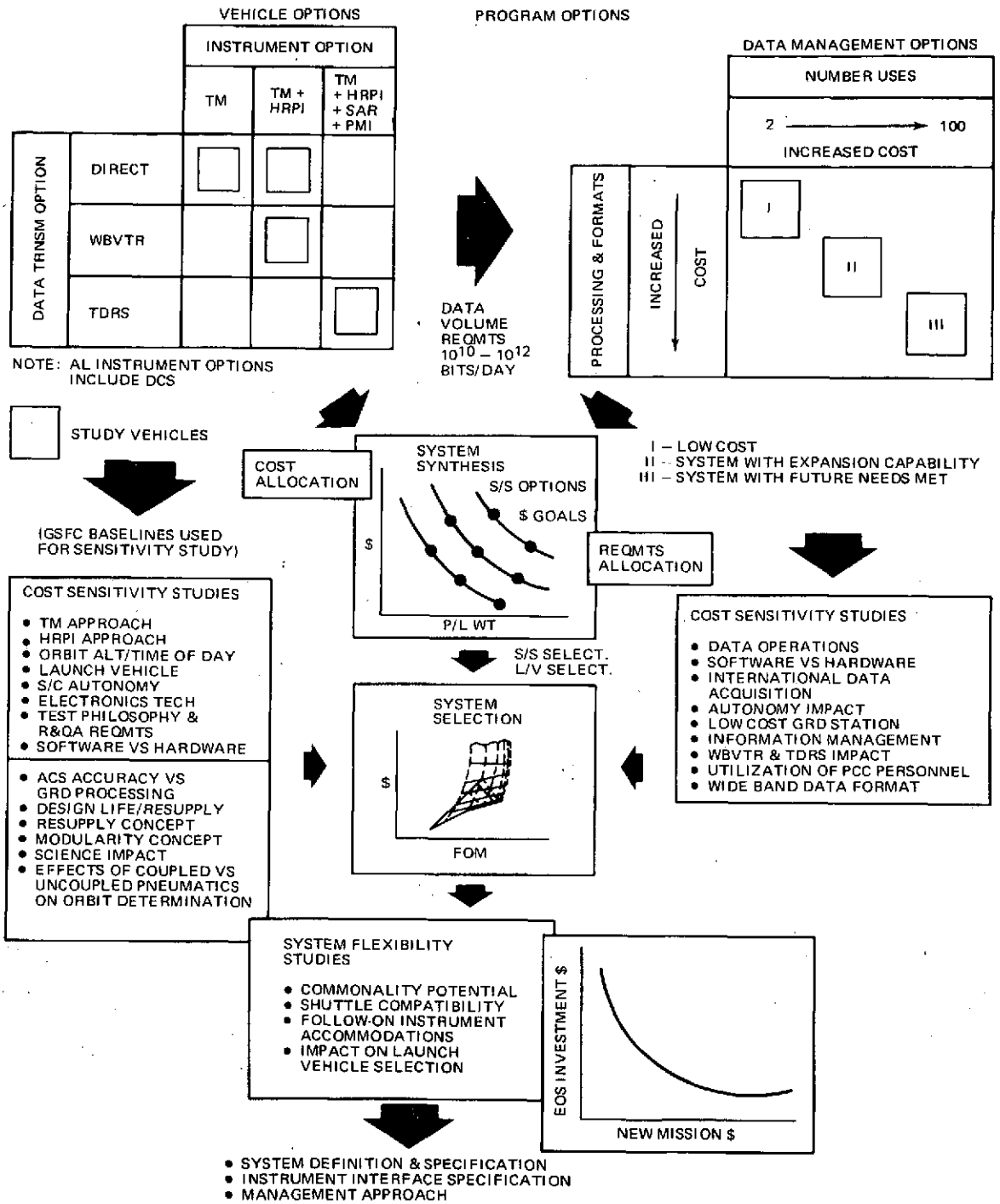

3-133
7-54
A7-43

Fig. B-1 System Design Approach. Cost is a Significant Factor in Our Design Approach.

and importance of the amount of data it returns to the users. In our approach the FOM is calculated directly from the hardware parameters of each design alternate. In this case the performance of an alternate is uniquely evaluated in measurable terms which include each element's contribution to the overall performance. In our model the following parameters are included:

- Instruments
  - quality of data
  - quantity of data
  - uptime
- Spacecraft
  - quality of subsystems
  - uptime of subsystems
- Launch Vehicle
  - Reliability
- Data Processing System
  - quantity (throughput)
  - quality of processing
  - uptime of hardware and software
- Data Products
  - quantity
  - quality
  - timeliness.

For the EOS the FOM should count the number of useful output products delivered to the users. For simplicity in understanding of results and for ease of comparison more of the products counted should be preferred than fewer. Since the FOM is a measure of value, all alternative designs may be compared in benefit by their corresponding values expressed by their FOM. In this case alternative designs may be compared in benefit by the FOM

in the same manner in which they can be compared in outlay by their dollar costs. In fact the ratio of the FOM to the dollar cost of an alternate expresses a measure of the marginal change in system cost-effectiveness achieved by any proposed change in the system configuration. A dimensional FOM allows us not only to rank alternatives but also provides for a means of determining what is the magnitude of the difference between alternatives.

Computation of the EOS FOM allowed us to solve the three design evaluation problems posed in Subsection B. 2 in the following ways:

1. The System Optimization Problem

   We can select the "best" design for the budget constraint as the one which achieves the highest value of the FOM.

2. The Design/Cost Trade Problem

   We can directly compute the improvement or decrease in performance expected by a design change and the associated increased or decreased cost to determine if the cost increases are justified and if the cost decreases, produce a system which remains acceptable.

3. The System Effectiveness Problem

   We can evaluate directly how well each alternate EOS system performs.

The model also allows for evaluation of synergistic affects of trades on the entire system which may not be evident on an individual trade basis, and enables easy identification of primary and secondary system drivers.

Of course the items given above are the most obvious benefits gained from the use of an effectiveness model. However, perhaps the most valuable benefit gained from the performance of this analysis is much more subtle. The mental exercise and frame of mind produced by the act of laying out the structure of the effectiveness tree causes the analyst and the designers which are supporting him to think systemmatically about how the design gets together. Use of this systemmatically disciplined logical thought process often brings to the surface previously unsuspected combinations of design features.

These combinations may be of great benefit even though each individual feature may not appear to be particularly attractive.

B.4 THE EOS FIGURE OF MERIT

As we have said, for the EOS system the FOM should count output products produced per unit time. Since the products and the instruments produced differ greatly they all must be related to some standard quality product so that the trades between quality and quantity of products can be made. In our analysis we have chosen a TM scene converted to a composite data product as the standard. The composite reflects the expected variation in both product mix and level of correction as deduced from a combination of previous studies using ERTS data and the expert opinion of our user consultant, Dr. M. Baumgardner. The TM scene has the following characteristics:

- 185 x 185 km ground size
- 7 spectral bands
- $\pm$ 15 meter spatial resolution.

If the operation of the system were perfect, useful output products produced per unit time would be an adequate FOM for the EOS. However no system is perfect. System failures, degraded operation, and delays are possible, and in fact probable for long term operational systems. The probabilities of occurrence of these units reduce the potential effectiveness of the system. These probabilistic factors are accounted for by that fraction of the total time which the system is operational. This fraction is called the "uptime ratio" or uptime.

Thus the FOM we have chosen is an expected value. In general the quality and quantity of the output of each system component must be combined with its uptime to express the effectiveness of the component. The effectiveness of the components is then combined by the model to measure the performance of the system. A single numerical value is thus given for our FOM which expresses the "expected number of useful data products delivered to the users per unit time". The term "expected"

indicates all the contributions of reliability and availability for the various subsystems expressed as uptime fractions. "Numbers of data products" expresses the number of physical composite products representing processed instrument scenes related to the TM standard. "Useful" indicates that the information from different instruments, presented in different formats has different values to users.

B.5 CONSTRUCTING THE EFFECTIVENESS MODEL

Once the dimensions of the FOM have been determined, counting the quantity of system output is straight-forward. Standard methods exist for computing the availabilities and uptimes of the system components. Evaluating the quality of the output, however, requires subjective values and weighting factors. A weighted sum of scores is computed to express the quality of each component's output.

The steps which were accomplished in constructing the EOS effectiveness model were:

1. Define System and Components
2. Define Mission Objectives
3. Perform User Requirements/System Capability Match--Determine the system capabilities needed to satisfy the objectives to some degree
4. Assess impacts of constraints of System Elements
5. Select Figure of Merit--How do all elements contribute to overall system performance? (Proper FOM depends on system peculiarities. Choose best of suitable FOM candidates.)
6. Develop Effectiveness Tree
7. Develop Weighting Factors
8. Generate Mathematical Expression
9. Determine Parameter Performance Ranges.

In order to insure that the FOM is directly computable from hardware parameters, an "effectiveness tree" is developed. This tree relates the top-level FOM to design parameters in step-by-step fashion. The tree is generated by determing which lower-level elements contribute to the next higher-level parameter. For example, to determine the availability of data and the timeliness of its delivery, it is necessary to discover what causes the data to be delayed. This in effect "partitions" the set of delays into two subsets: "known" delays (delays for which a point estimate of total delay time can be made) and "unpredictable" delays (delays for which only probability estimates are possible.) The set of unpredictable delays can be further broken down into subsets. Based on historical data, it is known that five subsets define well the set of unpredictable delays for spacecraft. These are: human error ground station hardware failures, false starts, software failures, and tracking errors. At this point the partitioning ceases, since the delay estimates for each of these subsets can be readily developed from probability distributions based on historical data.

Once the effectiveness tree is completed, the units of measurement for each of the parameters in the tree are determined, and the relative contribution each of the subsets makes to the higher-level set is estimated. These estimates provide the framework within which performance weighting factors are developed.

Our EOS model is designed hierarchical and modular. A hierarchical structure is one in which inputs to the model are accepted for any stage in the design process--from concept formulation to component fabrication--no matter what the degree of definition of the system and the level of detail achieved. In particular, if detailed information about a system is lacking, the model can still evaluate it on the basis of the gross design goals which do exist. The hierarchical levels evaluated for EOS were:

1. Program Level
2. System Level
3. System Component Level
4. Subsystem Level
5. Subsystem Component Level.

Thus the model is useful throughout the design process in identifying promising and unpromising avenues.

The hierarchical effectiveness model guided our design process by identifying promising paths among possible alternatives. It did not require n re detail than existed in the system specification. Therefore, it identified and rejected npromising concepts before much effort was expended in defining them.

A modular structure is one in which system effectiveness is calculated along functional hardware lines; i.e., as the system is actually put together. The effectiveness of any system is made up of the effectivenesses of all its components; the effectiveness of a system component is made up of the effectivenesses of all of its subsystems; and so forth. The structure appears as shown in Figure B-2.

With a modular structure, the effectiveness of any portion of the system may be evaluated independently of the rest of the system, by using only the relevant portion of the model or by changing the inputs to only that section and observing the effect on the system figure of merit.

Finally, a mathematical expression was generated to relate the lower level parameters to each higher level one in turn, taking into account the diverse units of these parameters and any weighting factors, until all the parameters are contained as variables in the expression. This expression results in a value for the system FOM for each set of lower-level parameters. Since a set of design variables defines a system design, a quantitative estimate can be made of the goodness of each design in terms of the FOM.

If the performance range for each parameter is specified, the performance of the "best" design can be quantitatively estimated in terms of the FOM by simply choosing the set of parameters made up of the values at the high end of the range in each case. In a similar fashion, the "worst" design can be specified and the system design range can be bounded. Within these bounds, low-, acceptable-, and high-performance design regions may be defined in terms of ranges of FOM values.

Page intentionally left blank

B.6 THE EOS MODEL

B.6.1 The EOS Problem

The broad-scoped EOS program includes the development of a common, low-cost, flexible spacecraft that can be used in conjunction with a great variety of sensor payloads.

The system comprises the satellites and a data management system which processes the data, converts them to usable form, and delivers them to users on time. One group of EOS satellites will perform Land Resource Management Missions (LRM missions). The objectives of the LRM mission are:

EOS - LRM Mission Objectives

- Develop sensor and other spacecraft systems to acquire spectral measurements and images suitable for generating thematic maps of the earth's surface.
- Operate these systems to generate a data base from which land use information such as crop or timber acreages or volumes, courses and amount of actual or potential water run-off and the nature and extent of stresses on the environment will be extracted.
- Demonstrate the application of this extracted information to the management of resources, such as food and water, the assessment and prediction of hazards, such as floods, and the planning and regulation of land use, such as strip mining and urbanization.

To provide the system with the capab ity to satisfy these user requirements, NASA defined a sensor complement for the LRM Mission.

- Thematic Mapper - A multiband scanning spectral radiometer with 30-meter ground resolution over a swath of about 185-km width
- High Resolution Pointable Imager - A multi-band, narrow swath, ten-meter resolution instrument which can be pointed to either side of the nadir track.

The capabilities of these sensors were reviewed against the known requirements of the users in order to determine the priorities to be placed on the spatial, spectral, and temporal resolution capabilities. The first mission objective expressed a need to generate images suitable for thematic maps. It was found from a user requirement analysis that this requirement could be fulfilled by sensor images if a certain radiometric accuracy was maintained. Thus a measure of the radiometric accuracy was included in the definition. The second objective implied a ground resolution requirement, so ground resolution was included in the definition. The third objective implied a requirement for timely delivery of the data to the users. so temporal resolution, or data timeliness, was included in the definition. The probabilistic part of the problem is addressed in terms of the reliability of the individual system elements. From this reduction of the mission objectives into measurable quantities, the FOM is selected. It should measure a quantity of delivered products, include the probability of their delivery, and the quality of the products delivered, measured by their spectral, spatial, and temporal resolution. The FOM chosen for this mission was "The Expected Number of Useful Data Products per Week Delivered to the Users". This FOM could be calculated from the data throughput rate and reproduction capacity of the system, weighted by the number and importance of the user applications satisfied. Starting from this top-level definition, the Effectiveness Tree was developed. The top level FOM is broken down into lower level elemental measures of the performance of the data processing system and the satellite system.

At first, when the system was poorly defined, the tree consisted of only the effectiveness of the instruments. This quantity was estimated by the number and type of sensors on board, and their associated quality and quantity of output. In this case, the system was assumed to be completely reliable, and it was assumed that all the data could be processed. As information about the system became available, more details were added to the Tree. The number of equivalent products produced depends on both the capacity of the system and how well the data product set satisfies the users. The capacity depends in turn on the quality, quantity, and availability of the system throughput. The availability of the throughput depends on the scheduled and unscheduled times the system is down. These downages

can now be estimated in terms of system hardware parameters. In each branch of the tree, this is the case, so that the FOM can, in fact, be calculated for each hardware configuration.

The mathematical expression developed for the calculation is straight-forward but extensive. However, in most cases, simple sums or products, in some cases modified by weighting factors, were sufficient at each stage.

B.6.2 Use of the Model Within the FOS Systems Engineering Process

The System Effectiveness Model aided our systems engineering process significantly in the following areas:

- Concept selection
- Major subsystem design
- Minor component design
- Design optimization within budget constraint
- Optimization of system design with variable mission mix.

The system design process proceeded in an iterative fashion from simple concept description to detailed subsystem component design definition. At each stage, the hierarchical effectiveness model was defined to the extent that the system is anticipated. The model was kept one step ahead of the system definition, so decisions can be made in sufficient time to influence the design process. The model therefore acted as a succession of finer and finer screens, eliminating less effective alternatives from consideration at each stage of the design process.

The first usage of the effectiveness model was to evaluate program concepts: number of spacecraft, instrument complement, launch schedule, launch vehicle, program life, satellite design life, use of resupply and refurbishment of the satellite, modularity concept, data volume requirements, processing options.

Later, as alternatives were eliminated, a specific hardware design, defined to the subsystem level, emerges. The ratio of incremental effectiveness to incremental cost msy be calculated for all proposed design changes to indicate the most promising areas for modifications. The effectiveness model is thus useful as a design tool. There is a strong sensitivity of the effectiveness model to the design-cost tradeoffs which are normally performed as part of the system engineering process.

B.7 EOS DESIGN EVALUATION AND SELECTION OF PREFERRED APPROACH

The design cost trades, which were reported in Report 3 of this study, were performed on an individual basis. For this reason, although the conclusions were and still are applicable for an individual trade area, a method must be applied to tie the conclusions together from an overall design standpoint. This method must be capable of integrating sometimes diverse trade outputs into an evaluation of the overall proposed designs and provide an insight into which overall approach is preferred.

The approach we have chosen is to develop an effectiveness model. The model relates system and hardware design and performance parameters to a single effectiveness Figure of Merit which reflects top level program objectives. We are then able to; (1) evaluate the effectiveness of alternate designs in meeting program objectives, and (2) relate effectiveness of the alternate designs to cost. This latter step is a clear representation of system cost effectiveness.

B.7.1 USER REQUIREMENTS WEIGHTING FACTORS

Information from different instruments provided in different formats have different values to the users. These values are estimated by the weighting factors given in Table B-1. The factors were derived by analysis of the results of the extensive user requirements survey performed during the system definition study. They represent, in each user area, the percentage of the applications in the areas which would be served by the value of the parameter indicated in the table.

Table B-2 shows the quantity, quality, and availability of the data output of each potential EOS instrument. The quantity of data is expressed by the number of equivalent TM scenes which the instrument can produce in one week, based upon its data rate in bit/sec and the anticipated usage of the instrument. The quality of the data produced by each instrument is measured by the weighting factors. The ratio of two weighting factors expresses the relative value of one scene from each instrument to an "average user". Thus weighting factors should be indicative of the economic value expected to be gained from utilizing the information provided by each instrument. The availability of an instrument is expressed by its uptime fraction. The expected number of equivalent scenes producible by an instrument is the product of these three numbers. This product is the primary measure of system effectiveness. It is multiplied by other factors expressing: the reliabilities of the launch vehicles (Table B-3), the success of the subsystems at meeting design objectives (Table B-4), the scores of orbit parameters relative to design goals (Table B-5), and the ability of the data processing system to transform the data into desired products. The resulting number of the "expected number of equivalent scenes produced". The factors mentioned above have the effect of reducing the expected number of equivalent scenes below that produced by the instruments, because the other systems are not perfect. The figure of merit then goes through two additional weightings to express its success at meeting specific mission and program objectives. Table B-6 shows the Land Resources Management mission objectives identified in the Requirements Document (Report 3, Appendix C). Objectives 1-5 express the goal of providing data to the application areas named. Objectives 6-9 are requirements on the orbit chosen for the satellite. Objectives 10-18 are requirements on the satellite design. The design in question is scored for each objective, and the weighted sum of the scores is multiplied by the expected number of scenes. Table B-7 shows how the scores of the applications areas mission objectives are computed. The analysis of user needs yielded information about the fraction of applications requiring a certain standard of information: frequency of observation, resolution, and spectral bands. The orbit and instrument complement of the satellite determine how many applications are satisfied.

Table B-1 Instrument Weighting Factors

FACTORS AFFECTING AVAILABILITY OF DATA PRODUCTS	WEIGHTING FACTORS
1. Timeliness of Delivery to Users	0.3
2. Availability of Product Formats	0.05
3. Responsiveness to Special Requests	0.2
4. Reliability of Delivery System	0.4
5. Formats Available Through LUS	0.05

Table B-2 Instrument Data Output

INSTRUMENTS	UPTIME FRACTIONS	SCENES/WEEK	WEIGHTING FACTORS
TM	0.927	300	0.89
HRPI	0.846	250	0.86
MSS-4	0.935	200	0.42
MSS-5	0.935	300	0.47
SAR	0.895	20	0.10
PMMR	0.865	20	0.10

Table B-3 Launch Vehicle Reliability

LAUNCH VEHICLE	RELIABILITY
Delta	0.89
Weight-Constrained Titan	0.89
Titan - 3 - B	0.96
Titan - 3 - D	0.91
Shuttle	1.00

Table B-4 Subsystem Success at Meeting Design Objectives

SPACECRAFT SUBSYSTEMS	WEIGHTING FACTORS
1. Attitude Control	0.125
2. Communication & Data Handling	0.125
3. Power	0.125
4. Mission Peculiar	0.125
5. Propulsion/Orbit Adjust/Reaction Control	0.125
6. Wide Band Communication	0.125
7. Tape Recorder	0.125
8. Solar Array	0.125
AVAILABILITY OF SUBSYSTEMS = 0.95	

Table B-5 Orbital Parameter Scores

ORBIT PARAMETERS	WEIGHTING FACTORS
1. Repeat Cycle	0.07
2. Swath Overlap	0.07
3. Orbit Adjust Frequency	0.07
4. Swath Sideslip Rate	0.07
5. Ground Station Coverage	0.07
6. Sufficient Shuttle Payload	0.08
7. Time of Day	0.07
8. Per Cent of Land IIRPI Revisitable	0.08
9. Mapping Coverage	0.07
10. Minimum-Cost Booster	0.07
11. Sun Angle	0.07
12. Tracking & Data Acquisition	0.07
13. Full Earth Coverage Time	0.07
14. Time Between Resupply Visits	0.07
Satellite MMD = 2.75 yr Availability of Instruments = 1.00	

Table B-6 LRM Mission Objectives

LRM MISSION OBJECTIVES	WEIGHTING FACTORS
1. Agricultural Applications	0.2
2. Forestry Applications	0.05
3. Land Use Applications	0.1
4. Water Resources Applications	0.1
5. Geology Applications	0.05
6. Sun-Synchronous Orbit	0.02
7. 5% Overlap Orbit	0.03
8. 17-Day Repeat Cycle Orbit	0.01
9. 3-Day HRPI Offset Revisit	0.06
10. Sensor Complement	0.05
11. Mission Lifetime	0.03
12. Satellite Lifetime	0.03
13. Data Product Options	0.05
14. Processing Level Options	0.04
15. Data Throughput Time	0.05
16. Data Throughput Quantity	0.04
17. Spectral Bands	0.05
18. Resolution	0.04

Table B-7 Mission Objectives Application Areas

FRACTION OF APPLICATIONS SATISFIED BY:

	FREQUENCY OF OBSERVATIONS WEEKS^{-1}				RESOLUTION			AVAILABLE SPECTRAL BANDS		
	3	2-3	1-2	1	60	30	10	4	5	7
Agriculture	.60	.65	.71	1.00	.29	.88	1.00	.40	.60	1.00
Forestry	.34	.38	.72	1.00	.0	.44	1.00	.60	.75	1.00
Land Use	1.00	1.00	1.00	1.00	.60	.60	1.00	.34	.50	1.00
Water Resources	.56	.64	.87	1.00	.96	.96	1.00	.78	.85	1.00
Geology	.86	.86	.86	1.00	.35	.85	1.00	.85	.90	1.00
Total	.70	.72	.84	1.00	.11	.77	1.00	.72	.83	1.00

Finally, Table B-8 identified the major program objectives for EOS and estimates of their relative importance. A program concept is evaluated for each objective and the weighted sum of scores is multiplied by the expected number of equivalent scenes, giving the overall figure of merit.

The System Effectiveness Model combines the design parameters for each alternate with the value to the users (as measured by the weighting factors) of the products produced by this particular set of parameters (e.g., particular complement of instruments and particular swath width), and determines the value of the FOM which should be applied to the alternate. The resulting data for design alternates considered in this study and an application of this data to the identification of the design to be preferred is given in the following paragraphs.

Table B-8 Major EOS Program Objectives

EOS PROGRAM OBJECTIVES	WEIGHTING FACTORS
1. Accommodate TM and HRPI Together	0.1
2. Accommodate Follow-on Instruments	0.025
3. Reduced Costs Using Shuttle	0.1
4. Shuttle Revisit Compatibility	0.1
5. Modular Design	0.1
6. Resupplyable	0.1
7. Accommodate Follow-on Instruments	0.025
8. Compatible with Expendable Boosters	0.08
9. Meet Operational Requirements of D.O.I.	0.1
10. Maintain Capability Through 1989	0.05
11. Long-Life Satellite	0.05
12. Quick System Throughput Time	0.1
13. Goal-Number of TM Scenes Throughput	0.08
14. Initial Launch Year	0.07

B.7.2 Program Evaluation

B.7.2.1 Conclusions

Program Design Options were evaluated in terms of the cost/performance (effectiveness) of design options versus the resulting FOM (Equivalent Scenes) for an EOS A and A' operational mission of two observatories, each with a two-year mission with one year of overlap. The results of this evaluation is shown in Fig. B-3 which plots the total EOS A and A' mission observatory recurring plus Operational Cost per Equivalent Scene (cost effectiveness) versus the total number of Equivalent Scenes (program effectiveness) produced during the operational missions. In examining this curve the following conclusions can be reached:

- The recommended EOS A and A' program with a TM/MSS, 30 meter resolution, and TDRS is a cost/performance effective approach within the constraints of using a conventional launch vehicle and the baselined TM 185 km swath width.
- TDRS has a significant positive effect on program cost and performance effectives (Option 1-6 vs 6-13).
- The inclusion of provisions for Shuttle compatibility in the EOS design will permit a significant increase in performance at a very small cost increase when the Shuttle becomes operational (Option 1 vs 4 or 8 vs 7).
- The TM with its 30 meter resolution has a significant positive impact on program cost and performance effectiveness. (Options 5 vs 6).
- Increase of the TM Swath width to 330 KM should be further studies since it produces a significant increase in effectiveness. (Options 5 vs 4).

It should be noted that the on-orbit resupply cost and performance effectiveness, is not truly represented in this evaluation, because it's benefit it not realized for missions of less than 2.75 years as described in our Shuttle utilization studies.

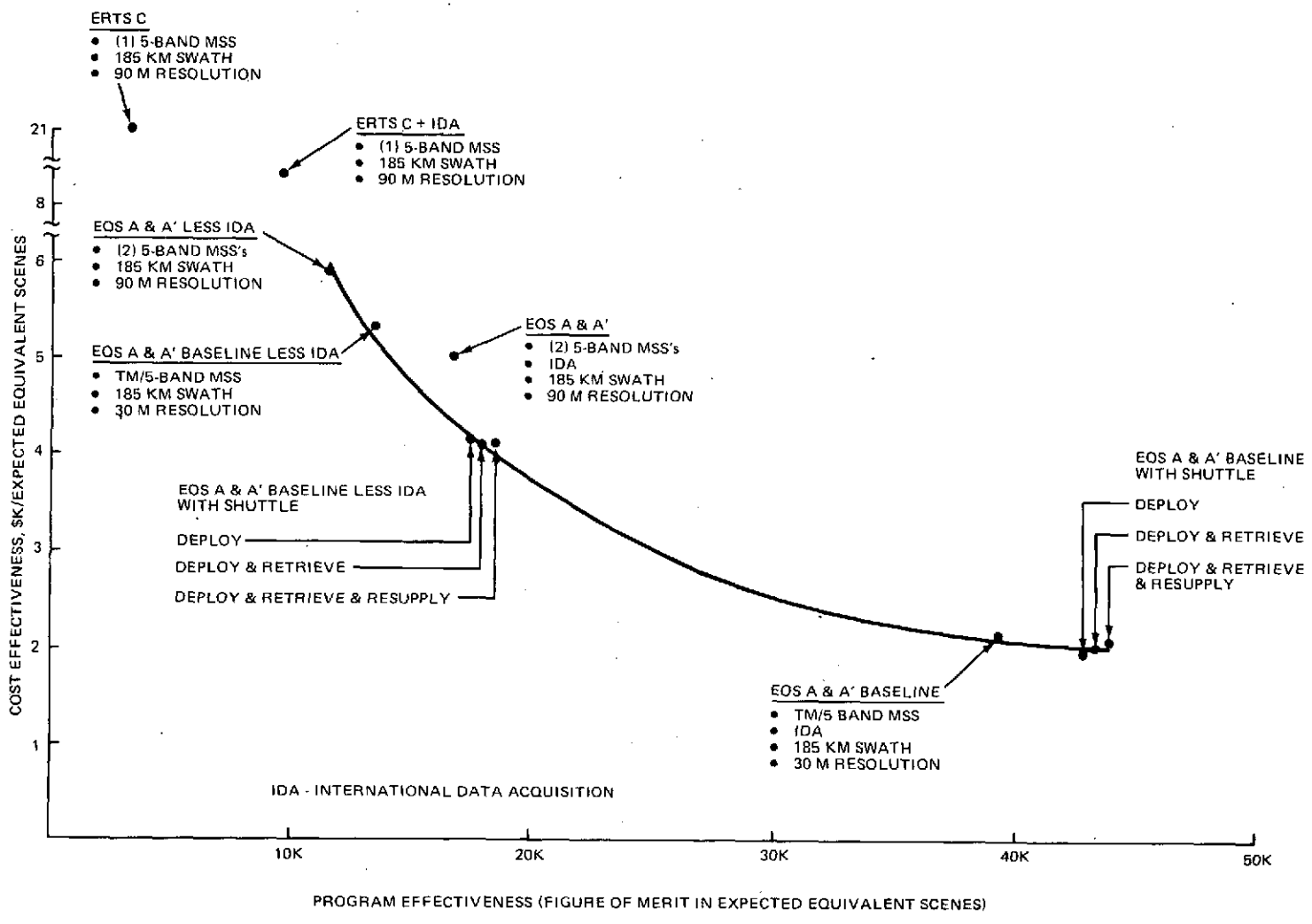

A7-44

Fig. B-3 Design Option Cost Effectiveness vs Program Effectiveness

B.7.2.2 Methodology

The program design approach cost and performance effectiveness curve was generated by first establishing the resulting Equivalent Scenes/year for each Design Option using the methodology described in Subsection B.7.1. The observatory recurring and operational cost of each design alternative, based on our EOS program design option cost (See Section 6), was then identified. The results of these two steps are shown in Table B-9.

Design alternatives were then synthesized to create each program design option, FOM, cost and cost/FOM (cost effectiveness). These parameters are shown in Table B-10. The cost effectiveness vs program effectiveness (FOM) in cost/equivalent scenes versus number of equivalent scenes was then plotted as represented in Fig. B-3.

Table B-9 Design Option Figure of Merit and Costs

Design Option	FOM 4 Mission Yrs	OBS. REC. & Operational Cost (2 OBS/2 Yr Ea.)
Reference Option EOS • TM/MSS • Direct data • 185 km SW • 30 m resolution	13204	$72.520M
Design Options		
• TDRS	+25456	$ 14.500M
• SS Deploy	+ 3924	1.086M
• SS Retrieve	+ 580	1.820M
• SS Resupply	+ 436	2.526M
• Incl TM SW to 330 km	+ 3488	0.900M
• Red. TM resolution to 90 m	- 6820	- 10.800M
• Red. TM SW to 100 km	- 7128	- 0.300M

Table B-10 Design Approach Performance Vs Cost

	DESIGN ALTERNATIVES										
	TDRS	DEPLOY	RETRIEVE	RESUPPLY	TM + MSS	90 M RES (2 MSS's)	330 KM SW (TM)	100 KM SW (TM)	EXP EQ. SCENES FOR 2 2-YR OBS WITH 1-YR OVERLAP	OBS SYSTEM RECURRING COST	COST PER EQ. SCENE
OPTION 1	x	x	x		x		x		46688	$90.226M	1.93
2	x	x			x				42620	$88.106M	2.06
3	x	x	x	x	x				43636	$92.452M	2.11
4	x				x		x		42183	$87.920M	2.08
5	x				x				38695	$87.020M	2.24
6	x					x			31875	$76.220M	2.39
7		x	x		x		x		21232	$76.326M	3.59
8		x	x		x				17744	$75.426M	4.25
9		x	x	x	x				18180	$77.952M	4.28
10		x			x				17164	$73.606M	4.28
11					x				13240	$72.520M	5.47
12		x	x			x			10924	$64.626M	5.91
13					x			x	10616	$75.126M	7.07

B.7.3 BIBLIOGRAPHY

1. NASA Tech. Brief No. B73-10104. "A Summary Report on System Effectiveness and Optimization Study. September, 1969.

2. Mathematica Incorporated, Economic Analysis of the Space Shuttle System, Chapter 3 "The Theory of Benefit-Cost and Cost-Effectiveness Analysis." January, 1972.

3. Fragola, J. R. and Spahn J. F.; "Economic Models for Satellite System Effectiveness", 1973 Annual Reliability and Maintainability Symposium.

4. Fragola, J. R. and Diamond, E., "Satellite Long Life Assurance--The Impact of the Shuttle Era", AIAA Man's Role in Space Conference; Cocoa Beach, Florida, March 27 - 28, 1972.

5. D.C. Thompson, "Decision Modeling: The art of Scientific Guessing", Machine Design, November 12, 1970. pp. 132 - 141.

6. OAO-A2 Monthly Reports. NASA-GSFC.

7. OAO-C Copernicus Monthly Reports. NASA-GSFC.

APPENDIX C WEIGHT STATEMENT

The launch weights of the Basic Spacecraft, the EOS-A, B, and C are summarized in Table C-1. This shows the functional weight breakdown for each spacecraft.

The Basic Spacecraft is a basic modular spacecraft incorporating minimum practical redundancy, a power supply capable of providing 200 W average power to the instrument section interface, and no provisions for Shuttle retrieval or resupply.

Major differences between the Barebones Spacecraft and EOS-A are:

a) Basic Structure - EOS-A adds a six-segment Orbiter interface structure (14 lb), PDRM interface fitting installation (4 lb), and Positioning Platform docking probes (9 lb) to provide for Shuttle deploy and retrieve. In addition, stowage lock assemblies (1 lb) must be added to the solar array installation to hold the array in the restowed position for Shuttle retrieval.

b) Electrical Harness - Adds wiring required for Shuttle compatibility (10 lb), including special EOS negative bus with provisions for isolation from Single Point Ground.

c) Reaction Control - Adds pressure relief and vent valves (4 lb) to limit RCS tank pressures for Shuttle deploy and retrieve.

d) Communications & Data Handling - Adds S- Band transponder (12 lb) for TDRSS link. Adds redundant equipment (24 lb) for fail-safe design required for Shuttle crew safety, and dedicated C&W and command override wiring and orbiter interface (2 lb). Adds memory module (6 lb) to computer.

e) Mission Peculiar - Adds propellant, tankage, and x-axis thrusters (27 lb) for orbit correction and adjustment. Adds instrument support structure (80 lb), IMP Box structure (25 lb) and TDRSS Antenna support, deployment mechanism and stowage locks (19 lb) plus stowage locks for the X-Band Antennas (1 lb). Adds insulation (11 lb) for the instrument support structure. In addition, EOS-A adds the TDRSS (87 lb) and X-Band (40 lb) communication systems, WB data compaction (14 lb), and spacecraft/instrument signal conditioning (34 lb).

f) Instruments - Adds the instrument complement for EOS-A of a Multi-Spectral Scanner (160 lb) and a Thematic Mapper (400 lb).

g) Contingency - Adds the contingency impact of the above changes (56 lb).

The EOS-B and C launch weights are built up similarly with weight changes reflecting such things as local structure reinforcement for launch vehicle compatibility, additional batteries and larger solar arrays, enlarged ACS reaction wheels and torquer bars, increased orbit adjust propellant requirements, and, in the case of EOS-C, the installation of an SRM for circularization at the mission altitude, as well as changes to the instruments and instrument data handling equipment. In addition, since EOS-B and C must be capable of resupply by the Shuttle, the necessary resupply mechanisms, blind mate connectors and spacecraft thermal shielding are added.

Table C-2 depicts the weight build-up from the Basic S/C for EOS-A, B, C and the follow-on missions. The resulting launch weights are compared to the payload capabilities of the selected launch vehicles, and weight saving options applied as required to obtain a positive payload margin. EOS-D makes use of a roll-out solar array to achieve the savings (including contingency reduction) shown. EOS-B and D require a Delta 3910 launch vehicle in the configuration shown, but if necessary, can be flown on a Delta 2910 launch vehicle by undertaking the weight reduction program described in Table C-3 which, in the case of EOS-D, includes the surrender of one or more program options.

Table C-1 EOS Weight Summary

FUNCTIONAL ELEMENT	BASIC	EOS- A	EOS-B	EOS-C
– BASIC STRUCTURE	360	388	440	460
– ELECTRICAL POWER	169	169	169	201
– ELECTRICAL HARNESS & S/C	35	45	90	90
– SOLAR ARRAY & DRIVE	195	195	195	279
– ATTITUDE CONTROL	161	161	161	306
– RCS (HYDRAZINE)	36	40	40	40
– C & DH	102	146	146	146
– THERMAL CONTROL	62	62	80	80
– INTERSTAGE ADAPTER	95	95	95	135
• BASIC S/C SUBTOTAL	1215	1301	1416	1737
• MISSION PECULIAR	(–)	(338)	(399)	(984)
– ORBIT ADJUST/TRANSFER	–	27	27	340
– INSTR SUPPORT	–	136	189	445
– TDRSS COMM	–	87	87	87
– WB COMM	–	88	96	112
• INSTRUMENTS	(–)	(560)	(800)	(1700)
– MSS	–	160	–	–
– TM	–	400	400	800
– HRPI	–	–	400	400
– SAR	–	–	–	500
• CONTINGENCY	146	202	222	322
•, TOTAL S/C	1361 LB	2401 LB	2837 LB	4743 LB

A7T-1

The weights described above were derived from a detailed weight analysis which was performed on the Basic and EOS-A Spacecraft. Preliminary stress and dynamic analyses were used to size the major structural members. Theoretical structure weights were computed, and non-optimum factors applied to determine total assembly weight. These factors have been developed over the course of several spacecraft (an numerous aircraft) programs, and have been proven quite accurate. Detailed calculations were performed on the latches and mechanisms, increasing our confidence in the lightweight latching concept. Subsystem equipment weights are based on actual weights of existing components, or quoted vendor weight. Thermal control weights are based on non-optimum factors developed from the actual weights of Lunar Module MLI blankets. Instrument and instrument data handling weights are either vendor estimates or government-specified.

Table C-2 EOS and Follow-on Mission Weight and Launch Vehicle Performance

ITEM DESCRIPTION	EOS-A	EOS-B	EOS-C	EOS-D (SEASAT-B)	EOS-E (TIROS-O)	EOS-F (SEOS)	SEASAT-A	SMM
• BASIC SPACECRAFT WEIGHT-LB[1]	1361	1361	1361	1361	1361	1361	1361	1361
– ORBITER DEPLOY PENALTY	67	67	67	67	67	64	67	67
– ORBITER RETRIEVAL PENALTY	1	1	1	2	1	1	2	2
– ORBITER RESUPPLY PENALTY	–	115	115	128	115	115	128	128
– 2-YEAR SERVICE LIFE (BATTERY)	–	–	32	32	–	–	32	–
– INCREASED STRUCTURAL CAPABILITY	–	–	60	–	–	80	–	–
– Δ CONTINGENCY	11	21	36	26	21	36	26	23
• BASIC SPACECRAFT	1440	1565	1672	1616	1565	1657	1616	1581
– SPACECRAFT MISSION PECULIAR	(47)	(47)	(629)	(200)	(718)	(59)	(175)	(59)
○ THERMAL CONTROL	–	–	–	60	–	75	60	60
○ SOLAR ARRAY	–	–	84	84	–	-60	61	-75
○ ATTITUDE CONTROL	–	–	145	–	–	6	–	37
○ COMM & DATA HANDLING	18	18	18	18	18	9	18	18
○ ORBIT ADJUST/TRANSFER	27	27	340	27	682	41	27	27
○ Δ CONTINGENCY	2	2	42	11	18	-12	9	-8
– INSTRUMENT MISSION PECULIAR	(354)	(425)	(742)	(431)	(428)	(344)	(431)	(467)
○ INSTRUMENT SUPPORT[2]	136	189	445	235	198	214	235	231
○ TDRSS COMMUNICATION	87	87	87	87	87	–	87	87
○ WIDE BAND COMM & DATA HANDLING	88	96	112	46	88	88	46	88
○ Δ CONTINGENCY	43	53	98	63	55	42	63	61
– INSTRUMENTS	(560)	(800)	(1700)	(706)	(770)	(2300)	(587)	(1431)
○ MULTI-SPECTRAL SCANNER	160	–	–	–	–	–	–	–
○ THEMATIC MAPPER	400	400	800	–	–	–	–	–
○ HIGH-RESOLUTION POINTABLE IMAGER	–	400	400	–	–	–	–	–
○ SYNTHETIC APERTURE RADAR	–	–	500	–	–	–	–	–
○ SEASAT-B (OCEAN DYN & SEA ICE)	–	–	–	706	–	–	–	–
○ TIROS-O (WEATHER & CLIMATE)	–	–	–	–	770	–	–	–
○ SEOS (GEOSYNCHRONOUS EOS)	–	–	–	–	–	2300	–	–
○ OTHER EXPERIMENTS	–	–	–	–	–	–	587	1431
• SUBTOTAL – SPACECRAFT WEIGHT SAVING OPTIONS[3]	2401 –	2837 –	4743 –	2953 -133	3481 –	4360 –	2809 –	3538 –
• TOTAL SPACECRAFT WEIGHT - LB	2401	2837	4743	2820	3481	4360	2809	3538
• LAUNCH VEHICLE PAYLOAD CAPABILITY	2660	3730	5150	2825	3550	4700	3350	3900
• PAYLOAD MARGIN - LB	259	893	407	5	69	340	541	362
• LAUNCH VEHICLE[4]	D2910	D3910	TIIIB	D2910	D3910	TIIIC-7	D3910	D2910

NOTES: (1) BASIC SPACECRAFT WEIGHT INCLUDES 146 LB CONTINGENCY.
(2) INSTRUMENT SUPPORT WEIGHT INCLUDES RETRIEVAL STOWAGE LOCKS AND RESUPPLY MECHANISMS (EXCLUDING EOS-A) FOR IMP AND INSTRUMENTS
(3) WEIGHT SAVING OPTIONS EMPLOYED ARE ROLL-OUT SOLAR ARRAY (EOS-D) INCLUDING CONTINGENCY REDUCTION
(4) TIIIB PAYLOAD LIMITS ARE FOR TITAN IIIB (SSB)/NUS.

1T-8
7T-2
A7T-2

Table C-3 Lightweight EOS Weight Derivation (Delta 2910 Launch Vehicle)

CONFIGURATION & WEIGHT REDUCTION ITEMS	WEIGHT, LB			
	EOS-B		SEASAT-A	
	POTENTIAL SAVINGS	PREFERRED ITEMS	POTENTIAL SAVINGS	PREFERRED ITEMS
• CURRENT OBSERVATORY	2837	2837	2775	2775
– LIGHTWEIGHT DESIGN FEATURES	(-299)	(-197)	(-320)	(-320)
– ROLL-OUT SOLAR ARRAY	–93	–	–114	–114
– HYBRID GR/EP STRUCTURE				
○ SPACECRAFT	–135	–135	–135	–135
○ INSTRUMENT SUPPORT	–29	–29	–27	–27
– CONTINGENCY CHANGE	–42	–33	–44	–44
• LIGHTWEIGHT WITH OPTIONS	2538	2640	2455	2455
– ELIMINATE PROGRAM OPTIONS	(-267)	(–)	(-356)	(-228)
RESUPPLY PROVISIONS				
○ SPACECRAFT	–115	–	–128	–128
○ INSTRUMENT	–49	–	–73	–73
– RETRIEVAL PROVISIONS	–5	–	–15	–
– SHUTTLE DEPLOY CAPABILITY	–67	–	–67	–
– REDUNDANCY - 2 YR. LIFE	–	–	–32	–
– CONTINGENCY CHANGE	–31	–	–41	–27
• LIGHTWEIGHT EOS	2271	2640	2099	2227
• D-2910 PAYLOAD CAPABILITY	2660	2660	2250	2250
• PAYLOAD MARGIN	389	20	151	23

A7T-3

The contingency weight is based on a detailed assessment of each assembly or component, generally using a factor of 20% for structure and new equipment, and 10% for modified existing equipment. No contingency exists for existing (off the shelf) equipment or specification weights. A detailed weight statement for EOS-A is found in Table C-4. The mass properties for EOS-A have been tabulated for several significant configurations in Table C-5 and the EOS Reference Axis System is illustrated in Fig. C-1.

Table C-4 EOS-A Weight Statement (Sheet 1 of 3)

ITEM	WEIGHT, LB.
STRUCTURE	**388**
• CORE STRUCTURE	(150)
– CORE BEAM	64.8
– FWD BULKHEAD	19.4
– AFT BULKHEAD	19.4
– OUTRIGGER TRUSS (6)	46.8
• ORBITER INTERFACE STRUCTURE	(27)
– PDRM FITTING INSTALLATION	4.0
– CORNER BRACE (3)	2.2
– INTERFACE SEGMENT (6)	11.5
– POSITIONING PLATFORM PROBE (3)	9.0
• MODULE STRUCTURE (3)	(185)
– H/C BULKHEAD	66.6
– H/C SHELF	15.9
– SIDE TRUSS	102.6
• ORBIT ADJUST STAGE	(25)
– H/C BULKHEAD	3.7
– BEAM (6)	9.0
– SUPPORT TRUSS	10.1
– TANK SUPPORTS	2.3
• SOLAR ARRAY STOWAGE LOCK	1
ELECTRICAL POWER	**169**
• POWER SUPPLY	(91)
– BATTERY	64.0
– BATTERY CHARGER	27.0
• POWER DISTRIBUTION	(67)
– CENTRAL POWER CONTROL UNIT	23.0
– GROUND CHARGING DIODE ASS'Y (2)	11.0
– BUS PROTECTION ASS'Y	5.0
– BUS ASSEMBLY (3)	2.0
– CONNECTORS	3.0
– WIRING & INSTALLATION	15.0
– S/C INTERFACE ASS'Y	8.0
• SIGNAL CONDITIONING & REMOTES	(11)
– SIGNAL CONDITIONING ASS'Y	3.0
– REMOTE UNIT (2)	8.0
ELECTRICAL HARNESS & SC	**45**
• BASIC HARNESS	(35)
– SPG BUS	0.5
– CONNECTORS	3.4
– WIRING & INSTALLATION	31.3
• PYRO CONTROL	5
• LAUNCH INSTRUMENTATION	5
SOLAR ARRAY & DRIVE	**195**
• RIGID DEPLOY/RETRACT	170
• SOLAR ARRAY DRIVE	25
ATTITUDE CONTROL	**161**
• SENSORS	(44)
– COARSE SUN SENSOR	0.3
– DIGITAL SUN SENSOR	5.0
– RATE GYRO ASS'Y	15.0
– FIXED STAR TRACKER	17.0
– MAGNETOMETER	6.5
• EVALUATION, CONDITIONING & REMOTES	(21)
– CONTROL LOGIC ASS'Y	13.0
– REMOTE UNIT (2)	8.0
• CONTROL	(61)
– REACTION WHEEL (3)	30.0
– TORQUER BAR (3)	30.6
• ELECTRICAL INTEGRATION	(35)
– BUS ASS'Y (3)	2.0
– BUS PROTECTION ASS'Y	5.0
– CONNECTORS	8.0
– WIRING & INSTALLATION	20.5

A7T-4(1)

Table C-4 EOS-A Weight Statement (Sheet 2 of 3)

ITEM	WEIGHT, LB
REACTION CONTROL	**40**
• HYDRAZINE SYSTEM	(18)
– THRUSTER (16)	5.6
– TANK	2.9
– COMPONENTS	
○ PROPELLANT FEED SYS	1.4
○ PRESSURE RELIEF SYS	3.5
– LINES	3.6
– SUPPORTS	1.0
• SIGNAL CONDITIONING & REMOTES	(7)
– SIGNAL CONDITIONING ASS'Y	3.0
– REMOTE UNIT	4.0
• ELECTRICAL INTEGRATION	(12)
– CONNECTORS	9.5
– WIRING & INSTALLATION	3.0
• PROPELLANT (N_2H_4)	3
COMMUNICATION & DATA HANDLING	**146**
• COMMUNICATIONS	(30)
– S-BAND ANTENNA (2)	2.4
– INTEGRATED TRANSPONDER	13.0
– S-BAND TRANSPONDER (TDRSS)	12.0
– COAXIAL CABLE INSTALLATION	3.0
• DATA HANDLING	(77)
– COMPUTER	26.0
– CLOCK	5.0
– CONTROLLER/FORMATTER (2)	8.0
– COMMAND DECODER (2)	15.6
– SENSORS	20.0
– CAUTION & WARNING INTERFACE	2.0
• SIGNAL CONDITIONING	(14)
– SIGNAL CONDITIONING ASS'Y (2)	6.0
– REMOTE UNIT (2)	8.0
• ELECTRICAL INTEGRATION	(25)
– BUS ASS'Y (3)	2.0
– BUS PROTECTION ASS'Y	5.0
– CONNECTORS	11.0
– WIRING & INSTALLATION	7.0
THERMAL CONTROL	**62**
• THERMAL SKINS	(26)
– CORE	10.1
– MODULE (3)	12.4
– RCS/ORBIT ADJUST STAGE	3.1
• INSULATION	(33)
– CORE	10.9
– MODULE (3)	17.3
– RCS/ORBIT ADJUST STAGE	4.6
• INSTALLATION	1
• HEATERS	(2)
– CORE (5)	0.6
– MODULE (15)	1.8
INTERSTAGE ADAPTER	**95**
• LAUNCH ADAPTER	(84)
– SKIN	27.9
– LONGERON (6)	4.6
– FWD RING	10.9
– AFT RING	8.1
– STIFFENER (12)	11.2
– SEPARATION SYS	21.5
• SPACECRAFT INSTALLATION – SEPARATION I/F	11
MISSION PECULIAR	**338**
• ORBIT ADJUST/TRANSFER	(27)
– THRUSTER (4)	2.8
– TANKAGE	2.9
– COMPONENTS	1.7
– PROPELLANT	20.0

A7T-4(2)

Table C-4 EOS-A Weight Statement (Sheet 3 of 3)

ITEM	WEIGHT, LB
MISSION PECULIAR (CONT)	
• INSTRUMENT SUPPORT	(136)
– STRUCTURE	
○ BOX BEAM	28.3
○ TRUSS	22.8
○ PLATFORM	29.3
○ IMP BOX	25.0
○ TDRSS TRUSS	5.0
– WB ANTENNA MECH	
○ TDRSS DEPLOYMENT	10.8
○ TDRSS STOWAGE	3.0
○ X-BD STOWAGE (2)	1.0
– THERMAL INSULATION	10.9
• TDRSS COMMUNICATIONS	(87)
– KU BAND STEERABLE ANTENNA	70.0
– TRANSMITTER	15.0
– COAXIAL CABLE INSTALLATION	2.0
• WIDEBAND COMMUNICATIONS	(88)
– X-BAND STEERABLE ANTENNA (2)	12.0
– ELECTRONICS	28.5
– WB DATA HANDLING UNIT	14.0
– SIGNAL CONDITIONING	33.5
INSTRUMENTS	**560**
• MULTI-SPECTRAL SCANNER	160
• THEMATIC MAPPER	400
CONTINGENCY	**202**
• STRUCTURE	(78)
– BAREBONES STRUCTURE	72.0
– RETRIEVAL I/F	5.4
– SOLAR ARRAY STOWAGE LOCK	0.2
• SUBSYSTEMS	(62)
– ELECTRICAL POWER	11.3
– ELECTRICAL INTEGRATION	2.0
– SOLAR ARRAY & DRIVE	19.5
– ATTITUDE CONTROL	14.6
– REACTION CONTROL	2.3
– C&DH	12.5
• LAUNCH ADAPTER	19
• MISSION PECULIAR	(43)
– INSTRUMENT SUPPORT	
○ STRUCTURE	22.1
○ STOWAGE MECHANISM	3.0
– IMP EQUIPMENT	
○ TDRSS COMMUNICATIONS	17.0
○ SIGNAL CONDITIONING	0.6
EOS-A SPACECRAFT LAUNCH WEIGHT	*2401*
OPTIONS	
• A. 5-YR SURVIVAL LIFETIME – ADD BATTERY	32
• B. 4-YR AVERAGE LIFETIME – ADD REDUNDANCY	(91)
– EPS	8
– ACS	40
– RCS	4
– C&DH	39
• CONTINGENCY INCREASE	(12)
– OPTION A	3.2
– OPTION B	8.6
TOTAL OPTIONS	*135*

A7T-4(3)

Table C-5 EOS-A Mass Properties Summary

CONFIGURATION	WEIGHT, LB	CENTER OF GRAVITY(1), IN.			MOMENT OF INERTIA, SL–FT²			PRODUCT OF INERTIA, SL–FT²		
		X	Y	Z	I_{xx}	I_{yy}	I_{zz}	I_{yz}	I_{xz}	I_{xy}
• SOLAR ARRAY STOWED										
– BASIC SPACECRAFT	1346	81.3	–3.5	0.2	212	796	817	1.3	31.9	–108.2
– S/C PLUS MISSION PECULIAR ITEMS	1727	94.3	–3.7	–0.2	271	1240	1255	–5.7	–6.0	–102.3
– TOTAL OBSERVATORY (INCL. INSTRUMENTS)	2287	109.3	–1.3	1.3	300	1658	1676	–0.2	28.8	–53.9
– TOTAL OBSERVATORY PLUS ADAPTER – LAUNCH	2401	105.6	–1.3	1.2	335	1824	1842	–0.2	31.2	–56.3
• SOLAR ARRAY DEPLOYED										
– TOTAL OBSERVATORY INITIAL DEPLOYMENT	2287	100.9	–8.1	1.3	844	1542	1807	4.1	34.2	94.3
– ARRAY ROTATED 90°	2287	103.1	–8.1	3.5	715	1559	1953	–104.0	42.5	–13.9
– ARRAY ROTATED 180°	2287	105.4	–8.1	1.3	844	1581	1846	4.1	31.3	–122.1
– ARRAY ROTATED 270°	2287	103.1	–8.1	–0.9	720	1564	1953	112.3	23.0	–13.9

NOTES: (1) REFERENCE AXIS SYSTEM IS SHOWN IN Fig. C-1
(2) SOLAR ARRAY DEPLOYMENT IS FOR 1030 DNTD (KNUCKLE ANGLE = 21 DEG)

A7T-5

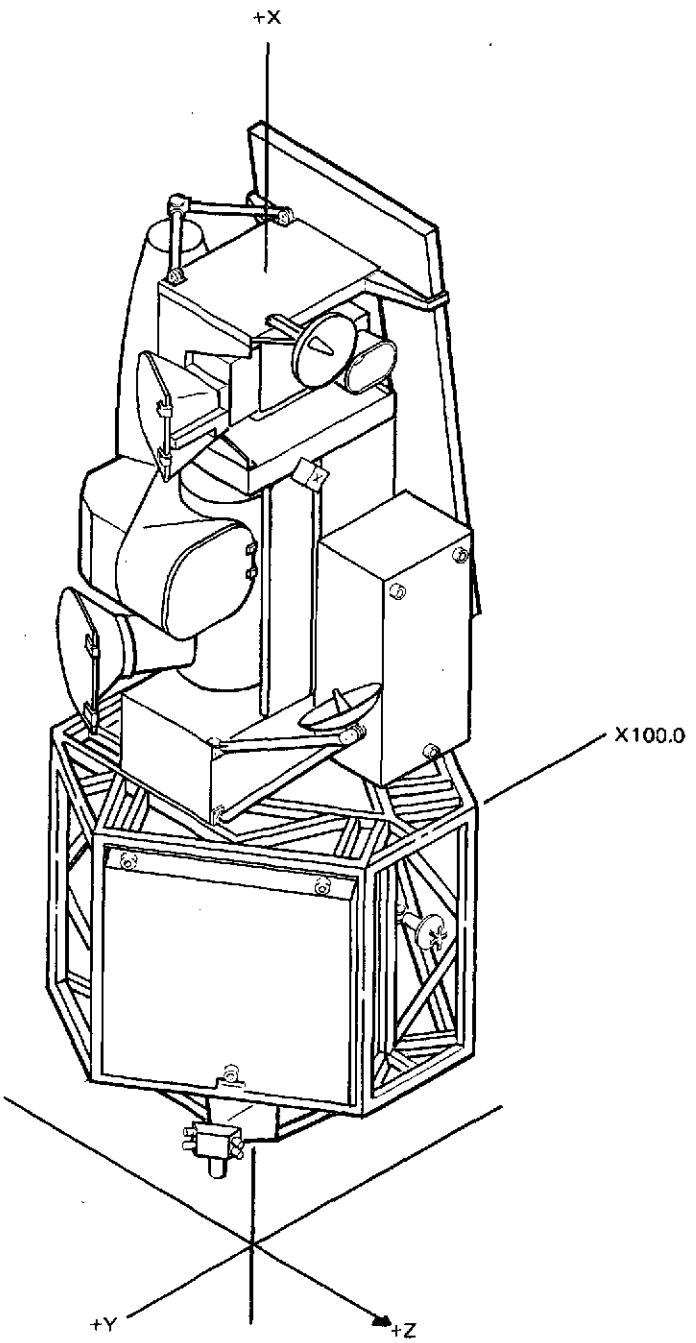

A7-7

Fig. C-1 EOS Reference Axis System

APPENDIX D

OPTICAL ATMOSPHERIC SCATTERING LIMITATIONS ON OFFSET POINTING

D.1 INTRODUCTION

The ability of the TM and HRPI to discriminate targets of interest from background is limited by atmospheric scattering and absorption. When viewing the Earth at some offset angle from the vertical, these effects are magnified because of the increased atmospheric thickness that must be looked through. There are therefore some limits on the amount of offset from the vertical that can be tolerated under different circumstances. Beyond these limits, some objects of interest are no longer visible. The purpose of this study is to assess the factors which serve to limit the observability of various ground objects by calculating atmospheric transmissions and path radiances, and consequent apparent contrast levels of various targets of interest for different solar illumination angles and angles of observation.

In this study, emphasis is placed on calculations of contrast levels of ground objects as seen from Earth orbit. Our results are therefore most relevant to remote sensing applications requiring border following rather than actual target recognition, e.g., delineation of the boundary of a corn field as opposed to distinguishing corn from wheat, etc. The latter is a more complex problem and would be a logical extension of this work in possible future studies.

D.2 ATMOSPHERIC SCATTERING PROGRAM

It is recognized that both man and nature can affect the atmospheric environment of the Earth in both obvious and subtle ways. Apart from localized thermal sources, the two big products of our industrial society that produce important optical atmospheric effects are carbon dioxide and suspended particulate matter (aerosols). Also, natural

NOTE

Cited references are listed in Paragraph D.7.

contributions such as molecular constituents and suspended moisture droplets can have a great optical effect on the atmosphere. Because of the difficulty in performing controlled experiments in the atmosphere and the long time constants associated with these experiments, the most practical way of assessing the effects of increasing the concentrations of these constituents is by computer modeling. We are specifically interested in the effect of change in apparent contrast (as seen from a satellite) of various ground objects caused by atmospheric scattering and absorption as a function of sensor viewing direction and solar radiation incidence angle.

In order to set up a mathematical model (Braslau and Dave[1]) of the Earth's atmosphere consisting of 41 plane parallel nonhomogeneous layers with a continental distribution of ozone and aerosols, and bounded at the lower end by a Lambert ground of known reflectivity, we require the optical complex index of refraction (refraction and absorption) of the atmospheric aerosols. The Earth's atmosphere contains silicates and other aerosol particulates, and the optical complex index of refraction is rather poorly known for these constituents over a wide wavelength range. Grumman Research is in the process of measuring the optical complex index of refraction of appropriate atmospheric constituents over a wide wavelength range using a unique equipment and analysis technique.

Using the optical complex index of refraction, and a single particle scattering theory (Mie scattering), we may evaluate the effect of a single size particle in the atmosphere. An appropriate particle distribution must be superimposed upon the single particle scattering, and the coordinates must be transformed by using a Fourier series expansion to permit calculations to be made in terms of an earth centered coordinate system; thus we consider the coordinates as the sun incidence angle θ_o, the offset viewing angle θ, and the azimuth angle ϕ between. Multiple scattering must be included in any scattering atmospheric model as an important effect. In any type of calculation involving a series expansion (Fourier series), a sufficient number of terms must be used to insure convergence. Since the atmospheric particulate and moisture content changes throughout the year, a particular season must be chosen for the mathematical modeling.

For the purposes of evaluating the effect of the atmosphere on offset pointing, we will use an average midlatitude, summer atmospheric model described by McClatchey et al[2]; this model specified the atmospheric pressure, temperature, density, water vapor, and ozone as a function of height above the ground to 100 km. Superimposed upon this atmosphere is an aerosol distribution, typically shown in Fig. D-1 for a clear sky and for severe atmospheric loading (from Deirmendjian[3]). The model atmosphere that we use is meant to be representative of atmospheric conditions over CONUS. Fluctuations in ground level visibility and, in particular, in haze and dust levels have not been considered here.

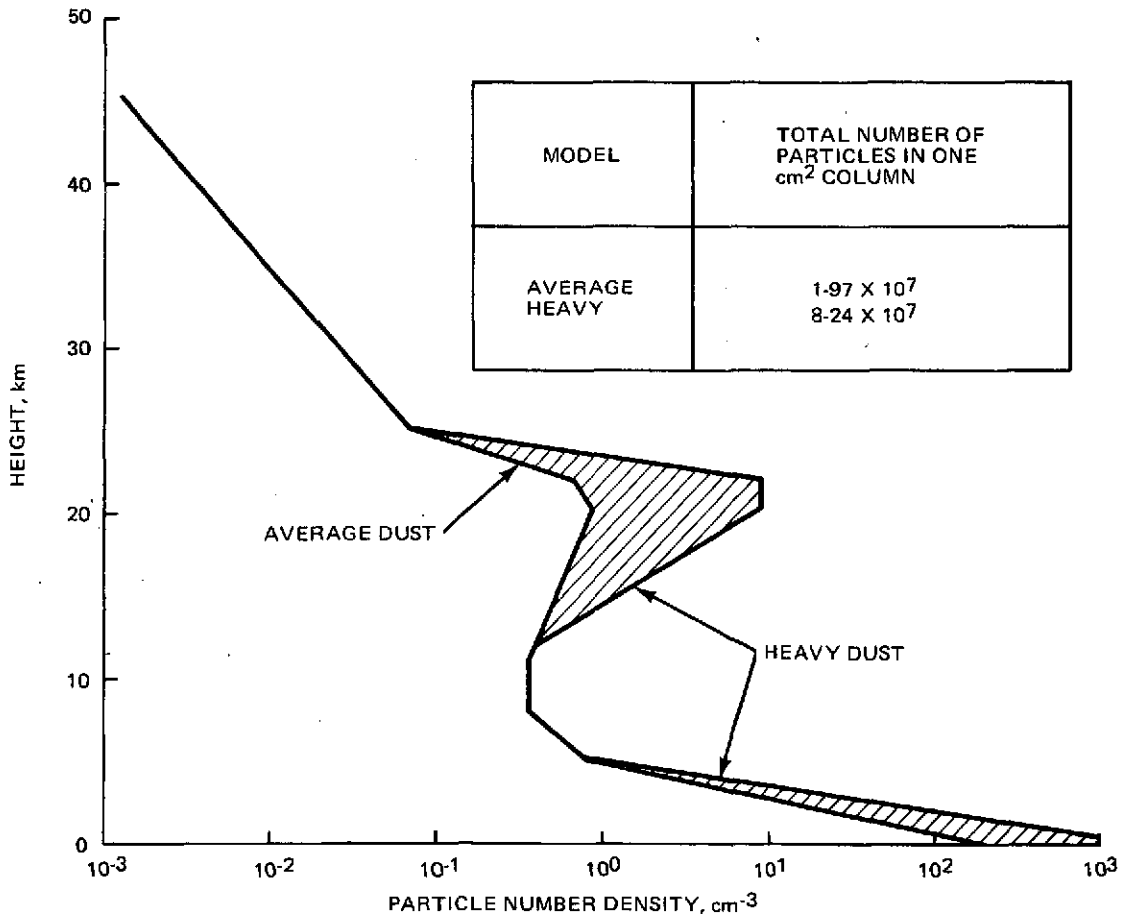

Fig. D-1 Aerosol Height Distributions for Two Different Particle Loadings

The atmospheric model that we use assumes particles with a real index of refraction of 1.5 as a general average, with the absorption portion between zero and 0.03. Our most detailed calculations are in the green region of the spectrum (EOS Band 1, from 0.5 to 0.6 μm), because the scattering is greatest at the shortest wavelengths and Band 1 of EOS is the shortest wavelength region observed. Our normal absorption is taken as 0.03, but for clean sand, the absorption is closer to 0.01. However, our calculations were relatively insensitive to the choice of absorption in this range. We have used a clean atmosphere model, having a visibility of 20 km in the visual region as the standard of comparison. This is because a 20-km or less visibility occurs in the United States for the percentages of times shown in Fig. D-2 (Eldridge[4]). It is seen that 20 km is fairly representative of viewing conditions over CONUS.

For the purpose of estimating the effect of a more heavily dust laden atmosphere, we doubled the aerosol concentration at each altitude in the model. This has the effect of decreasing the ground level visibility by 5%, while decreasing the visibility at 20 km altitude by 50% (because the major aerosol concentration is at 20 km). The overall atmospheric transmission is decreased 30% by this doubling of the aerosol concentration.

In order to evaluate the effects on contrast of offset pointing, we have tabulated the Lambert (diffuse) ground sperical reflectances of typical targets (Table D-1, (Egan[5, 6]), in the EOS bands 1-6). Some typical combinations will be presented to illustrate the effect of the atmosphere on contrast degradation. It must be noted that many targets have specularity effects, and these must be taken into account for more accurate work (Egan[5, 6]). Note however, that for an ensemble of objects, each characterized by some directionally dependent reflectivity, a random orientation of these objects will tend to wash out the directionality to some degree. Thus, for example, a single corn leaf has a characteristic bidirectional reflectance but a corn field can still be characterized by a diffuse reflectance (to a first approximation) because of the random orientation of the corn leaves. Many objects in remote sensing applications may be characterized by a diffuse reflectance by this argument.

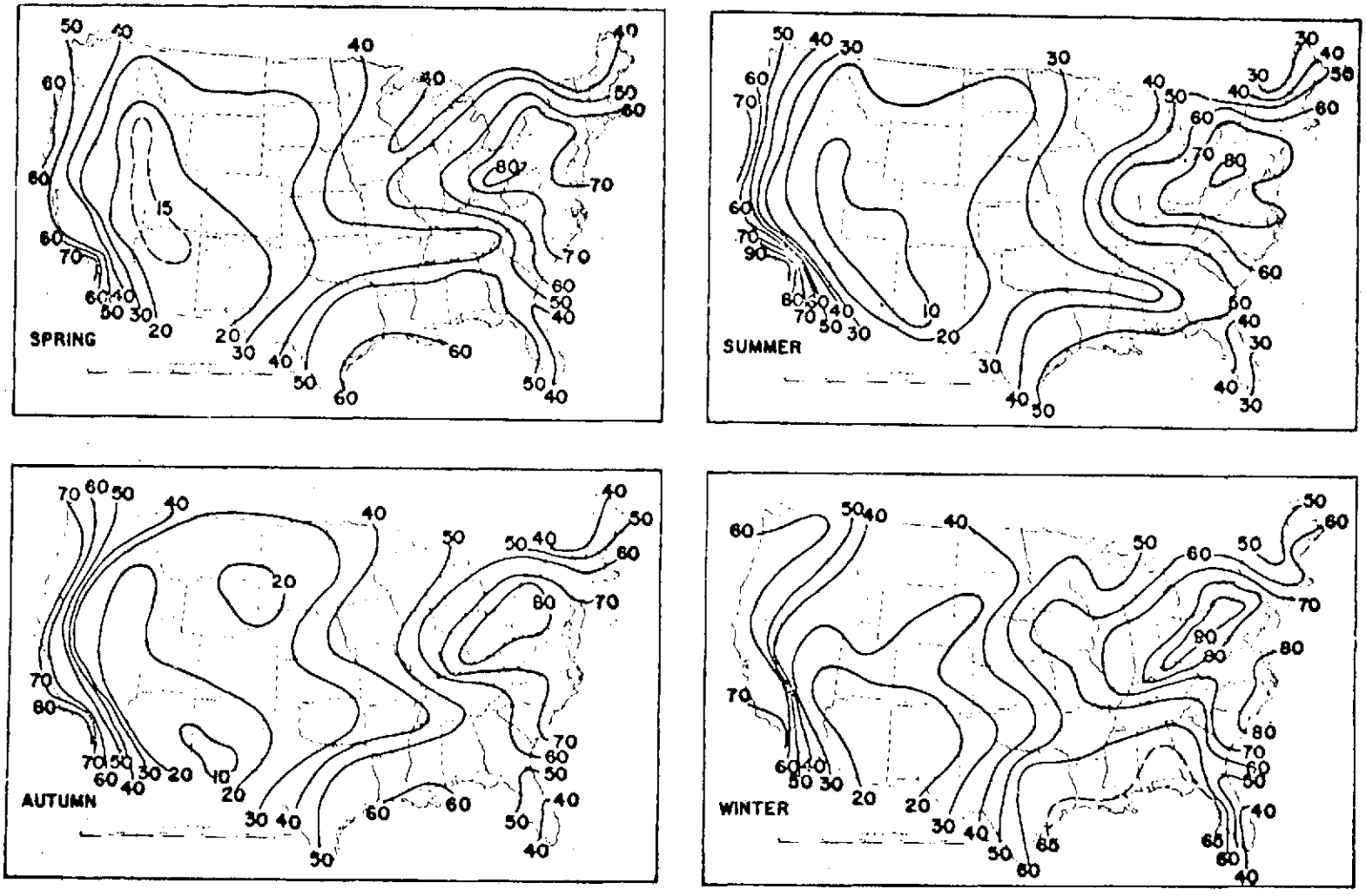

NOTE: VALUES INDICATED ARE PERCENTAGES OF THE TIME VISIBILITY IS 20 KILOMETERS OR LESS

A7-24

Fig. D-2 Seasonal Ground Level Visibility for CONUS

Table D-1 Reflectivities of Typical Remote Sensing Targets

BAND	WAVELENGTH, μm	FORESTRY			AGRICULTURE			FARM SOIL MOISTURE		ICE	SNOW ICE
		PINE	STRESSED PINE	OAK	ALFALFA	CORN	WATER	WET	DRY		
1	0.5-0.6	.10	.25	.25	.20	.25	.04	.10	.30	.04	.50
2	0.6-0.7	.15	.25	.30	.45	.20	.04	.15	.35	.04	.50
3	0.7-0.8	.40	.40	.50	.60	.50	.04	.20	.40	.04	.50
4	0.8-1.1	.70	.70	.95	.70	.70	.04	.20	.45	.04	.50
5	1.55-1.75	.20	.45	.45	.30	.35	.04	.15	.50	.01	.50
6	2.1-2.35	.15	.45	.25	.15	.20	.01	.20	.65	.01	.50

A7T-6

D.3 CALCULATIONAL RESULTS

Using the U.S. Standard Summer Atmosphere as discussed in the previous section, the Braslau-Dave model was employed to calculate the upward monochromatic light fluxes leaving the top of the atmosphere as a function of viewing angle, sun angle, and ground reflectivity.

Figure D-3 indicates the geometry of the problem. The EOS is assumed to be looking at the Earth at some offset angle θ from the vertical and at some azimuth ϕ from the solar direction. The direction $\phi = 180^{\circ}$ corresponds to the forward solar direction. If L_t represents the light flux of a particular target object seen at the EOS and L_b is the light flux of the background against which the object is being observed, then we define the apparent contrast as

$$C = \frac{L_t - L_b}{L_b}$$

Atmospheric scattering and absorption of light will tend to reduce the apparent contrast by reducing the amount of target and background light reaching the EOS and by increasing the path radiance or scattered (non-target and background light) sunlight reaching the EOS from all other directions. Hence, even if the atmospheric transmission is high, contrast may be reduced by a large amount of scattered sunlight.

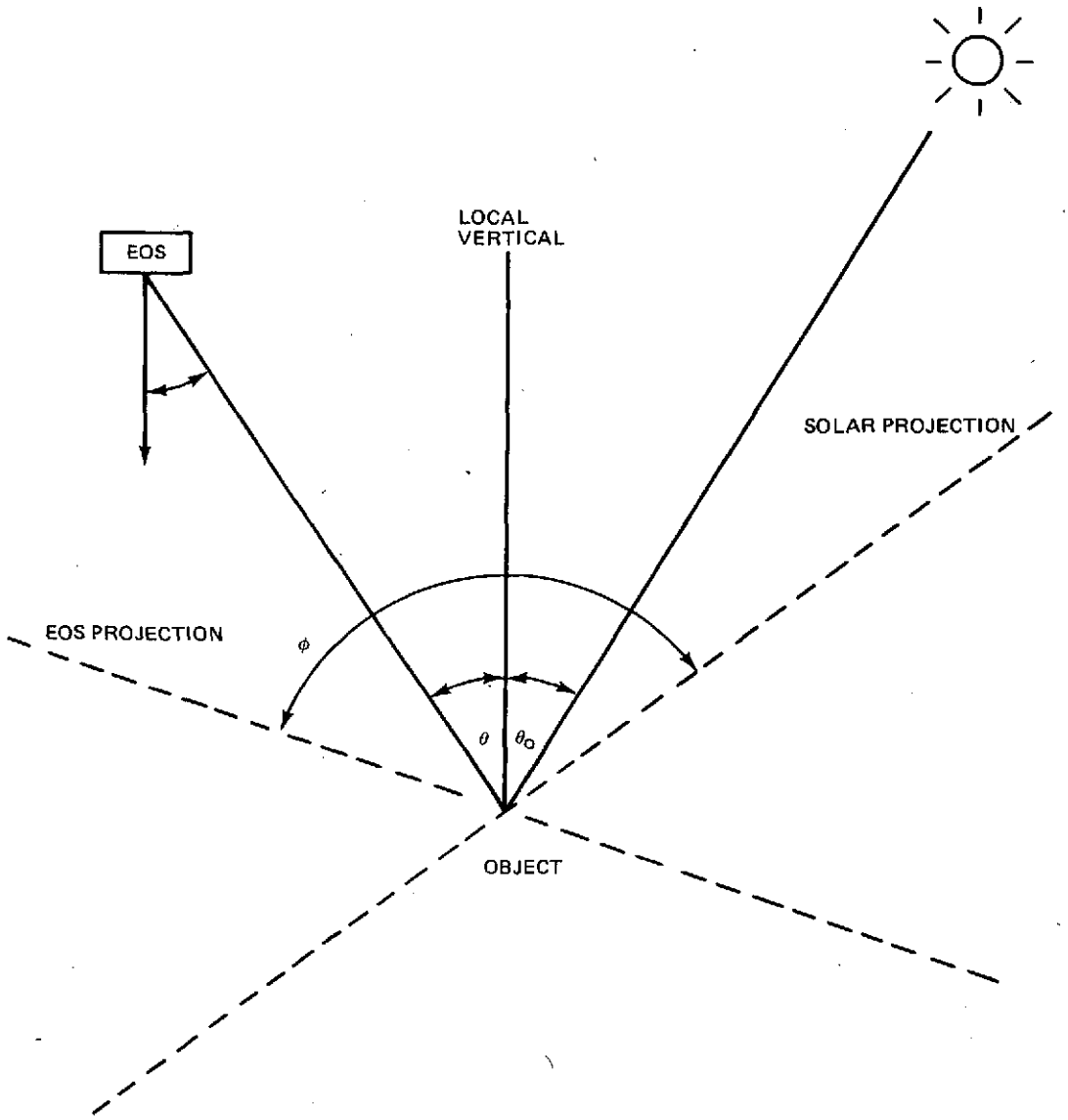

- θ_O = SOLAR ZENITH ANGLE
- θ = EOS OFFSET ANGLE
- ϕ = EOS VIEWING DIRECTION AZIMUTH ANGLE RELATIVE TO THE SOLAR PROJECTION

A7-16

Fig. D-3. Viewing Geometry of the EOS

Ground level contrast can be expressed as

$$C_o = \frac{R_t - R_b}{R_b}$$

where R_t and R_b are target and background Lambert (diffuse) reflectivities. Note that, in fact, R_t and R_b are really dependent on the direction of illumination and viewing. However, for our purposes, we will not consider this effect.

The degree to which the atmosphere tends to reduce visibility is now measured by contrast transmittance defined as

$$T_c = C/C_o$$

As may be expected, T_c is highest for small solar zenith angles θ_o (high solar elevation) and for $\phi = 0^o$ (anti-solar viewing).

In some cases, we discuss relative contrast which we define to be the ratio $c(\theta,\phi)/c(0,0)$ (all other quantities held constant) to illustrate the relative dependence on viewing angle.

The effect of solar elevation (θ_o dependence) is seen in Fig. D-4. Here we consider the case of a target reflectivity of 20% as seen against a background reflectivity of 10% at a wavelength of 0.55 μm (average λ for EOS Band 1). Apparent contrast levels are shown as a function of offset pointing angle θ in the forward solar direction ($\phi = 180^o$) for four solar zenith angles $\theta = 20^o$, 40^o, 60^o and 80^o. Thus, for example, the ground level contrast of 1.0 is reduced to 0.69 for nadir viewing at a sun angle of 20^o and is reduced to 0.29 at a sun angle of 80^o. This graph illustrates the gain in contrast performance obtained at high solar elevations. Note the large gain in going from $\theta_o = 80^o$ to $\theta_o = 60^o$ compared to the small gain in going from $\theta_o = 40^o$ to $\theta_o = 20^o$. In cases where target and background reflectivities are close, even a small reduction in apparent contrast may render the target object invisible.

The largest reductions in contrast occur for forward-solar viewing conditions. For other than forward solar viewing, loss of contrast is slower with offset angle.

This is illustrated in Fig. D-5 where we show contrast relative to nadir viewing for azimuthal viewing directions $\phi = 90^\circ$, 120°, 150° and 180°, at $\lambda = 0.55\mu m$ with $\theta_o = 60^\circ$ and $R_T/R_B = 20$ vs 10%. For this case contrast starts to drop rapidly with offset angle only as ϕ increases beyond 120°.

Contrast attenuation is largest when viewing dark objects against dark backgrounds and least for highly reflecting targets and backgrounds. This is illustrated in Fig. D-6 where we show contrast relative to nadir viewing versus offset angle for four sets of target and background reflectivities, 50 vs 40, 40 vs 30, 30 vs 20, and 20 vs 10 percent respectively. In this case, we assume a sun angle of 60° and a viewing angle $\phi = 180^\circ$ and $\lambda = 0.55\mu m$. It is apparent that contrast loss with offset angle is more rapid at the lower reflectivities. Hence, we may expect to satisfy more EOS user applications involving highly reflecting targets of observation at the larger offset angles than those applications for which reflectivies are small.

Contrast reductions from atmospheric effects will be largest for EOS Band 1 since scattering increases with decreasing wavelength. The dependence of loss of contrast on wavelength is shown in Fig. D-7. Again for sun angles $\theta_o = 40^\circ$, $\phi = 180^\circ$, $R_T/R_B = 20$ vs 10 percent, contrast levels are shown for $\lambda = .55, .75, 1.0$ and $2.0\mu m$ corresponding roughly to EOS Bands 1, 3, 4 and an average of Bands 5 and 6. As expected, contrast transmittances are higher at the larger wavelengths. Note also that the falloff with offset angle is about the same independent of wavelength. Hence, the same performance penalty as measured by a percentage loss compared to nadir viewing is incurred at a given offset angle in all bands (1 through 6). Note that the thermal band (Band 7) is not included in this discussion since in this band atmospheric emission is a significant factor in contributing to path radiance and is not calculable with the Dave-Braslau model.

We have also considered the case of a hazy atmosphere for purposes of comparison with the U. S. Standard Summer Atmosphere. As a first approximation to a reduced visibility atmosphere we doubled the aerosol levels of the clear atmosphere at each altitude. Note that in reality the increases are greater near the ground for a hazy

atmosphere, however, this effect is neglected here. Figure D-8 indicates contrast levels for the same target and viewing conditions at 0.55 μm for clear and hazy conditions. One can conclude that considerably larger offset angles are permissible for clearer viewing conditions.

D.4 RADIOMETRIC CORRECTIONS

The scattering program that we have used to predict the effects of atmospheric scattering and absorption on target contrast may be used to correct the EOS imagery for these effects. These corrections have been applied in our analysis of data from the NASA ERTS-1 Experiment No. 589 conducted by Grumman to determine the boundaries of ERTS and aircraft data within which useful water quality information can be obtained. Essentially, the correction for scattering requires the subtraction of the atmospheric scattering (under the appropriate sun angle and viewing conditions) from the radiance levels sensed by the EOS sensors. Then an absorption correction is made by multiplying this corrected value by a factor greater than one, deduced from the mathematical model (Egan[7]); calibrations were accomplished using a large beach area (high reflectivity) that was readily resolvable by the ERTS-1 together with ground truth and aircraft calibration programs.

The result of this calibration procedure was an improvement in the radiometric accuracy of the data to a level of 10%, which is comparable to currently achievable levels of accuracy.

D.5 CONCLUSIONS

In summary, the following observations may be concluded from the analysis.

- Contrast levels improve considerably for the EOS when going from a sun zenith angle $\theta_o = 80^\circ$ to $\theta_o = 60^\circ$ and improve only moderately when θ_o goes from 40° to 20°. This can be an important factor in the selection of orbit time of day
- Contrast degradation with offset angle is most severe at $\phi = 180^\circ$ but is still significant in other scan directions as well

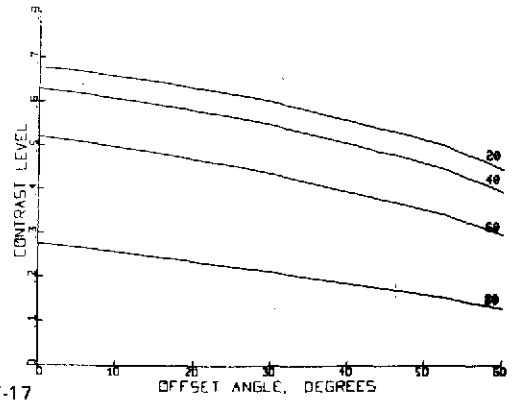

A7-17

Fig. D-4 Computer Plot of Apparent Contrast at Four Solar Zenith Angles, θ_0 = 20, 40, 60, and 80° (For R_t = 20%, R_b = 10%, ϕ = 180°, λ = 0.55 μm)

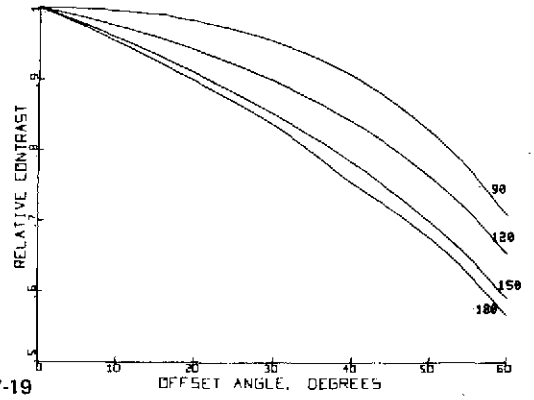

A7-19

Fig. D-5 Computer Plot of Relative Contrast in Four Viewing Directions, ϕ = 90, 120, 150, and 180° (For R_t = 20%, R_b = 10%, θ_0 = 60°, λ = 0.55 μm)

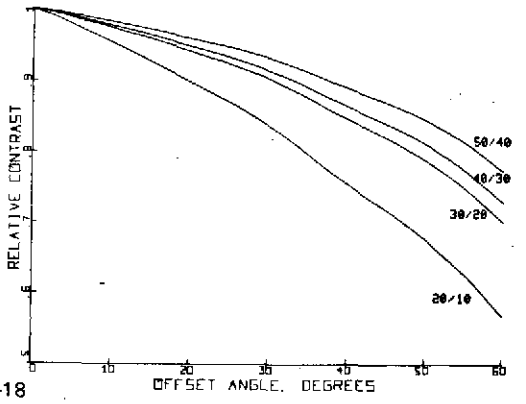

A7-18

Fig. D-6 Computer Plot of Relative Contrast at Four Lambert (Diffuse) Target and Background Reflectives R_t and R_b = 50 and 40%, 40 and 30%, 30 and 20%, and 20 and 10%, Respectively (For λ = 0.55 μm, θ_0 = 60°, and ϕ = 180°)

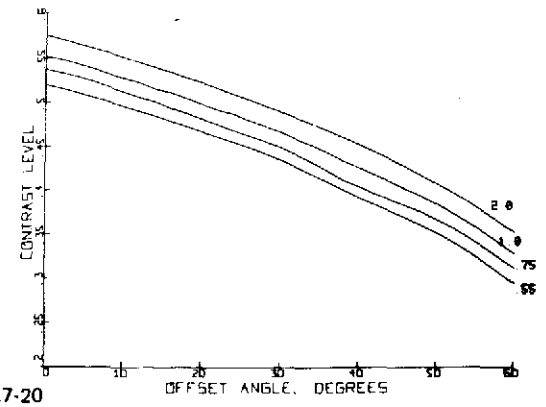

A7-20

Fig. D-7 Computer Plot of Apparent Contrast at Four Wavelengths, λ = 0.55, 0.75, 1.0, and 2.0 μm (For θ_0 = 40°, ϕ = 180°, R_t = 20%, R_b = 10%)

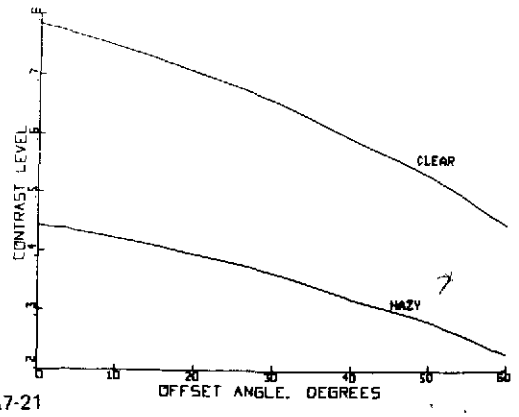

A7-21

Fig. D-8 Computer Plot of Apparent Contrast for Clear and Hazy Viewing Conditions (For R_t = 20%, R_b = 10%, λ = 0.55 μm, θ_0 = 60°, ϕ = 180°)

C - 3

D.5 CONCLUSIONS (Cont)

- User applications for which ground target and backgrounds have reflectivities less than 30% are most sensitive to loss of contrast with offset angle
- Performance penalties in loss of contrast are the same throughout EOS Bands 1 through 6
- In general, less offset pointing can be tolerated for hazy viewing conditions. Even moderately hazy viewing conditions can make offset viewing impossible for some targets of interest
- Wide angle systems can be expected to show considerable variation in contrast performance over the field of view
- In general there is some finite angle off the vertical at which a sensor may be canted which will yield optimal contrast performance.

D.6 FUTURE STUDY AREAS

Future studies should be performed in the following areas:

- Analysis of the optimal orientation of a sensor for best contrast performance, e.g., best orientation of a canted sensor
- Evaluation of the effects of directionally dependent reflectivities
- Evaluation of the effects of alternate choices of atmospheric profiles
- Evaluation of contrast performance in the thermal IR Band (Band 7), including the effects of atmospheric emission in the IR
- Analysis of the problem of target recognition as opposed to contrast performance.

D. 7 REFERENCES

1. Braslau, N. and Dave, J. V., "Effect of Aerosols on the Transfer of Solar Energy Through Realistic Model Atmospheres", J. Appl. Meterology, Vol. 12. No. 4, June 1973, pp 601-615.

2. McClatchey, R. A., Fenn, R. W., Selby, J. E. A., Volz, F. E., and Garing, "Optical Properties of the Atmosphere", (Third Edition) AFCRL-72-0497, 24 August 1972, U. S. Air Force Cambridge Research Laboratories.

3. Deirmendjian, D., "Electromagnetic Scattering on Spherical Polydispersions," American Elsevier Publishing Co., Inc., New York 1969, 260 pp.

4. Elridge, R. G., "Climatic Visibilities of the United States", J. Appl. Meterology, Vol. 5, June 1966 pp 277-282.

5. Egan, W. G., "Optical Stokes Parameters for Farm Crop Identification", Remote Sensing of Environment, Vol. 1, 1970 pp 165-180.

6. Egan, W. G., "Nonimaging Optical Differentiation of Forest Foliage", Forest Science, Vol. 16, No. 1, March 1970, pp 79-94.

7. Egan, W. G., "Boundaries of ERTS and Aircraft Data Within Which Useful Water Quality Information Can be Obtained", Proceedings of the Ninth International Symposium on Remote Sensing of Environment, Environmental Institute of Michigan, University of Michigan, April 15-19, 1974.